Behavioural, electrophysiological and pharmacological investigations on cell type-specific neural processing in different cortical and hippocampal brain regions

Sanne Beerens

A thesis submitted to the University of Strathclyde in accordance with the requirements for award of the degree of Doctor of Philosophy at the Strathclyde Institute of Pharmacy and Biomedical Sciences

August 2022

Declaration of Authenticity and Author's Rights

This thesis is the result of the author's original research. It has been composed by the author and has not been previously submitted for examination which has led to the award of a degree.

Signed:  Date: 16 August 2022

Published work

The following papers were published during the course of this PhD:

Webster, J.F., Vroman, R., **Beerens, S.**, Sakata, S., and Wozny, C. (2021). NDNF is selectively expressed by neocortical, but not habenular neurogliaform cells. Eur. J. Neurosci. *53*, 3561–3575.

Beerens, S., Vroman, R., Webster, J.F., and Wozny, C. (2021). Probing subicular inputs to the medial prefrontal cortex. iScience 24, 102856.

Beerens, S., Winterer, J., Lukacsovich, D., Földy, C., and Wozny, C. (2022). Transcriptomically-Guided Pharmacological Experiments in Neocortical and Hippocampal NPY-Positive GABAergic Interneurons. eNeuro 9, ENEURO.0005-22.2022.

Webster, J.F., **Beerens, S.**, Wozny, C. (2022). Effects of early life stress and subsequent re-exposure to stress on neuronal activity in the lateral habenula. Neuropsychopharmacology. 10.1038/s41386-022-01493-0 .

Acknowledgements

First and foremost, I would like to thank my supervisor Prof. Christian Wozny for his excellent guidance. Even though we spent almost half of my PhD in different countries, there was always time to discuss something if needed. The pandemic also did not help in terms of the research, but you always kept believing in the project and my PhD and that really helped me to get through. It was not an easy time, but your continued support definitely made it better.

Next, I would like to thank Dr. Jack Webster for teaching me most of the techniques in the lab. Whenever the ephys setup stopped working I could always message you and you would help me fix it. I would probably still be in the lab today trying to fix the setup if it wasn't for you. I hope you enjoy your new position in Edinburgh and I hope to hear great things about you in the future.

I would also like to thank Dr. Rozan Vroman for helping me to get started in the lab. Your pilot work on the subiculum project gave me something to work on from the start and turned out to be a big part of my PhD.

A special thanks goes to the BPU technical staff, for taking great care of the mice and helping with experiments and advisement on experimental design.

I would also like to thank everyone from the 4th floor of the Hamnet Wing for the coffee breaks, one-pint Fridays and other fun activities that made my PhD so much better.

Finally, I would like to thank my family and friends for their continued support and listening to the occasional scientific rant.

Abstract

In this thesis, three different projects are presented that are centred on cellular diversity and hippocampal processing in health and disease. We used *in vitro* electrophysiology combined with optogenetics to study active and passive properties and connectivity in the subiculum, prefrontal cortex and retrosplenial cortex. In summary, in Chapter 3 we characterize the projection from the dorsal subiculum (dSUB) to the medial prefrontal cortex (mPFC) in detail. We show that the dSUB mainly projects to the dorsal regions of the mPFC. The projection was stronger more posterior in the mPFC compared to the anterior mPFC, showing maximal projection to the dorsal and ventral anterior cingulate cortex (ACC). In terms of cell-type specificity, the dSUB projects to both excitatory and inhibitory neurons in the mPFC, apart from neurogliaform cells.

In Chapter 4 we continue to investigate the dSUB but in relation to depression. We show that maternal separation of pups results in mild depressive-like behaviour and that adult mice can be subsequently grouped in resilient and susceptible to the early-life stress. The main findings from this chapter are an increase in acute stress-induced activation of dSUB neurons and an increase in the excitatory drive onto fast-spiking interneurons in the retrosplenial cortex (RSC) from the dSUB that may lead to a strengthening of the feedforward inhibition in the RSC following maternal separation.

Chapter 5 investigates differences in NPY-positive neurons between the cortex and hippocampus. This study provides a proof of concept to investigate electrophysiological and gene expression differences between brain regions for specific cell types and to validate these using pharmacology. The example used in this chapter reveals differences in gene expression between the auditory cortex and CA3 NPY-positive neurons, which is potentially related to the differential developmental origin of interneurons in these brain regions. Whereas it is thought that transcriptomically-defined inhibitory cell types are largely similar across brain regions, this research challenges that idea, at least for NPY-positive interneurons.

To conclude, this thesis stresses the point that accurate cell type classification is essential for improvement of cell-type specific investigations, which provides more insight into the pathology of disorders on a cellular and circuitry level. Subsequently, this could lead to a better understand of various brain disorders and potentially discover targets for more selective and specific treatments.

Table of content

List of Figures and Tables

List of Abbreviations

5-HT	Serotonin
5-HT_{1A}	Serotonin Receptor 1A
5-HT_{2A}	Serotonin Receptor 2A
5-HT_{3A}	Serotonin Receptor 3A
AAV	Adeno-associated virus
ACC	Anterior cingulate cortex
AMPA	Alpha-amino-3-hydroxy-5-methyl-4-isoxazole-propionic acid
ANOVA	Analysis of Variance
BDNF	Brain-derived neurotrophic factor
CCK	Cholecystokinin
CGE	central ganglionic eminance
Chodl	Chondrolectin
ChR2	Channelrhodopsin-2
CMS	Chronic mild stress
CRACM	Channelrhodopsin-assisted circuit mapping
CT	Corticothalamic
DAPI	4′,6-diamidino-2-phenylindole
DREADD	Designer receptor exclusively activated by designer drug
DSM	Diagnostic and Statistical Manual of Mental Disorders
dSUB	Dorsal subiculum
EPM	Elevated plus maze
FST	Forced swim test
GABA	Gamma-aminobutyric acid
GAD65/67	Glutamate decarboxylase 65/67
HCN1	Hyperpolarization Activated Cyclic Nucleotide Gated Potassium Channel 1
HPA	Hypothalamic-pituitary-adrenal
IL	Infralimic cortex
INTRSECT	Intronic recombinase sites enabling combinatorial targeting
IT	Intratelencephalic
LED	Light emitting diode
LHb	Lateral habenula
MDD	Major depressive disorder
MGE	Medial ganglionic eminance
MM	Mammillary nuclei
mPFC	Medial prefrontal cortex

MS	Maternal separation
MWM	Moris water maze
NA	Noradrenaline
NAc	Nucleus accumbens
NGFC	Neurogliaform cell
NMDA	N-methyl-D-aspartate
NOL	Novel object location test
NOR	Novel object recognition test
NOS	Nitric oxide synthase
NPY	Neuropeptide Y
OFT	Openfield test
PL	Prelimbic cortex
PT	Pyramidal tract
PTSD	Posttraumatic stress disorder
PV	Parvalbumin
RMP	Resting membrane potential
RNA	Ribonucleic acid
RSC	Retrosplenial cortex
scRNA-seq	Single-cell RNA sequencing
SPT	Sucrose preference test
SSRI	Selective serotonin reuptake inhibitors
SST	Somatostatin
TST	Tail suspension test
UCMS	Unpredicted chronic mild stress
VGLUT2	Vesicular glutamate transporter 2
VIP	Vasoactive intestinal peptide
vSUB	Ventral subiculum
VTA	Ventral tegmental area

Chapter 1: Introduction

1.1 Cellular diversity

Over time, different types of neurons have been discovered and classified in different ways. The first neuronal cell types were found and described based on morphological characteristics (Ramón y Cajal, 1899). Later, the implementation of electrophysiological recordings refined this even further, using active and passive properties to group neurons. Over the last few decades additional techniques including morphological, immunohistochemical, electrophysiological and molecular techniques have been developed, which introduced markers to define individual cell types and to refine classification schemes.

Interestingly, a recent study showed that neuroscientists have difficulty classifying some cell types by solely looking at their morphology, indicating that morphological characterization alone is not sufficient to accurately ascribe individual cells to cell types (Defelipe *et al.*, 2013; Mihaljević *et al.*, 2019). Therefore, additional information like molecular marker expression and electrophysiological characteristics are considered to be needed for a unified classification of neurons.

Indeed, molecular techniques such as RNA sequencing have demonstrated many valuable results on cellular diversity and discovered differences or subclasses of cell types that otherwise would have been left undiscovered. An advantage of this molecular information is that some of the information is stable over time, whereas morphological and electrophysiological characteristics might vary depending on many factors, including temperature or sensory input. However, not all molecular properties are static, e.g. some genes might only be expressed during development (e.g. Gurok et al., 2004; Lim et al., 2018).

Further developments of molecular techniques have resulted in single-cell RNA sequencing, which provides more information on a cellular level, enabling comparison of molecular profiles of single cells. Patch-seq, i.e. patch-clamp recordings combined with dye injection for post hoc visualization followed by sequencing techniques, allows to collect electrophysiological and morphological characteristics in addition to a gene expression profile from single neurons (Fuzik *et al.*, 2015; Cadwell *et al.*, 2016). The multifaceted information obtained from single cells makes this technique even more informative, however, it is considered a very laborious method. Recent advances in spatial transcriptomics might provide more information than classical single-cell RNA sequencing. Multiplexed error-robust fluorescence in situ hybridization (MERFISH) allows for spatially resolved

RNA profiling in single cells with a high throughput (Chen *et al.*, 2015; Lein, Borm and Linnarsson, 2017). Additionally, the development of in situ sequencing might provide more information on cell types (X. Chen *et al.*, 2019). It has also become evident that single-cell RNA sequencing misses out on information by focussing on gene-level analysis. Detection of isoforms of genes, as a consequence of alternative splicing, are masked in gene-level analysis and are shown to add another level of specificity to cell types (Booeshaghi *et al.*, 2021). As overall expression of a certain gene, including all isoforms, might not differ between cell types, some specific isoforms of this gene might actually be differentially expressed (Booeshaghi *et al.*, 2021). Dysregulation of splicing has also been associated with psychiatric diseases (Gandal *et al.*, 2018). However, isoform detection has a low throughput and therefore it also misses clusters that are identified with regular single-cell RNA sequencing. On the other hand, it also discovers clusters that were not identified with regular methods. Combining regular single-cell RNA sequencing results with isoforms detected in SMART-seq and merging this with spatial transcriptomics might be a solution for this, resulting in a gene-isoform-space single-cell atlas (Booeshaghi *et al.*, 2021).

However, these recent developments add valuable knowledge to the field, but classical methods such as morphological and electrophysiological characteristics remain essential for cell classification as they provide functional information. Finding appropriate markers to define neuronal cell types is key to understand neuronal connections and, importantly, neuronal circuits that mediate behaviour. Thus, numerous attempts have been made to come up with a unified classification (Ascoli *et al.*, 2008; Yuste *et al.*, 2020), but a final consensus has not been reached yet.

Cell types, and especially clusters resulting from RNA sequencing analysis, are usually depicted in a taxonomy (Figure 1.1). This branching tree refines cell type definition in each layer. When focussing on neuronal cells, the first major branches are referred to as classes, such as glutamatergic and GABAergic neurons, followed by neighbourhoods focussing on developmental origin. The next level of division are subclasses followed by the most defined layer of individual clusters. The first major split in the tree is the class distinction of neurons in inhibitory (GABAergic) and excitatory (glutamatergic) neurons. Transcriptomic studies of the neocortex have confirmed that these have least in common and are the first split in the hierarchical taxonomy (Tasic *et al.*, 2018). Overall, the mammalian neocortex consists of about 85% excitatory pyramidal cells and around 15% inhibitory interneurons. Single-cell transcriptomics has found 360 different cell

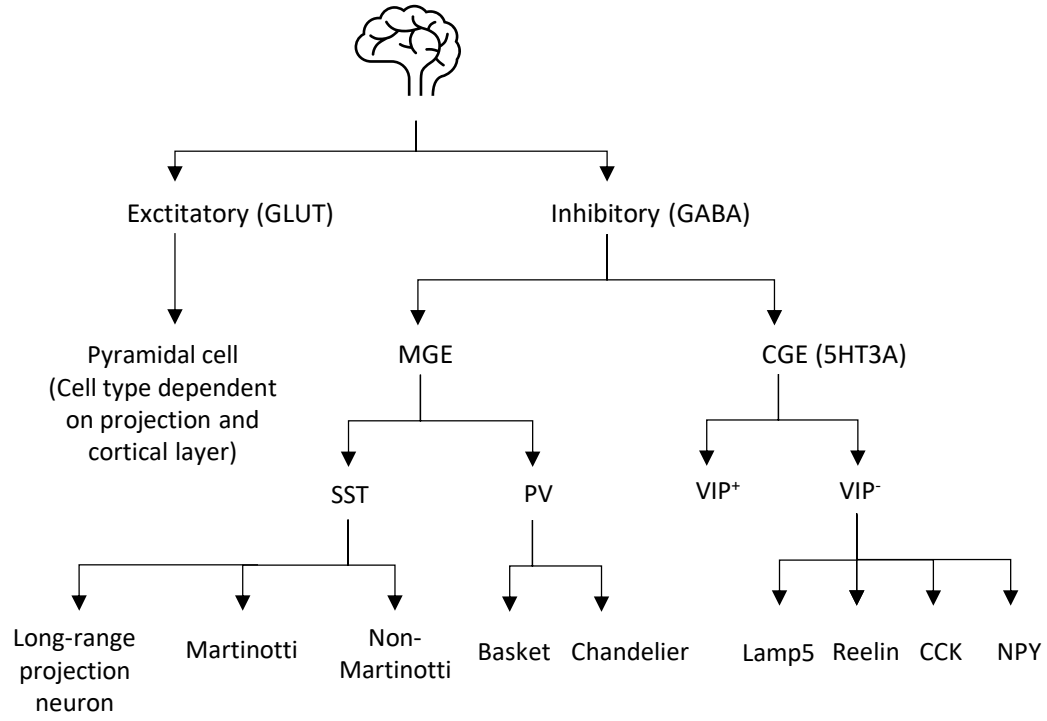

Figure 1.1: Simplistic cell type taxonomy of the neocortex
The first split divides cells into classes (GLUT/GABA). For inhibitory neurons, this can be further split into neighbourhoods (MGE/CGE) which can be further divided into subclasses. Each subclass consists of individual cell clusters or cell types.

types in the neocortex and hippocampus, with 119 GABAergic types and 241 glutamatergic clusters (Tasic *et al.*, 2018).

1.1.1 Excitatory neurons

In terms of morphology, excitatory neurons have a typical triangular-shaped soma, making them easy to distinguish from other types of neurons. They have two distinct dendritic domains on the base and apex of the soma. The apical dendritic organisation is typical for different types of pyramidal cells, allowing identification of individual pyramidal cell types by the apical dendritic arborization (Kanari *et al.*, 2019). When taking the somatosensory cortex as an example, this resulted in at least 17 pyramidal cell types exhibiting different apical dendritic arborization, with deeper layers expressing a larger diversity in cell types as the complexity of branching types increases from superficial to deeper layers. Projection pattern is also an important classification of long-range projecting pyramidal cells. This is still a challenge, since this information is not available for a large number of cells. However, pyramidal cells across the cortex can largely be classified in 3 major

classes based on their projection pattern. First, intratelencephalic neurons (IT) which project to regions within the telencephalon like the neocortex and corticoid structures like the amygdala. These neurons are found throughout layer 2 to 6. Secondly, pyramidal tract (PT) neurons, also known as subcerebral projection neurons, project to regions like the brainstem and spinal cord. These are large pyramidal neurons located in layer 5B. The last major class of pyramidal cells are corticothalamic (CT) neurons. They project to the ipsilateral thalamus and are only found in layer 6. All excitatory neurons form recurrent connections with neurons of the same class, but connectivity between classes is asymmetric (Harris and Shepherd, 2015). IT cells project locally to both CT and PT cells and receives input back from CT cells, but PT neurons do not project locally in the cortex (Harris and Shepherd, 2015). The intracortical projection of CT neurons is shown to be related to their thalamic projection target, however, they mainly project to IT neurons but no evidence is presented for projections onto PT cells (Zhang and Deschênes, 1997; Harris and Shepherd, 2015).

In terms of electrophysiology, pyramidal cells are highly recognisable by their typical firing pattern (Mason and Larkman, 1990). Their firing frequency is slowing down during prolonged current injection, also known as accommodating firing. Additionally, they show a sag potential during negative current injections. However, firing patterns might differ between subclasses of pyramidal cells and for different brain regions. Transcriptomic studies showed that pyramidal cells form different subclasses for individual cortical layers (Yao *et al.*, 2021). Furthermore, pyramidal cell types are barely shared between cortical regions with a gradual transition in cell types between regions (Yao *et al.*, 2021).

1.1.2 Inhibitory neurons

The other major class of neurons are inhibitory interneurons, characterized by their ability to produce GABA and their expression of glutamate decarboxylase (GAD) 65 and/or 67, an enzyme that is essential for the production of GABA. This group of neurons is a highly diverse group and can be classified into many different subclasses, which are shared among different brain regions (Tasic *et al.*, 2018). The first distinction between types of interneurons is the region they derive from during development as the temporal and spatial origin of interneurons relates to the mature cell type (Butt *et al.*, 2005). Interneurons are derived mainly from the caudal and medial ganglionic eminence (CGE/MGE; Figure 1.1) (Butt *et al.*, 2005; Yao *et al.*, 2021). Additionally, the preoptic area (POA) has been shown to produce interneurons during development (Lim *et al.*, 2018). The origin of interneurons is

reflected in their gene expression profile, with specific transcription factors being associated with different regions of origin (Lim *et al.*, 2018). For example, neurons originating from the CGE express *Sp8* and *Prox1*, whereas expression of *Nkx2-1*, *Lhx6* and *Satb1* is specific to MGE-derived interneurons (Kessaris *et al.*, 2014). This differential origin during development is also the first split in the hierarchical taxonomy of interneurons (Figure 1.1).

MGE-derived neurons can be split into two major classes depending on protein expression: somatostatin (SST)-expressing and parvalbumin (PV)-expressing interneurons (Figure 1.1), which make up ~30% and ~40% of the total interneuron population in the neocortex, respectively (Rudy *et al.*, 2011). Interneurons can also be classified according to their firing pattern in two major classes: fast-spiking and non-fast-spiking, whereas the non-fast spiking firing patterns may be adapting or accelerating. Fast-spiking interneurons are characterized by their high firing frequency and these neurons are all PV-positive interneurons. These PV-positive neurons can be further classified anatomically in chandelier and basket cells. Chandelier cells have a very distinctive morphology, where the axonal arbour resembles a chandelier light fixture. In terms of electrophysiological differences, chandelier cells show immediate firing whereas basket cells exhibit delayed spiking upon a depolarising current injection (Woodruff *et al.*, 2009). Basket cells are the most abundant type of interneuron in the neocortex. In terms of connectivity, chandelier cells synapse onto the axon initial segment of pyramidal cells, whereas basket cells form synapses onto the soma and proximal dendrites of pyramidal cells and other interneurons (Hu, Gan and Jonas, 2014; Lim *et al.*, 2018). Fast-spiking interneurons mainly receive excitatory input from pyramidal cells, but also some inhibitory input from other PV-positive interneurons (Hu, Gan and Jonas, 2014).

Non-fast-spiking cells have a lower frequency than fast-spiking cells, but generally higher than pyramidal cells. These cells can be both MGE- or CGE-derived, depending on molecular marker expression. For the MGE, these are SST-positive neurons. These cells preferentially target dendrites of postsynaptic neurons. Two major types of SST-positive neurons are Martinotti and non-Martinotti cells. Martinotti cells are transcriptionally heterogeneous. They are particularly abundant in layer 5 but can also be found in layer 2 and 3 of the neocortex and are characterized by an ascending axon that arborizes in layer 1. Non-Martinotti cells are found throughout layer 2 to 6 and lack axons in layer 1. They are particularly abundant in layer 4 where they target PV-positive basket cells. The somatostatin-expressing group of interneurons also contains a type of

long-range GABAergic projection neuron. These cells frequently co-express chondrolectin (Chodl), nitric oxide synthase (NOS), and neuropeptide Y (NPY). These neurons project to other regions of the cortex and are located in the deep layers.

CGE-derived interneurons make up the remaining ~30% of the total interneuron population in the neocortex, which also express the serotonin receptor 5-HT_{3A} (Rudy *et al.*, 2011) (Figure 1.1). As mentioned above, all CGE-derived neurons are non-fast spiking interneurons. These 5-HT_{3A}-positive neurons can be further divided into vasoactive intestinal peptide (VIP)-positive and -negative neurons, the latter group containing more markers for subtypes, like Reelin, cholecystokinin (CCK) and neuropeptide Y (NPY) (Lee *et al.*, 2010). Very recent transcriptomic studies have resulted in even more markers for very specific subclasses of neurons, including Lamp5, a marker for mainly neurogliaform cells (NGFCs). These NGFCs have a clearly distinct electrophysiological print from other interneurons (e.g. Kawaguchi, 1995; Schuman et al., 2019). They exhibit a late-spiking phenotype, show a sag potential and the firing pattern is accelerating when applying near-rheobase current injections and non-accommodating with larger current injections. Also, in terms of output these neurons are shown to have special characteristics. NGFCs elicit slow long-lasting IPSPs on their postsynaptic targets by a combined activation of slow-kinetic $GABA_A$ receptors and extrasynaptic $GABA_B$ receptors (Tamás *et al.*, 2003). These cells are probably the most abundant type of interneuron in layer 1 of the cortex. This cell type plays a central role in Chapter 5.

Another type of interneuron that is highly present in layer 1 is the canopy cell. They share some characteristics with NGFCs, like their horizontal elongated axonal arbour and the expression of NDNF, but they also have some distinct features (Schuman *et al.*, 2019). For example, canopy cells have a wider axonal arbour, less branches and the axon extends further from the soma than NGFCs. Additionally, in contrast to NGFCs, canopy cells do not express NPY and they do not elicit $GABA_B$-mediated inhibitory potentials in connected pyramidal neurons.

Although single-cell RNA sequencing has provided much information on the developmental origin and existence of many subtypes of neurons, a combination of morphology, electrophysiology and transcriptomics is still essential to properly assign neurons to different classes (Taniguchi *et al.*, 2011; Kim *et al.*, 2020). Two cell types might be similar in morphology and electrophysiology, but transcriptomics might show that these cells are indeed different types or from a different origin. Hence even though they may therefore seem similar, they might

still have different functions or are differentially modulated and might also be part of different networks and therefore differentially involved in behaviour. Additionally, cells with similar molecular print might have different morphological characteristics or project to different regions (Peng *et al.*, 2021). On the other hand, projection targets overlap with RNA sequencing results for major branches, but finer transcriptomic cell types might have the same projection targets, as shown for the visual cortex (Tasic *et al.*, 2018). Since long-range connectivity patterns might be important during early development this might not be accurately reflected in adult gene expression.

This classification and identification of very specific cell types has allowed for the development of techniques targeting these fine cell types to further characterize their function. The next part of this chapter will review some of the cell -type specific investigation techniques that have been developed.

1.2 Cell type specific investigations

The discovery of different subclasses of neurons has extended the knowledge of the cellular composition of the brain. Especially the genetic markers for individual cell types are highly informative and has allowed for very specific investigations of individual cell types. The use of Cre- and Flip-mediated expression is essential in this process.

1.2.1 Cre-driver lines

Genetic engineering has enabled specific recombination of sequences to manipulate protein expression and add or delete sequences. Cre recombinase affects sequences between two loxP sites and depending on the orientation of these loxP sites it can initiate deletions, inversions and translocations. By expressing Cre-recombinase under a promotor that is cell-type specific, a protein-encoding sequence containing an inverted sequence between two loxP sites is only subjected to recombination and successfully read in that cell type, resulting in cell-type specific protein expression. By expressing reporter genes or proteins that allow neuronal manipulation in a Cre-dependent matter this results in protein-specific manipulation. This enables cell-type specific investigation of structure and function, but also of the position in neural networks and involvement in behaviour. Additionally, this strategy can be used to express a virus into a specific brain region, but not surrounding regions, if this region has cells with a selective promotor (Harris *et al.*, 2014). Because this technique has great value in dissecting neural circuitry and increasing cell-type specific knowledge, the GENSAT project

developed over 250 Cre-driver lines for cell-type specific expression (Gerfen, Paletzki and Heintz, 2013). Whereas these Cre-driver lines would facilitate the investigation of broad subclasses of cell types, it would not be selective enough for individual clusters. Cell types can be classified by gene expression profiles, but it is not possible to recognize individual cell type clusters by expression of a single gene, as cell types are usually defined by expression of multiple genes or other characteristics. Therefore, single gene promotor driven Cre-expression might give insight into heterogeneous cell classes but is not selective enough for individual cell types which express multiple marker genes. The lack of genetic tools to study individual cell types is especially evident for pyramidal cells. There are transgenic lines that label broad classes of pyramidal neurons, but there are only a few lines that are restricted to more specific subpopulations (Gerfen, Paletzki and Heintz, 2013). Laminar-based transcriptomics and projection-based gene profiling has revealed specific genes that are restricted to laminar and sublaminar expression, enabling layer-specific targeting of pyramidal neurons (Sorensen *et al.*, 2015). Moreover, the temporary inducible Cre/Flip expression has recently enabled driver lines that are specific for glutamatergic cell types related to their origin and development (Matho *et al.*, 2021). The same is true for GABAergic neurons, single-gene approaches only capture broad classes of interneurons. Combinatorial genetic and viral approaches target more restricted GABAergic subpopulations (He *et al.*, 2016).

Additionally, the use of a second recombinase might help investigate individual cell types (Fenno *et al.*, 2014). Flippase is another recombinase like Cre, but it flips a sequence between two FRT sites in the same manner as Cre recombinase. By using a combination of loxP and FRT sites, one can design conditional expression dependent on two conditions: Cre-expression is dependent on one condition and Flippase on another condition. This system, known as INTRSECT (intronic recombinase sites enabling combinatorial targeting), was designed and validated by Fenno and colleagues (Fenno *et al.*, 2014). For example, Cre is expressed in a specific cell type, and flippase is expressed in neurons projecting to a specific brain region. This allows the expression of a fluorophore or modulator specifically in neurons from that cell type that project to that specific brain region. This strategy can also be used to more specifically target cell types, by using two marker genes. It is estimated that ~200 strategically designed Flip- and Cre-driver lines will be sufficient to target most of the individual cortical cell types (Huang, 2014). The Allen Institute for Brain Science is also highly involved in the development of Cre-driver lines with the aim of advancing cell-type

specific investigations (Madisen *et al.*, 2010; Harris *et al.*, 2014). For example, they have used Cre-driver lines to include rare cell types for single-cell RNA sequencing and were able to characterize the transcriptomic profile of these cells, discovering even more subclasses (Tasic *et al.*, 2018).

1.2.2 Channelrhodopsin-assisted circuit mapping

As mentioned above, the design of cell-type specific Cre expression enabled the investigation of structure and function of individual cell types, including network position. Several techniques exist to study efferent and afferent projections. For example, cholera toxin B or phaseolus vulgaris leukoagglutinin (PHA-L) can be used to trace afferent and efferent projections, respectively, in a non-cell specific manner. On the other hand, retrograde or anterograde travelling viruses can be used to trace projections of specific cell types in a Cre-dependent manner. There are several techniques to study efferent and afferent projections, including the use of retrograde and anterograde tracers. Additionally, channelrhodopsin can be used to study functional connectivity both *in vitro* and *in vivo*.

Channelrhodopsin-2 (ChR2) is a light-activated nonspecific cation channel, which was discovered in algae where it gave the organism the ability to move towards or away from light (Nagel *et al.*, 2005). The channel has kinetics in the order of milliseconds which is fast enough for neuronal control. When ChR2 is expressed on the membrane of neurons, blue light stimulation allows Na^+, among other cations, to flow inwards across the membrane and this leads to depolarization of the cell inducing action potential generation (Boyden *et al.*, 2005). This enables the investigation of functional connectivity *in vivo* by expressing channelrhodopsin and recording electrophysiological activity in different brain regions or elucidating the role of certain neurons or projections in behaviour.

However, channelrhodopsin can also be applied *in vitro* to study long-range connectivity in a single-cell manner. For example, when ChR2 is expressed in the presynaptic neuron optogenetic stimulation increases the Ca^{2+} concentration in the axonal terminal inducing vesicle release and synaptic transmission. Neurons do not need to be intact for ChR2 to facilitate synaptic transmission, meaning that synaptic connectivity of long-range projections can also be studied in slices (Petreanu *et al.*, 2007). This technique is called channelrhodopsin-assisted circuit mapping (CRACM), which is one of the central techniques used in this thesis. A virus containing ChR2 is injected into brain region A to study its connectivity with brain region B (Figure 1.2). The virus can also be expressed in a cell-type specific manner using Cre-dependent expression. ChR2 will then be expressed around the

soma but also along the axon of the neurons, even for long-range projections. When the brain is subsequently sliced for *in vitro* patch clamp recordings, the axons of long-range projections are severed from the soma. Photostimulation of these axon terminals in the target region is sufficient to induce neurotransmission and elicit currents in the postsynaptic cell (Petreanu *et al.*, 2007). An advantage of *in vitro* optogenetics compared with *in vivo* is that more information about the postsynaptic cells is available. Whereas *in vivo* multi-unit electrophysiology is able to distinguish only between excitatory and inhibitory neurons, *in vitro* patch clamp recordings result in more electrophysiological characteristics of the neuron, and if combined with post hoc visualization, morphology and exact location of the recorded neuron. This provides valuable information on the cell types receiving input from another brain region.

More recently, optogenetics using two types of opsins has been developed. This dual-channel photostimulation uses one blue-shifted opsin (excitation wavelength ~470nm), like ChR2 or Chronos, and one red-shifted opsin (excitation wavelength ~590 nm), like ReaChR or Chrimson, to stimulate two cell types or

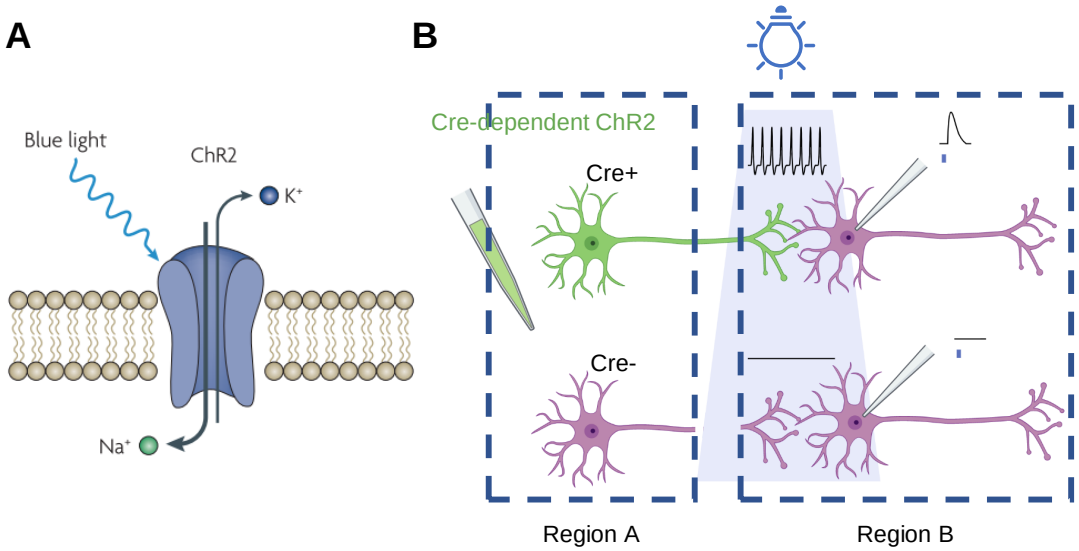

Figure 1.2: Channelrhodopsin-assisted circuit mapping

A) Schematic depiction of the mechanism of channelrhodopsin. Blue-light stimulation opens the cation channel allowing Na+ to flow into the cell and K+ out of the cell, resulting in depolarization of the neuron. Adapted from Zhang et al., 2007. B) Schematic depiction of channelrhodopsin-assisted circuit mapping, where the connectivity between region A and B is studied *in vitro*. The virus containing Cre-dependent ChR2 is injected in region A which is then expressed in Cre-positive neurons along the axon all the way to the terminals in region B. If a postsynaptic cell shows a response after blue-light stimulation this indicates that region A and B are connected.

projections independently and/or simultaneously (Klapoetke *et al.*, 2014; Hooks, 2018). Although red- and blue-shifted opsins have different optimal excitation wavelengths, the first generation of red-shifted opsins can still be activated by blue light (Hooks *et al.*, 2015). Therefore, research is still ongoing to further improve red -shifted opsins. This would allow activation independently of ChR2 activation. In addition to that, red light is better at penetrating biological tissue which is especially relevant for *in vivo* experiments of the deep brain regions in rodents and potential clinical applications (Lehtinen, Nokia and Takala, 2022). This dual-channel technique is especially useful to understand signal integration in single cells. For example, double-channel experiments showed that input from somatosensory cortex and thalamus innervate the same neurons in the motor cortex (Hooks *et al.*, 2015).

Optogenetics, but also other cell-type specific investigations using chemical-induced activation by designer receptors exclusively activated by designer drugs (DREADDs; chemogenetics), make it possible to study cell-type specific network composition and behavioural function. This can also be used to study network dysfunctions in animal models of disease, like depression, which is the central theme of Chapter 4.

1.3 Depression

Depression is a prevalent mood disorder that is still not well understood. Overall, it affects emotional, cognitive and physical functioning, but it can express itself in different severities with a variance in number of symptoms and persistence. Currently, major depressive disorder (MDD) is diagnosed when a patient exhibits at least 2 core symptoms for a minimum period of 2 weeks as classified by the Diagnostic and Statistical Manual of Mental Disorders (DSM). Possible symptoms include reduced feelings of joy, also known as anhedonia, low mood or mood changes, sleep changes, feelings of guilt and suicidal thoughts. MDD also presents itself with cognitive symptoms, mainly affecting memory and attention. These symptoms might even exist separately from low mood symptoms, but the cognitive deficits in MDD are much overlooked and understudied (Rock *et al.*, 2014).

Symptoms are variable among patients as patients can have different comorbidities making diagnosis and sometimes even distinction between the individual mood disorders difficult. Several treatment options exist for depression, however, the success rate is low and varies between patients, probably due to the high variety and combination of symptoms. One of the classical treatments for depression is monoamine reuptake inhibitors, like selective serotonin reuptake

inhibitors (SSRI), based on the monoamine theory of depression. However, the treatment only works in a small proportion of patients and there are a lot of patients exhibiting treatment-resistant depression. The remission rate for most-used medication is 30-40%, which is very low (Krishnan and Nestler, 2011). However, the monoamine theory was formed many years ago and therefore the basis of most drugs might be obsolete. Mood disorders seem to be more complex than just an alteration in monoamine levels. Additionally, the subjective diagnosis of depression, instead of being based on objective biomarkers, makes it challenging to study depression or find working treatments. There is currently no objective diagnostic criteria or biomarkers for depression, which holds back the research and understanding of the underlying mechanism and the development of new treatments. In the next section, the different theories on depression that have been developed over time are described.

1.3.1 Theories of depression

The recent review by Lui and colleagues describes the theories formed over the years (Liu et al., 2017). Many theories have been developed and a few of the main theories will be described below, including the monoamine theory, the monoamine receptor theory, the neuroplasticity theory and the excitatory synapse theory.

The monoamine theory was one of the first theories of the pathology of depression and is based on the finding that inhibiting the reuptake or metabolism of monoamines alleviates depressive symptoms. This hypothesizes that low levels of serotonin (5-HT) and/or norepinephrin (NE) lie at the basis of depressive symptoms. However, subsequent research contradicts this theory. For example, reuptake inhibitors take a short time to restore monoamine levels to a normal level, whereas the symptoms are usually alleviated in patients in the order of weeks after starting of the treatment. This indicates that the monoamine levels are not solely responsible for depressive symptoms.

As a consequence, the monoamine receptor theory was formed. This theory hypothesizes that not the monoamine levels but reduced monoamine autoreceptor levels play a pivotal role in depression. Autoreceptors, like the serotonin 1A (5-HT_{1A}) receptor, inhibit presynaptic 5-HT signalling and thereby form a negative feedback loop to regulate 5-HT release. Increasing the monoamine levels using reuptake inhibitors will increase autoreceptor activation which will result in a reduction of monoamine release. However, chronic activation of autoreceptors results in desensitization which reduces the level of autoreceptors expressed at the membrane resulting in an increase of monoamine release. This is a slower process

and therefore may correspond with the onset of antidepressant effects after starting SSRI treatment. However, some crucial evidence supporting this theory is lacking. For example, contradictory results regarding changes in 5-HT_{1A} levels or function have been found in MDD patients (Savitz, Lucki and Drevets, 2009; Ruhé *et al.*, 2021). Additionally, 5-HT_{1A} antagonists do not show antidepressant effects. This indicates that monoamine autoreceptors might be involved in depressive symptoms, but do not play a pivotal role in the pathology of depression.

Furthermore, depression is a complicated mental health disorder and displays a variation in symptoms indicating also a mechanism that is more complicated that an imbalance of monoamine receptors. A shift of focus towards a circuitry mechanism has taken place more recently, providing a role for monoaminergic brain regions and other regions involved in reward value and mood status in the pathology of depression (Chaudhury, Liu and Han, 2015; Spellman and Liston, 2020). One theory incorporating this is the neuroplasticity theory of depression (Serafini, 2012). It is based on the fact that depression is often a result of stress or that depressive symptoms can be induced by prolonged periods of chronic stress. It hypothesizes that since prolonged stress causes changes in neuroplasticity this might underly the pathology of depression. Decreased plasticity in the hippocampus and PFC has also been observed in MDD patients. For example, it is hypothesized that neurogenesis, especially in the dentate gyrus of the hippocampus, is affected in depression and this is shown to be restored by antidepressant treatment, contributing to this neuroplasticity theory of depression (Kempermann and Kronenberg, 2003; Boldrini *et al.*, 2009). Reduced levels of neurotrophic factors, which are involved in neuroplasticity, like brain-derived neurotrophic factor (BDNF), have also been found in depressed patients (Chen *et al.*, 2001; Karege *et al.*, 2002, 2005). Interestingly, antidepressants have been shown to increase neurotrophic factors and neuroplasticity in the PFC and hippocampus, indicating that this plays an important role in depressive symptoms.

Somewhat related to this, it has also been shown that excitatory synapse changes play a role in depression and this has been the basis for recent novel drug development like ketamine and S-ketamine. This theory hypothesizes that chronic stress underlies changes in a subset of glutamatergic synapses in selective brain regions like the prefrontal cortex, hippocampus, nucleus accumbens and the lateral habenula (e.g. Thompson et al., 2015; Yang et al., 2018). In agreement with this, reduced AMPA and NMDA receptor-mediated excitation has been observed in depression. Ketamine is thought to counteract these synaptic changes by blocking NMDA excitation and potentiating AMPA signalling (Maeng *et al.*, 2008). Since the

mechanism of action is a direct process and not dependent on plasticity measures like reuptake inhibitors, ketamine is shown to have short-term alleviating effects. Since glutamatergic receptors are also involved in BDNF expression regulation and neuroplasticity, this might also be key to ketamine's antidepressant effect. Understanding the exact mechanisms of the antidepressant effects of ketamine could therefore give better insight into the mechanism of depression.

The neuroplasticity theory is not exclusive for MDD, it has also been implicated in the pathologies of other disorders, like schizophrenia and bipolar disorder (Liu *et al.*, 2017). Therefore, this theory could be a common ground for multiple psychiatric disorders. The ENIGMA consortium is designed to discover structural and functional brain alterations for individual psychiatric disorders in patients, including MDD, but also to compare these changes between disorders (Schmaal *et al.*, 2020; Ho *et al.*, 2022). Since similar but different severity of changes has been found between schizophrenia, bipolar disorder and MDD, an "affective-psychotic severity continuum" has been proposed (Schmaal *et al.*, 2020). This raises the question on how changes in neuroplasticity can account for different symptoms and different disorders. This might imply a role for circuitry-specific alterations underlying specific symptoms. Additionally, a shift of view to circuit-specific alterations underlying MDD symptomology has taken place and therefore has increased research into circuitries of depression over the past years (Spellman and Liston, 2020). Increasing our knowledge on single cell transcriptomics and refining cell type classification enables us to investigate the position of these refined cell types in networks and therefore the role of these cell types in disorders like MDD.

1.3.2 Animal models of depression

Many different models exist to induce depressive-like behaviour in rodents. These models have been reviewed and discussed extensively (Krishnan and Nestler, 2011; Scheggi, De Montis and Gambarana, 2018; Hao *et al.*, 2019; Planchez, Surget and Belzung, 2019). The optimal model to use depends on what type of depression is the target of the study since different models represent different causes of depression, exhibit different symptoms or show differences in responses to antidepressant treatment. Furthermore, individual models have advantages and disadvantages (Hao *et al.*, 2019). The caveat of using animal models to study depression is that it is not certain in what way and amount they correctly model MDD as seen in humans. There are many structural and functional alterations that are seen in both rodents and humans, stressing the point that these models

resemble the human situation. In addition to this, depressive-like behaviour in rodents can often be ameliorated using antidepressant commonly used to treat MDD, showing that both are probably based on a common underlying mechanism. However, depressive-like behaviour can only insufficiently be tested in rodents, and this is not comparable with the way of diagnosing MDD patients. Especially, feeling of guilt, suicidal thoughts and low mood are specific for humans and are not translatable to or testable in rodents. Therefore, we can assume that animal models resemble certain behavioural aspects of MDD seen in humans, but we cannot be certain that it mimics the disorder as a whole. Therefore, it is better to use the term “depressive-like behaviour” and use rodents to model this type of behaviour, instead of depression as a whole psychiatric syndrome. The models provide a great way to study how situations similar in rodents and humans result in similar behavioural changes and what changes in the brain are associated with these induced behavioural alterations. Therefore, for studies using rodent models it needs to be noted that only conclusions on depressive-like behaviour can be drawn, and suggestions towards human situations can be made, but it is most likely not one-on-one translatable.

The following criteria have therefore been developed to evaluate animal models of disorders in general, not only for depression models: face validity, construct validity and pharmacological validity (Krishnan and Nestler, 2011). Face validity entails that the rodent models exhibit behaviour comparable to MDD patients. For example, symptoms are comparable, or physiological changes correspond between humans and animals, as far as that is possible. Construct validity focusses on the origin and causation of the disorder, that the way the behaviour is induced in rodents is comparable to the human situation. For example, stress is highly associated with the development of depression and therefore the majority of rodent models use a form of stress to induce depressive-like behaviour. However, since the exact mechanism and cause of depression is not known, this makes it difficult to be certain of the construct validity and other causes of depression might be overlooked. Pharmacological validity entails that the depressive-like behaviour is ameliorated using antidepressants that are currently used in treatment for MDD. Especially the pharmacological validity brings a halt to further research, especially in terms of patients that are resistant to current treatments. The major problem of treatment-resistant depression is not addressed by using models responding to conventional therapies, and thus, the development of novel models for treatment-resistant depression is urgently required to investigate new treatments. However, current animal models of depression might

still provide information on depressive-like behaviour-associated neural circuitries. Below, the most used rodent models and tests for depression are described. Apart from these models there are also pharmacologically-induced models for depressive -like behaviour. We have decided to not go into detail here since we focussed on stress-induced models, which we believe are more translatable to the human situation.

Chronic mild stress

Chronic mild stress (CMS) uses chronic stress in the adult to induce depressive-like behaviour. This paradigm can be executed by multiple alternating mild stressors (unpredicted CMS: UCMS) or fixed stressors like chronic restrained stress. Possible stressors in the UCMS include restricted space, wet bedding, no bedding, cage tilt at 45-degree angle, shallow water bath, food and/or water deprivation, day/night cycle disruption and predator smells (e.g. rat urine for mice). The stressors are applied in a random fashion, both in order and in timing. On average, it takes about 4 weeks of stress exposure to induce depressive-like behaviour.

The way this model is executed can vary greatly between studies (Willner, 2017). For example, the number of stressors per day differs between studies, as well as the duration of the applied stressors or the total duration of the protocol (number of weeks). Consequently, results for this model are variable indicating that the model is very sensitive to alterations in the protocol. Additionally, effects are dependent on the execution of the protocol and the intensity of the stressors (Willner, 2017). This also is in agreement with the human situation where a variety of symptoms can be present and different variations of depression exist.

Social defeat

Social defeat is another model based on chronic stress applied during adult life. An intruder rodent is introduced in the home cage of the subject mouse. This will result in social defeat as seen by freezing behaviour and submissive posture. Thereafter, the intruder is kept in a small compartment within the resident's cage so that the resident is protected from being attacked but still in olfactory, visual and auditory contact with the intruder. This results in a depressive-like phenotype, which is, for example, shown in a reduced sucrose preference, an increased HPA axis activation, reduced locomotion, and increased anxiety-like behaviour in the elevated plus maze test. This model can also be applied in juvenile mice (Iñiguez *et al.*, 2014).

Learned helplessness

Learned helplessness is based on the phenomenon that when animals are first presented with an inescapable foot shock they fail to learn to avoid escapable foot shocks. They accept that they are not able to escape the negative experience, and cease looking for a way to avoid experiencing the negative stimulus. The model can be used in both mice and rats.

This model will produce animals that exhibit this learned helplessness behaviour but also animals that still manage to avoid the escapable foot shock. These are called susceptible and resilient animals, respectively. Therefore, this model is highly useful to study the difference between animals susceptible or resilient to stress-induced depressive-like behaviour (Wang *et al.*, 2014; Svenningsen *et al.*, 2016).

Maternal separation

Whereas the above-mentioned models apply stress in adult life to induce depressive-like behaviour, the maternal separation protocol models the effect of early life stress. For this model, pups are separated from their mother for several hours a day for a period of several days. The duration of separation, number of days of separation and age of initiation of the protocol differs per study (e.g. Romeo *et al.*, 2003; George *et al.*, 2010; Chen *et al.*, 2022). On average, separation of 6 hours per day for a period of 10 days from postnatal day 6 (P6) is shown to be effective to induce depressive-like behaviour.

Maternal separation is repeatedly shown to affect behavioural despair and effects on locomotion (George *et al.*, 2010; Tractenberg *et al.*, 2016; Planchez, Surget and Belzung, 2019), although some studies have shown no behavioural effects (Tan *et al.*, 2017). Additionally, it's debated if maternal separation, or early life stress, induces anhedonia (Shalev and Kafkafi, 2002; Matthews and Robbins, 2003; Planchez, Surget and Belzung, 2019). However, when significant changes in the sucrose preference test have been observed, the effect is still not as pronounced as other tests (Tchenio *et al.*, 2017). On the other hand, effects of maternal separation on cognitive function have been found repeatedly across studies (Rocha *et al.*, 2021). Additionally, it has been suggested that maternal separation alters the response to stress in the adult, called stress inoculation (Qin *et al.*, 2019). Differences in the behavioural effects of MS in adolescent and adult mice have also been described, with anxiety-related behaviour only being present during adolescence whereas depressive-like behaviour was present during both adolescence and in the adult (Chen *et al.*, 2022). These differential effects

depending on developmental stage might also contribute to either increasing or decreasing sensitivity to stressors after maternal separation.

However, the differences found between studies, as for other animal models of depression, is probably due to the differences in the protocol used. Since maternal separation is applied while the mouse is still developing, this form of stress might have a different impact than stress during the adult life. Because of the neonatal timing of the stressor, it might interfere with the development of neurons or neuronal circuits. Therefore, we decided to utilize this model of depression as presented in Chapter 4 of this thesis.

1.3.3 Tests for depressive-like behaviour

Several procedures to evaluate depressive-like behaviour in rodents have been developed. The tests can be classified into different categories, measuring different aspects of MDD-associated symptoms: anhedonia, apathy, despair, and anxiety-like behaviour (Planchez, Surget and Belzung, 2019).

Anhedonia

The reduced motivation and liking of a reward, also known as anhedonia, is seen as a core symptom of depression. The sucrose preference test is the main test that is used in rodents to measure anhedonia. Rodents will be given the opportunity to freely choose between drinking water and sucrose solution, usually 1%. The preference is then calculated as the amount of sucrose consumed as a percentage of total fluid intake. In multiple studies, rodents are deprived of food and water before the test to increase the amount of fluid intake and the test is then executed during a short period of time, usually in the order of hours. However, this might create a bias in fluid consumption and is most likely driven by thirst and not a passive measure of the liking of sucrose vs water. Therefore, in this study, we have chosen to measure the fluid intake over a 24-hour period in the presence of food. Other tests for anhedonia also exist, as conditioned place preference and intracranial self-stimulation, but they are less used in previous studies (Papp, Willner and Muscat, 1991; Zacharko and Anisman, 1991; Cryan, Hoyer and Markou, 2003).

Apathy

Several measures of apathy exist, of which the coat state score is most used. Rodent models of depression tend to groom less resulting in a dirtier and not well-kept coat. A more quantifiable method for grooming can be achieved by performing the sucrose splash test. During this test, the dorsal coat of the mouse is sprayed

with a 10% sucrose solution and grooming is recorded over a 5-minute period. A reduction in grooming and latency to groom is observed for models of depressive-like behaviour (Hu *et al.*, 2017).

Despair

Tests of behavioural despair are the most used tests to study depression. They expose animals to an unavoidable stressor, comparable to the learned helplessness behaviour, and record the time point when the animal gives up escaping, recorded as immobility. One of these tests is the forced swim test (FST) (Yankelevitch-Yahav et al., 2015). During this test, a rodent model is placed in a cylinder with water and not provided with a platform to escape from the water. The time till the rodent stops swimming, and starts passively floating in the water, is used as a measure for behavioural despair. In models of depression a reduced latency to stop swimming and an increased duration of immobility is observed.

Another test for behavioural despair is the tail suspension test (TST), which can only be applied to mice. During this test, the mice are hung from their tails which induces mobility and, like the FST, mice will try to escape. Similar as to the FST, the time till the mouse stops trying to escape and total duration of immobility is recorded and found to be reduced in models of depression.

However, behavioural despair tests, the FST in particular, have recently been debated whether these are good measures of depressive-like behaviour (Commons *et al.*, 2017). Instead, it is thought to be a measure of stress coping mechanisms, but not depression per se. This is also reflected in the fact that models of autism spectrum disorder that are known to have problems with stress coping but do not show depressive-like behaviour, also show behavioural despair in the FST (Commons *et al.*, 2017). Therefore, stress coping mechanisms might be affected in models of depression but conclusions on the FST must be carefully taken and might not be one-on-one translatable to depression.

Anxiety-like behaviour

Tests for anxiety-associated behaviours are not exclusively for depression, however, depression is often accompanied by anxiety-like behaviour. One of the tests that is most commonly used is the open-field test. During this test a rodent is placed in an arena that is open at the top. Usually, mice are afraid of new surroundings and do not like to be in the middle of an empty environment without any protection. This is based on the innate response that they are more vulnerable for predators in that position. Therefore, mice usually walk along the walls of this environment and avoid the middle of the arena. The proportion of time spend in the

middle serves as a measure of anxiety. Besides this, the test also provides information on locomotor activity.

Another popular test is the elevated plus maze. During this test a rodent is placed in the middle of a plus-shaped maze with narrow arms. Two of the arms have high walls around them and the two other arms have no walls. Rodents prefer to spend time in the closed arms, since this provides shelter. The amount of time spent in open arms vs. closed arms in addition to the number of entries into the open arms is a measure for anxiety. These measures are reduced in models of depression but also in models of anxiety.

In summary, all behavioural tests have advantages and disadvantages (for review see Hao et al., 2019). In this study, we have decided to use the following tests: sucrose preference test to measure anhedonia, the sucrose splash test to measure apathy and the open field test to assess anxiety. These tests should determine if the protocol used is successful in inducing depressive-like behaviour and to further characterize behavioural changes.

1.3.4 Cell types and brain regions involved in depression

Using above mentioned models of depression, but also in MDD patients, alterations in and involvement of different brain regions and circuitries have been shown to be affected. A role for specific neuronal cell types has also been suggested. It has been shown that cell types have a unique transcriptional signature after unpredictable chronic mild stress (Newton *et al.*, 2022). Interestingly, gene expression was altered in both inhibitory PV, SST and VIP interneurons and excitatory pyramidal cells (Newton *et al.*, 2022). PV-expressing neurons have been more extensively studied in relation to depression, especially in the medial prefrontal cortex and hippocampus. Overall, a reduction in PV function has been found in both animal models of depression and post-mortem tissue of MDD patients (Perlman, Tanti and Mechawar, 2021). Whereas studies reported no changes in the number of PV neurons in MDD patients in the PFC and hippocampus (Knable *et al.*, 2004; Rajkowska *et al.*, 2006), a reduction in PV expression in the ACC and altered methylation for the PV promotor was shown (Tripp *et al.*, 2012; Thaweethee-Sukjai *et al.*, 2019). However, it has also been suggested that changes in PV neurons are more specific for bipolar disorder than MDD (Knable *et al.*, 2004; Sibille *et al.*, 2011). In animal models of depression, an increase in PV expression, number of PV neurons and increased PV activation in the prefrontal cortex has also been observed (Shepard and Coutellier, 2018; Page *et al.*, 2019). However, conflicting evidence exists and PV neurons might be

differently affected per brain region, since reduced PV expression and a reduction in PV neurons after early-life stress has been shown in the orbitofrontal cortex (Goodwill *et al.*, 2018). Furthermore, it has also been suggested that chronic stress does not alter PV maturation or induce PV cell loss in the PFC (Perlman, Tanti and Mechawar, 2021; Richardson *et al.*, 2021). All in all, GABAergic cells, and more specifically PV cells, are indicated to contribute to the pathology of depression even though there is a lot of contradictory evidence. Therefore, more research is necessary to elucidate how they are affected and how this contributes to the symptoms of depression.

Brain regions that have been shown to be affected in depression include the reward-processing or valence-conducting regions, but cortical structures have also been associated. Discoveries on the relevance of brain structure in depression have been derived from studies observing changes in brain activity and structure in MDD patients and animal models of depression, as well as the use of chemogenetic and optogenetic methods to elucidate the role of brain regions or specific projections in depressive-like behaviour (Biselli *et al.*, 2019; Planchez, Surget and Belzung, 2019). The main regions implicated in depressive-like behaviour are the medial prefrontal cortex (mPFC), anterior cingulate cortex (ACC), amygdala, nucleus accumbens (NAc), ventral tegmental area (VTA), hippocampus, lateral habenula (LHb) and raphe nuclei (Biselli *et al.*, 2019; Spellman and Liston, 2020). In the following sections, the role of the PFC and hippocampus in depression will be discussed in more detail, as these regions are studied in Chapter 3, 4 and 5.

Prefrontal cortex

The mPFC consists of three different regions: the infralimbic cortex (IL), prelimbic cortex (PL) and anterior cingulate cortex (ACC). These regions receive different inputs, the dorsal part predominantly from sensorimotor structures, the ventral part from limbic structures, suggesting diverse functions of these regions (Hoover and Vertes, 2007).

Overall, the mPFC is associated with higher cognitive functions like attention, planning, memory and decision making. The different regions of the mPFC have their own functions in different types of behaviour. The ACC is thought to be involved in behavioural control. Neural processing in the ACC would create context -dependent information by integrating task-related information to initiate a decisive strategy (Heilbronner and Hayden, 2016). The ACC has also been implicated in signalling behavioural error and deviations from expectations. This suggests a role for the ACC in learning using prediction errors by comparing expected events to

observed events independent of valence. (Alexander and Brown, 2019). For example, in rats, the ACC has been shown to encode expected outcomes based on previous outcomes of the same task (Hyman, Holroyd and Seamans, 2017). When the actual outcome did not match the expected outcome, the ACC would shift towards encoding the actual outcome. The prelimbic and infralimbic cortex have been shown to play opposing roles in different types of behaviour. For example, the PL is shown to drive fear expression, whereas the IL inhibits fear expression and promotes extinction (Vidal-Gonzalez *et al.*, 2006). Additionally, the PL is thought to increase goal-directed behaviour, whereas the IL promotes habitual behaviour (Killcross and Coutureau, 2003). This is demonstrated by continued lever pressing after reward devaluation after PL lesioning, indicating the formation of habitual behaviour. Furthermore, increased lever pressing after IL lesioning compared to controls points towards goal-directed behaviour and reduced habitual behaviour.

Apart from a dorsal-ventral organisation, the prefrontal cortex, like other cortical regions, is also arranged in different layers along the medial-lateral axis. Each layer has its own cell types, projections and functions (Narayanan, Udvary and Oberlaender, 2017). Layer I contains mainly multipolar cells. Layer II and III are often grouped as one layer. In general, this layer receives most of the input from other brain regions and projects this to other layers of the cortex. Layer IV is predominately involved in sensory-motor integration and is, therefore, not present in the prefrontal cortex and only exists in cortical areas involved in the processing of sensory information, like the somatosensory or motor cortex. Layer V and VI are considered the major output layers of the cortex. Layer V consists of different types of pyramidal cells and projects mainly to the basal ganglia. Layer VI is morphologically the most diverse layer of the cortex (Thomson, 2010). It contains both corticothalamic and corticocortical neurons, which are two distinct types of cells with specific firing properties. This deep layer receives input from thalamic structures but is also an important output structure.

A reduced volume of the medial PFC (mPFC) has been shown to be associated with major depressive disorder (Treadway *et al.*, 2015). Decreased activity is also observed in both MDD patients and in animal models of depression (Drevets *et al.*, 1997; Covington *et al.*, 2010). Lesioning the mPFC induces depressive-like behaviour (Klein *et al.*, 2010), suggesting that the decrease in mPFC activity plays a pivotal role in the development of depression. In contrast, restoration of mPFC activity by optogenetic stimulation in a mouse model of depression alleviated depressive-like symptoms (Covington *et al.*, 2010; Hamani,

Diwan, Macedo, *et al.*, 2010), further complementing this view. Interestingly, only stimulation of the PL but not the IL had an antidepressant effect (Hamani, Diwan, Isabella, *et al.*, 2010). This would suggest a specific role for the PL in depression. However, inhibiting the IL decreases depressive-like behaviour (Slattery, Neumann and Cryan, 2011), contradicting lesioning experiments. Additionally, the excitation/ inhibition (E/I) balance in the mPFC, and specifically the PL, has been implicated in the behavioural effects after maternal separation with differential effects depending on the developmental stage (Chen *et al.*, 2022). Increased excitation and E/I balance has been observed in adolescent mice, whereas excitation and E/I balance was decreased in adult mice that were exposed to maternal separation. Since lesioning and stimulation protocols in previous studies are affecting the overall activity of these brain regions, this might point towards a pivotal role for PL/ IL activity balance. However, projection-specific or cell-specific mechanisms within these regions are not ruled out. Altogether, this shows that more research into the role of the mPFC in depression is necessary.

Hippocampus

High-dimensional mapping of hippocampal structure in major depressive disorder patients and healthy control revealed alterations in hippocampal shape, but not size, in depressed patients, showing an inward deformation of the subiculum (Posener *et al.*, 2003). Whereas the overall volume analysis of the hippocampus might not show any alterations, analysing the shape might show more subtle differences in structure that are not reflected in hippocampal volume (Posener *et al.*, 2003). However, a reduction in CA1 volume has also been shown (Salminen *et al.*, 2019). The subiculum is specifically shown to be altered, even in the early stages of illness (Cole *et al.*, 2010; Ho *et al.*, 2022), indicating a pivotal role for the subiculum in depression. Additionally, resting-state functional connectivity was affected for the whole hippocampus in MDD patients (Hao *et al.*, 2020).

The effect on hippocampal structure and function has also been studied in animal models of depression. Expression of HCN1 channels were altered in dorsal, but not ventral, CA1 neurons after UCMS exposure and downregulation of these channels also had an antidepressant and anxiolytic effect (Kim and Johnston, 2018; Kim, Brager and Johnston, 2018). Furthermore, in a rat UCMS model, area CA1 was shown to be the first hippocampal region to show signs of atrophy, followed by a reduction in volume of the CA3, dentate gyrus and subiculum (Li *et al.*, 2017). The reduction in hippocampal volume was also correlated to Morris water maze (MWM) performance, the larger the reduction of volume the poorer the outcome in the MWM (Luo *et al.*, 2014). Another finding is that animal models of

depression show decreased neurogenesis in the dentate gyrus (de Andrade *et al.*, 2013). The role of the hippocampus in neurogenesis and neuroplasticity in MDD has been described in part 1.3.1. This effect of adult new-born hippocampal cells is most prominent for the ventral hippocampus (Tanti and Belzung, 2013). However, antidepressants act on both the dorsal and ventral part of the hippocampus, indicating that not only the ventral part of the hippocampus is affected. This will be discussed in more detail in section 1.3.5.

In addition to the mood symptoms, cognitive symptoms are prevalent in MDD patients, including deficits in memory and spatial navigation (Ravnkilde *et al.*, 2002). For example, MDD patients are shown to perform less well in a virtual spatial navigation task (Gould *et al.*, 2007). In animal models of depression, reduced performance is observed in MWM, novel object recognition, novel object location and working memory tests (e.g. Luo et al., 2014; Olave et al., 2022; Rocha et al., 2021; Yu et al., 2011), potentially preceding other, more typical, forms of depressive-like behaviour such as anhedonia and apathy (Maramis, Mahajudin and Khotib, 2020). Altogether, this highly implicates a role of the hippocampus in depression. The structure and function of the hippocampus will be explained in more detail in the next few sections.

1.3.5 The hippocampus: dorsal vs ventral

The hippocampal formation is an anatomically complex brain region that consists of many different subregions, including the subiculum (SUB). The structure and function of the hippocampus has been proposed to diverge along the longitudinal axis and this has been supported by seminal studies (e.g. Moser *et al.*, 1995; Kjelstrup *et al.*, 2002; Pothuizen *et al.*, 2004; Floriou-Servou *et al.*, 2018). The ventral part has been shown to be involved in emotional processes and the integration of the internal state during memory formation. For example, lesions of the ventral hippocampus affect stress responses and emotional behaviour. In contrast, the dorsal hippocampus facilitates cognitive processes, like navigational tasks and context-coupling of memories (Strange *et al.*, 2014). This dichotomy in function is also reflected in differences in gene expression and long-range connections. Gene expression in the dorsal hippocampus is similar to gene expression in cortical regions, whereas gene expression in the ventral hippocampus resembles gene expression of endocrine-involved regions, like the amygdala and the hypothalamus (Dong *et al.*, 2009).

However, it has recently been debated if this is a true dichotomy in function. For example, a role for the ventral hippocampus in spatial memory has also been

shown (Torromino *et al.*, 2019). In particular, the ventral hippocampus may be involved in the earlier phases of spatial learning, during which more global search strategies are deployed (Ruediger et al., 2012). Additionally, single-cell RNA sequencing (scRNA-seq) results revealed more of a gradual transition from dorsal to ventral hippocampus (Ding *et al.*, 2020). Therefore, the dichotomy view might need adaptation into a more transition from dorsal to ventral, with an intermediate zone in between (Strange *et al.*, 2014).

The same spread in functional difference is seen in animal models of depression and the action of antidepressants in the hippocampus (Tanti and Belzung, 2013). Stress models of depression seem to affect the ventral hippocampus more than the dorsal part, but the dorsal part still seems to play a role in depression (Tanti and Belzung, 2013). Both the dorsal and ventral part are shown to express stress-sensitive genes and gene expression is modulated by chronic stress exposure (Olave *et al.*, 2022). In addition to this, antidepressant therapies affect both the dorsal and ventral regions and could therefore possibly strengthen different hippocampal functions to drive remission. Alterations in the ventral subiculum would suit the mood symptoms associated with depression, whereas changes to the dorsal subiculum could contribute to cognitive alterations. Lesions of specific subregions along the dorsal-ventral axis have been shown to contribute to different depressive-associated behaviours, although hippocampus-dependent memory function was not tested (Levone, Cryan and O'Leary, 2021). Moreover, cognitive deficits are presented during depression, and especially spatial navigation is found to be affected in depressed patients (Ravnkilde *et al.*, 2002; Gould *et al.*, 2007), which is a function that is mainly present in the dorsal hippocampus. Taken together, this raises the possibility for the hippocampus to be involved in both the cognitive and mood symptoms of depression in a region-specific manner.

1.3.6 The subiculum

The subiculum is part of the hippocampal formation and plays a role in memory processing and navigation. It is specifically associated with the retrieval of episodic memories (Matsumoto, Kitanishi and Mizuseki, 2018). The subiculum follows the hippocampus along the longitudinal axis. It receives it main input from the CA1 area, and, together with the CA1, is considered the main hippocampal output structure as it is extensively connected to various cortical and subcortical regions (Aggleton and Christiansen, 2015; Bienkowski *et al.*, 2018; Cembrowski, Wang, *et al.*, 2018).

Structure of the subiculum

As discussed above, the subiculum, like the rest of the hippocampus, displays a dichotomy in function and structure along the dorsal-ventral axis. The dorsal subiculum (dSUB) is involved in navigation and contains navigation-specific cells (O'Mara et al., 2009; but see Torromino et al., 2019), whereas the ventral part of the subiculum (vSUB) is involved in mediating stress responses (Herman and Mueller, 2006).

This is also reflected in different projections along the longitudinal axis. Since the dSUB is involved in navigation and spatial memory it projects to cognitive regions like the retrosplenial cortex and mammillary nuclei (Namura *et al.*, 1994; Naber and Witter, 1998; Witter, 2006). Additionally, the dSUB sends efferent projections to the caudal part of the lateral septum and the nucleus accumbens (Naber and Witter, 1998; Fanselow and Dong, 2010). On the contrary, the ventral hippocampus is involved in more emotional processes and this is reflected in connectivity with the limbic system of the brain. The vSUB is shown to project to the olfactory bulb, bed nucleus of the stria terminalis, amygdala (Fanselow and Dong, 2010) and thalamic and hypothalamic areas (Namura *et al.*, 1994). Furthermore, the vSUB is shown to project to the medial prefrontal cortex (mPFC) (Jay and Witter, 1991; Naber and Witter, 1998; Witter, 2006; Liu and Carter, 2018). Even on a cellular level, the vSUB and dSUB are shown to be different regions containing region-specific cell types. Single-cell transcriptomic studies have enhanced our understanding of gene expression in subiculum neurons (Cembrowski, Wang, *et al.*, 2018; Ding *et al.*, 2020; Yao *et al.*, 2021) highlighting different neuronal cell-types in the dSUB and vSUB.

Apart from the dorsal-ventral axis, the subiculum also shows differences along the proximal-distal (i.e. lateral-medial) axis (Ishihara and Fukuda, 2016). The subiculum can be divided in the prosubiculum and the subiculum, also referred to as the proximal and distal parts of the subiculum. The composition in cell types are also shown to be different, with regular spiking cells located in the proximal part and burst-firing cells in the distal part (Kim and Spruston, 2012; Cembrowski, Phillips, *et al.*, 2018). Additionally, recent sequencing results have revealed that these regions are in fact separate regions containing different cell types and projecting to different regions (Bienkowski *et al.*, 2018; Ding *et al.*, 2020). Cell clustering analysis revealed even more subdomains within these two parts of the subiculum associated with different projections (Cembrowski, Wang, *et al.*, 2018). The proximal and distal parts of the dSUB have also been shown to exhibit distinct functions. Silencing of the distal subiculum resulted in reduced MWM performance,

whereas performance was unaffected when the proximal subiculum was silenced (Cembrowski, Phillips, *et al.*, 2018). This finding corresponds with burst-firing cells, which are located in the distal SUB predominantly, conveying spatial information (Simonnet and Brecht, 2019) and are involved in memory consolidation (Böhm *et al.*, 2015). Interestingly, the role of the proximal subiculum is not well understood. It is only speculated that the proximal subiculum is involved in object-based memory, the "what" component, in contrast to context-based memory, the "where" component, of the distal subiculum (Knierim, Neunuebel and Deshmukh, 2014; Aggleton and Christiansen, 2015) and this region is been shown to be activated in an memory-load dependent manner for non-spatial memories (Ku *et al.*, 2017).

Projections from the dorsal subiculum.

As mentioned above, the dorsal part of the subiculum projects to cognitive regions. The projections are distinct for the two different subregions of the dSUB (Witter, Ostendorf and Groenewegen, 1990). The distal subiculum is shown to project to the medial entorhinal cortex, presubiculum, retrosplenial cortex, and ventromedial hypothalamus (Kim and Spruston, 2012; Bienkowski *et al.*, 2018; Cembrowski, Phillips, *et al.*, 2018; Cembrowski, Wang, *et al.*, 2018). On the other hand, the proximal subiculum is shown to project to the amygdala, lateral entorhinal cortex, nucleus accumbens, and medial/ventral orbitofrontal cortex (Kim and Spruston, 2012; Bienkowski *et al.*, 2018; Cembrowski, Phillips, *et al.*, 2018; Cembrowski, Wang, *et al.*, 2018). Therefore, it is hypothesised that the proximal subiculum serves as a crossover between cognitive and limbic structures, whereas the distal subiculum links cognitive regions (Bienkowski *et al.*, 2018).

VGLUT2-expressing neurons are the main output neurons of the subiculum (Wozny *et al.*, 2018). This marker is evenly expressed among the distal and proximal dSUB and not prevalent in the neighbouring CA1 (Ishihara and Fukuda, 2016). Tracing experiments have shown collateral projections to the retrosplenial cortex and mammillary bodies, which are potentially VGLUT2 positive (Roy *et al.*, 2017; Kinnavane *et al.*, 2018; Yamawaki *et al.*, 2019). For the retrosplenial cortex (RSC) it is known that it receives both VGLUT1 and VGLUT2 projections from the subiculum. However, both cell types are shown to have different terminal fields in the RSC (Yamawaki *et al.*, 2019)

Additionally, it is thought that the dorsal subiculum, in addition to the well-known projection from the vSUB, projects to the mPFC. PL-projecting dSUB neurons have been shown, identified as S100b-expressing cells in the proximal subiculum (Cembrowski, Wang, *et al.*, 2018). This corresponds with injections of the proximal subiculum resulting in fibres in the prefrontal cortex (Bienkowski *et al.*,

2018). So far, the dorsal subiculum has only been shown to project to the IL and sparsely the PL (Witter, Ostendorf and Groenewegen, 1990; Bienkowski *et al.*, 2018), however, a recent tracing study raised the possibility of projections from the dorsal subiculum to the ACC as well (Bienkowski *et al.*, 2018). Electrical stimulation of dorsal subicular neurons also elicited responses in the ACC and PL (Nakamura, Katayama and Kawakami, 2010), showing that the different regions of the mPFC and dorsal subiculum are in some way connected but evidence for a direct functional connection is lacking. Chapter 3 will go into more detail on this.

As mentioned before, this thesis is divided in three different projects corresponding to three different result chapters. The aims and objectives of this thesis will be described below.

1.4 Aims and objectives

The work presented in this thesis is centred around cell diversity and the subiculum in health and disease and consists of three individual projects:

1. Characterize the dorsal subiculum to mPFC projection
2. Investigate the role of dSUB structure and function in an animal model of depression
3. Examine differential interneuron modulation: Serotonin receptor expression in cortical and hippocampal NPY interneurons

In the first project we investigate the projection from the dorsal subiculum to the mPFC since detailed information on a functional connection was lacking. We use *in vitro* patch clamp recordings combined with optogenetics to characterize the postsynaptic cells in the mPFC receiving input from the dorsal subiculum. Findings of this project are presented in Chapter 3.

For the second project we continue looking into the structure and function of the dorsal subiculum but related to depressive-like behaviour. Cognitive function and the hippocampus are shown to be affected in (animal models of) depression, but the subiculum has only been investigated in human patients. Since the subiculum is one of the major output regions of the hippocampus, this region might play a vital role in the cognitive symptoms of depression. In Chapter 4 we will go in more detail about this and present our findings.

The last project is centred around interneuron modulation and cell diversity in the hippocampus and cortex. Single-cell sequencing results showed differences in gene expression profiles for CA3 and auditory cortex NPY-positive interneurons, including expression of the serotonin receptor 5-HT_{2A}. We used *in vitro* patch clamp recordings combined with pharmacology to examine if differential gene expression also resulted in differential protein expression and if this affected electrophysiological characteristics. Results of this are presented in Chapter 5.

Chapter 2: Material and Methods

2.1 Animals

Both male and female mice were used for all experiments. VGLUT2-IRES-Cre mice Slc17a6tm2(cre)Lowl (on a C57BL/6 background) were used for optogenetic and maternal separation experiments, NPY-GFP mice on a C57BL/6 background were used for pharmacology and wildtype C57BL/6 mice were used for the cFOS experiments (Table 2.1).

Mice were kept on a regular 12:12 hour light/dark cycle with ad libitum access to water and food unless stated otherwise. Pups were housed with their parents until weaning at P21 unless stated otherwise. For the MS protocol, all mice were single housed the day before sucrose preference testing in order to allow testing for each individual mouse. All animal procedures were approved by the Ethics committee of the University of Strathclyde, Glasgow in accordance with the relevant UK legislation (License number P546B085A and PP0372838; the Animals (Scientific Procedures) Act, 1986).

Mouse Strain	**JAX stock #**	**Reference**
Slc17a6$^{tm2(cre)Lowl}$	016963	Vong et al., 2011
NPY-GFP	006417	Van den Pol et al., 2009
C57BL/6J	000664	N/A

Table 2.1: Overview of mouse lines used.

2.2 Maternal separation

At P5, half the litter was ear punched to mark the pups that would undergo maternal separation (MS). From post-natal day 6 (P6) until P16 earmarked pups were removed from the dam and placed in individual segments of a cage in a different room for 6 hours a day. Pups were provided with baby food and water and the cage was heated to ~ 37^{o}C using a heat mat. These pups underwent early weaning at P17 and were provided with baby food to maintain their bodyweight. The other half of the litter was left in the home cage with the dam and weaned at the normal age of P21. The pups were group-housed after weaning, and were split by sex after one week.

2.3 Stereotactic injections

VGLUT2-IRES-Cre mice (N = 19) underwent stereotaxic surgery at P27-P35 for PFC recordings and at P38-45 for the MS subicular (SUB, N = 15) and retrosplenial cortex (RSC) recordings (N = 15). They were deeply anaesthetized using isoflurane (5% for induction; 1-2% for maintenance), transferred to a stereotaxic frame (Narishige, Tokyo, Japan) and subcutaneously injected with the analgesics carprofen (5 mg/kg) subcutaneous and lidocaine (4 mg/kg) under the scalp. A small incision was made and the skull was exposed under aseptic conditions. Bregma and lambda were measured, and the head tilt was adjusted accordingly to ensure that the brain was level. A small burr hole was drilled above the subiculum in the left hemisphere. Glass micropipettes were pulled using a PC-100 vertical puller (Narishige, Tokyo, Japan). Table 2.3 contains the details for the injection coordinates and viruses that were used. Injections were made using a pressure injector (Narishige, Tokyo, Japan), injecting 100-200 nL of virus at a rate of 25 nL/min. For PFC recordings, the viral vector used is a AAV9-EF1a-SwitchON_mRubyNLS-hChR2(H134R)-EYFP-NO_WPRE (titre: 2 x 10^{13} vector genomes/mL; Table 2.2) which is an adeno-associated virus of serotype 9 that drives Cre-dependent expression of ChR2 and eYFP in Cre-positive cells and the expression of mRuby in the absence of Cre (Wozny *et al.*, 2018). The virus AAV9-EF1a-doublefloxed-hChR2(H134R)-EYFP-WPRE-HGHpA (titre: 1.8x10^{13} GC/ml; Table 2.2) was used for RSC and SUB recordings. Table 2.3 summarizes the viruses, volumes and coordinates used in mice. The pipette containing the viral vector was left in place for 10 minutes after injection before slow removal to minimize viral spread along the injection tract. The burr hole was covered with bone wax and the incision was closed using Vetbond tissue adhesive. Mice were given at least three days after surgery to recover before the sucrose behavioural testing was started and/or 2-3 weeks before slice preparation to allow sufficient viral expression.

2.4 Behavioural testing

Litters that underwent maternal separation underwent behavioural testing in the adult between P45 and P60 to assess depressive-like behaviour and memory function. The tests used are sucrose preference testing, open field test, splash test and novel object location and recognition test. Figure 2.1 gives an overview and timeline of the tests used.

2.4.1 Sucrose Preference Test

Sucrose preference was tested in adult mice between P46 and P53 and lasted 4 days (Figure 2.1B). Mice were single-housed during this period. First, mice were presented with two drinking bottles containing water for 24 hours to habituate them to having two spouts in their cage (day 0). Next, one of the bottles contained a 1% sucrose solution (day 1). After 24 hours the bottles were weighed, and the location of the sucrose and water bottle were swapped. This was repeated for the next two days (day 2 and 3) as testing days. Bottles and drinking spouts were used for the same solutions and the same mice every test to minimize variation. Bottles were weighed before and after presenting them to the mice. Sucrose preference was calculated as the volume of sucrose consumed as a percentage of the total volume of liquid consumed. The average of day 3 and 4 was used to correct for any possible side preference. If a mouse presented with unreliable high or low values, another day of SPT was performed for those mice.

Virus	**Derived from**	**Cat. number/LOT number**
AAV9-EF1a-SwitchON_mRubyNLS-hChR2(H134R)-EYFP-NO_WPRE	Provided by Viral Core Facility, Charité, Berlin	addgene #118279,
AAV9-EF1a-doublefloxed-hChR2 (H134R)-EYFP-WPRE-HGHpA	Addgene	addgene #20298 LOT:v65631

Table 2.2: Overview of viruses used.

Virus	**Amount**	**Mice**	**AP**	**ML**	**DV**
AAV9-EF1a-doublefloxed-hChR2 (H134R)-EYFP-WPRE-HGHpA	100 nL	8	-3.4	-2.2	-1.8
AAV9-EF1a-doublefloxed-hChR2 (H134R)-EYFP-WPRE-HGHpA	200 nL	7	-3.4	-2.2	-1.8
AAV9-EF1a-SwitchON_mRubyNLS-hChR2(H134R)-EYFP-NO_WPRE	100 nL	5	-3.4	-2.5	-1.8
AAV9-EF1a-SwitchON_mRubyNLS-hChR2(H134R)-EYFP-NO_WPRE	200 nL	21	-3.4	-2.5	-1.8
AAV9-EF1a-SwitchON_mRubyNLS-hChR2(H134R)-EYFP-NO_WPRE	100 nL	3	-3.4	-2.0	-1.8

Table 2.3: Coordinates and viruses used for stereotaxic injections

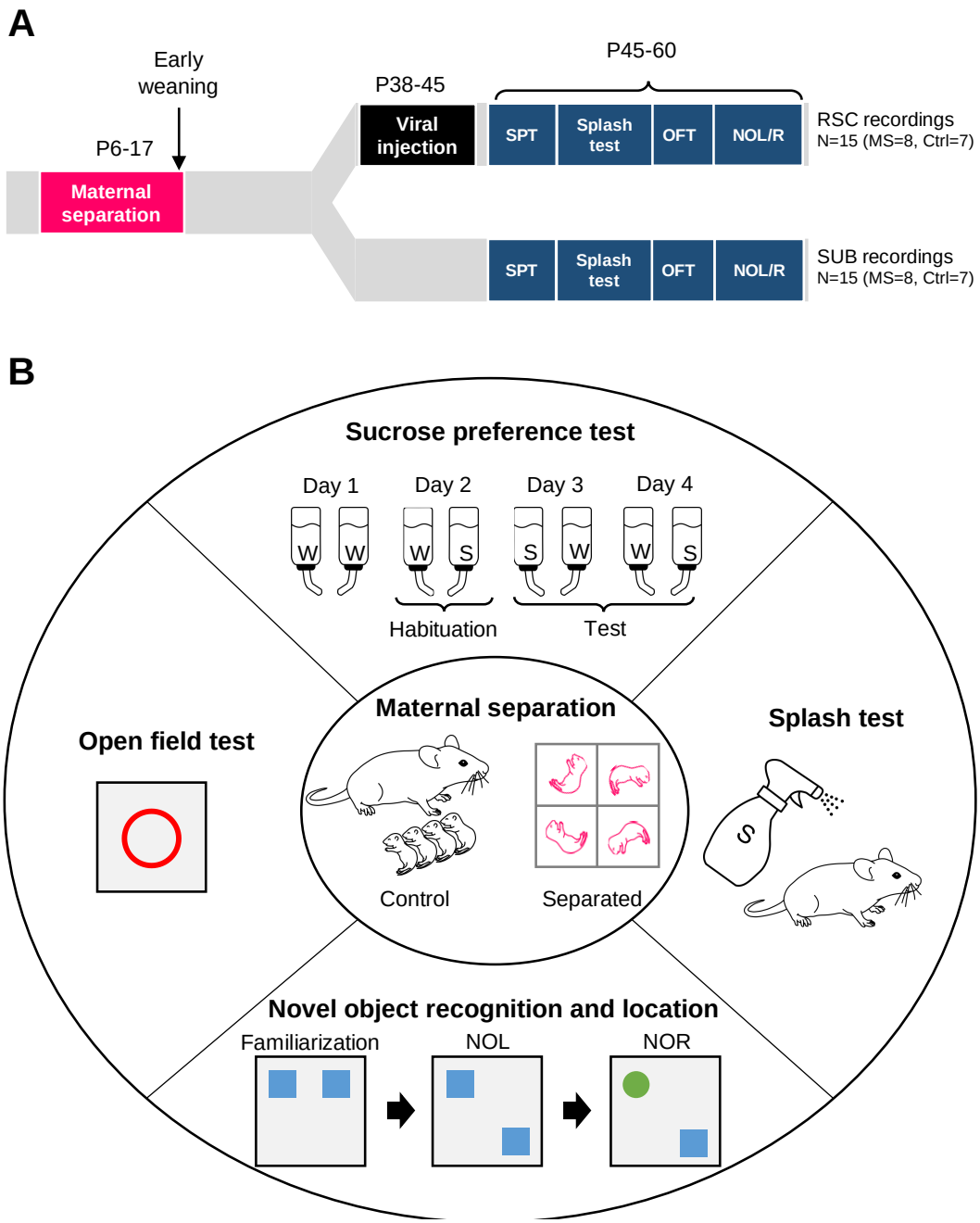

Figure 2.1: Timeline and tests performed.

A) Timeline of maternal separation, surgeries and tests performed to assess depressive-like behaviour. Mice that were used for SUB recordings did not have surgeries, whereas mice that were used for RSC recordings had stereotaxic surgery.

B) Overview of tests performed to examine depressive-like behaviour in maternal separated and control mice.

2.4.2 Splash test

The splash test was performed in the home cage to minimize novel environment stress that might influence the test results. Food, water and cage enrichment was removed before the test. Mice were sprayed with a 10% sucrose solution on their dorsal coat outside of the cage and placed back into their home cage. Their behaviour was recorded for 5 minutes using a GoPro camera. The cage walls were not high enough allowing the mice to jump and/or climb out of the cage. Therefore, the cage remained covered with the cage lid which allowed the mice to climb on the cage lid. Grooming, rearing and climbing was scored manually from these videos. Grooming was defined as reaching for and cleaning of their dorsal coat. Short bouts of grooming of the head was not scored as grooming as this might also be acute stress-induced behaviour (Estanislau, 2013; Rojas-Carvajal and Brenes, 2020).

2.4.3 Open field test

The habituation session of the novel object recognition/location task was used for the open field test. Dimensions of the box are 40 x 40 x 40 cm. One wall contained a directional mark to allow the mouse to orientate itself within the environment, which is important for the novel object location test. Each mouse was recorded for 10 minutes using a ceiling-mounted camera. Mouse location was subtracted using DeepLabCut and subsequently analysed using Matlab. DeepLabCut is designed for pose estimation by training a deep neural network to recognize specified parts of the animal from example videos (Mathis *et al.*, 2018). The nose, ears and tail base of the mice were manually labelled in 440 frames from 11 example videos to train a network using the ResNet-50 model. Subsequently, all recorded videos were analysed using this trained network. The resulting nose trace from DeepLabCut was then analysed using Matlab to calculate the time exploring each object. Exploration of an object was defined as the nose of the mouse being within a 2 cm range from the object, which was measured as a circle with a radius of 5 cm from the centre of the object. The time spent in the centre was calculated as total time that the nose of the mouse was within a 10cm radius from the middle of the box.

2.4.4 Novel object location and recognition test

The novel object location and novel object recognition test were used to test object and spatial memory function (Figure 2.1B). On day 1, mice were habituated to the environment by allowing exploration for 15 minutes without any objects. This session was also used to assess open field exploration. The familiarization phase

took place on day 2, where the mouse was presented with two identical objects: either a tower or a tube, balanced between groups. The square tower was lined with coloured taping and the dimensions were 12.5 x 5.2 x 5.2 (L x H x W) cm. The transparent tube was filled with paper and closed off at the top side to discourage climbing. The dimensions of the tube were 13 x 5.5 (L x D) cm. The objects were placed 10 cm from the walls. On day 3, one of the two objects was moved to a novel location for the Novel Object Location (NOL) test. The side of the moved object (left or right) was balanced between mice. For the Novel Object Recognition (NOR) test on day 4 the non-moved object of day 3 was changed for the other object, e.g. tower when tube was used during familiarization and NOL, or vice versa. Whenever a mouse managed to climb an object, this mouse was excluded from analysis for that and subsequent sessions, resulting in N = 22 for habituation, n = 20 for familiarization, n = 18 for NOL, n = 16 for NOR.

2.5 Acute slice preparation

Mice were humanely euthanized using cervical dislocation and immediate decapitation at P48-68 for PFC recordings and P59-82 for SUB/RSC recordings. Brains were quickly removed and submerged in oxygenated (95% O2; 5% CO2) ice-cold sucrose-containing artificial cerebrospinal fluid (ACSF) containing (in mM): sucrose 50, NaCl 87, $NaHCO_3$ 25, KCl 3, NaH_2PO_4 1.25, $CaCl_2$ 0.5, $MgCl_2$ 3, sodium pyruvate 3 and glucose 10. Sources of all reagents can be found in Table 2.4. Brains were kept in the dark after extraction until the end of the experiment. Brains were sliced in 300 µm coronal (PFC and RSC recordings) or horizontal (SUB recordings) slices using a vibratome (Leica Biosystems, VT1200S, Newcastle-upon-Tyne, UK). Slices were transferred to oxygenated ACSF containing sucrose at 35°C and after 30 min incubation transferred to 35°C normal ACSF containing (in mM) NaCl 115, $NaHCO_3$ 25, KCl 3, NaH_2PO_4 1.25, $CaCl_2$ 2, $MgCl_2$ 1, sodium pyruvate 3 and glucose 10. Slices were left to cool down to room temperature (~ 30 min) before recordings. The rest of the brain slices used for injection site analysis were directly transferred to 4% PFA in 0.1 M sodium-based phosphate-buffered saline (PBS) overnight and stored in 0.1 M PBS until further tissue processing.

2.6 Electrophysiology

For electrophysiological recording, slices were transferred to a recording chamber and continuously perfused with oxygenated ACSF at a flow rate of 2-3 ml/min.

Slices were visualized using a Luigs and Neumann LN-Scope System (Luigs and Neumann, Ratingen, Germany). The recording location was determined using a 4x objective, and cell patching was performed under a 60x objective. For PFC recordings, cells were recorded in the infralimbic cortex (IL), prelimbic cortex (PL) and the dorsal and ventral parts of the anterior cingulate cortex (ACC) using the MultiClamp 700B Amplifier (Molecular Devices, California, USA). Glass micropipettes were filled with an intracellular solution containing (in mM) potassium gluconate 125, HEPES 10, KCl 6, EGTA 0.2, $MgCl_2$ 2, Na-ATP 2, Na-GTP 0.5, sodium phosphocreatine 5, and 0.2 % biocytin. The pH of the intracellular solution was adjusted to 7.2 by adding KOH. Whole-cell patch clamping was performed, and cells were held at -60 mV in voltage-clamp to assess access quality and series resistance. Electrical properties were recorded in current-clamp using a 1 s current injection with increasing amplitude (range -500 – 500 pA; step size 10 – 100 pA). Resting membrane potential (RMP) was determined using multiple sweeps of 500 ms without current injection and input resistance was measured by injecting a 1 s pulse of -100 pA.

For subicular recordings, cells were recorded along the proximal-distal axis of

Chemical	**Company**
Sucrose	Fisher chemicals
NaCl	Fisher chemicals
$NaHCO_3$	Sigma
KCl	Sigma
NaH_2PO_4	Sigma
$CaCl_2$	Fisher Chemicals
$MgCl_2$	Fisher Chemicals
Sodium pyruvate	Sigma
Glucose	Sigma
Potassium gluconate	Sigma
HEPES	Sigma
EGTA	Sigma
Na-ATP	Sigma
Na-GTP	Sigma
sodium phosphocreatine	Sigma
Biocytin	Sigma

Table 2.4: Overview of chemicals used

the subiculum in horizontal slices of the dorsal and ventral hippocampus. Dorsal and ventral slices were distinguished based on the shape of the hippocampus, which is more elongated for dorsal slices and more round for ventral slices. This was confirmed by measuring the length:width ratio of the hippocampus, whereby a ratio of <1.09 would identify a slice as ventral and >1.09 as dorsal (Figure 4.6A,B). Ratios of selected slices ranged from 0.89 to 1.30. The threshold of 1.09 is the middle point of this range and was found to reliably distinguish between dorsal and ventral hippocampal slices based on anatomical features of the hippocampus. Electrical properties were recorded in current-clamp using a 1 s current injection with increasing amplitude (range -500 – 500 pA; step size 50 pA) at RMP and -70 mV. Resting membrane potential (RMP) was determined using multiple sweeps of 500 ms without current injection and input resistance was measured by injecting a 1 s pulse of -100 pA. Spontaneous activity was recorded in voltage-clamp at -50 mV to visualize both inhibitory and excitatory currents.

2.7 Optogenetic stimulation

Optogenetic stimulation was performed using a blue LED (pE-300ultra, Cool LED, Andover, UK; 2 ms pulse; power 11.5 mW) and responses were recorded in current clamp. Recordings were performed in darkness to prevent unintentional stimulation. All neuronal voltage and current signals were low pass-filtered at 2-10 kHz and acquired at 10-25 kHz using an ITC-18 digitizer interface (HEKA, Pfalz, Germany).

For PFC recordings, slices were stimulated with a 2 ms pulse at 100% LED intensity. The LED-induced response was averaged over 20 stimulations. For RSC synaptic strength recordings, slices were stimulated with a 1 ms pulse at the following LED intensities in order of increasing strength: 1, 2, 4, 6, 8, 10, 20, 40, 60%. Responses were recorded at RMP and at a holding potential of -70 mV and response size was calculated as an average of 5 stimulations per LED intensity.

2.8 Pharmacology

2.8.1 TCB-2

First, the effect of the 5-HT_{2A} agonist TCB-2 (Table 2.5) was tested in slices from NPY-GFP mice. NPY-positive auditory neurons were patched in current-clamp and baseline spontaneous activity was recorded for two minutes before 10 µM TCB-2 was added to the perfusion system and spontaneous activity was recorded for

another 10 minutes. The IV protocol (range -100 – 300 pA; step size 25 pA) was recorded both before and 10 minutes after application of the drug to see its effect on RMP, input resistance and spiking frequency. Spontaneous activity was always recorded at RMP with 0 pA injected and IV protocols were recorded with a current injection to reach an RMP of -70 mV to keep IV conditions the same throughout the whole recording in case of drug-induced RMP changes.

Deep-layer PFC pyramidal neurons were also recorded to test TCB-2 activity as previously published (Tian, Schmidt and Lambe, 2016). The same protocol was used as for auditory cortex NPY neurons except for a TCB-2 concentration of 5 µM and RMP was kept at -75 mV using current injection during IV protocol recording.

2.8.2 5HT and ketanserin

The effect of the 5-HT_{2A} receptor antagonist ketanserin (ketanserin tartrate; Table 2.5) after 5-HT (serotonin hydrochloride, Table 2.5) application was tested. Pharmacological responses were recorded using a continuous IV protocol (range -200 – 350 pA; step size 50 pA). Current injections lasted 1 s with 9 s in between current injection steps. The total duration of recording was 30 minutes with 5-HT (30 µM) and the ketanserin (10 µM) being added to the perfusion system 2 and 12 minutes after the start of the recording, respectively. The drugs take ~2 minutes to reach the recording chamber, meaning that the real timing of 5-HT is t = 4 minutes and t = 14 minutes for ketanserin.

Drug	**Company**	**Cat. number/LOT number**
TCB-2	Tocris	2592/10
Serotonin hydrochloride	Sigma	H9523-25MG LOT:SLCC3073
Ketanserin tartrate	Tocris	0908/50 Batch:4B/225704

Table 2.5: Overview of drugs used.

2.9 cFOS experiments: Acute restraint

To investigate stress-induced brain region activation after maternal separation, we subjected C57BL/6 mice that underwent MS (N = 8) or control mice (N = 9) to acute restraint stress. Mice were placed into a tube with a diameter of 5.5 cm. One end of the tube was closed and a removable closing was inserted at the other end. This was inserted as far till the mouse had minimal room to move. Both closings

had holes in them allowing ample airflow into the tube (Figure 4.11A,B). Mice were placed in the tube for 1 hour and were perfused 1 hour after being released from the tube to allow cFOS expression. Mice that were not exposed to acute restraint stress (MS N = 9; Ctrl N = 9) were perfused directly after being taken from their home cage.

2.9.1 Transcardial perfusion and sectioning

Mice were terminally anaesthetized by subcutaneous injection of 50% lidocaine and 50% euthatal. Once anaesthetized, the heart was exposed and mice were perfused through the left ventricle with 0.1 M PBS followed by 4% PFA dissolved in PBS. Brains were removed and fixed overnight in 4% PFA after which they were transferred to a 30% sucrose solution in PBS for cryoprotection. Brains were stored at 4° C until sectioning.

For sectioning, brains were imbedded in OCT compound (VWR, Leicestershire, UK) and sectioned in 60 µm slices on a Leica S2010 R microtome (Leica Biosystems, Newcastle-upon-Tyne, UK). Slices were collected in sequence in 6 Eppendorf tubes and selected slices containing the PFC or subiculum were used for cFOS staining.

2.10 Immunohistochemistry

Following electrophysiological recordings, slices containing neurons, which had been patched and filled with biocytin were processed as previously described (Wozny and Williams, 2011). Slices were blocked for 1.5 hours using 5% normal goat serum and 1% Triton X-100 dissolved in 0.1 M PBS. Slices were incubated with streptavidin conjugated to Alexa-647 (1:500 dilution) in 0.1M PBS containing 1% Triton X-100 for 3 hours at room temperature. After incubation, slices were washed with PBS and mounted using DAPI-containing Fluoromount-G mounting medium (ThermoFisher Scientific, Waltham, MA, USA). Non-recorded slices were washed with 0.1 M PBS and directly mounted with DAPI-containing Fluoromount-G mounting medium.

Subiculum injection site slices were stained for Satb2, which is used as a marker for CA1 neurons, following the same blocking procedure as recorded slices. Slices were incubated with Rabbit anti-Satb2 (1:1,000) overnight. After washing with PBS, the slices were incubated with Goat anti-Rabbit 647 (1:500) for three hours. The slices were mounted after washing with PBS and covered with DAPI-containing Fluoromount-G mounting medium.

For cFOS staining, slices were blocked in 5% normal goat serum and 0.3%

Triton X-100 dissolved in PBS for 30 minutes. Slices were incubated with a mixture of Rabbit anti-cFOS antibody (1:10,000) and Mouse anti-PV antibody (1:4,000) in PBS overnight at room temperature. The next day, slices were washed with PBS and incubated with Goat anti-Rabbit 647 (1:500) and Donkey anti-Mouse 488 (1:500) in PBS for three hours. After that, the slices were washed with PBS and mounted with DAPI-containing Fluoromount-G mounting medium. More information on the antibodies used can be found in Table 2.6.

Antibody	**Company**	**Cat. number**	**LOT number**
Streptavidin Alexa-647	Invitrogen	S32357	LOT:2179341
Rabbit α cFOS	Abcam	AB190289	LOT:GR3393951-1
Mouse α PV	Swant	235	(unknown)
Donkey α mouse (488 conjugate)	Invitrogen	A21202	LOT:1890861
Goat α rabbit (647 conjugate)	Invitrogen	A21245	LOT:1981173
Rabbit α Satb2	Abcam	AB92446	LOT:GR3252015-1

Table 2.6: Overview of antibodies used.

2.11 Imaging

All images were taken using a Leica SP8 confocal microscope. Tile scanning was used to create overview images, and stitching was done automatically by the Leica LASX software. Images were taken using a 10x objective. Z-stacks of prefrontal cortex slices were made with 5-8 µm steps with 6-8 steps for each stack in order to reconstruct recorded neurons and to visualize ChR2-positive fibres.

For cFOS imaging, stacks with 2 µm steps were made from the whole slice thickness of 60 µm. The subiculum was imaged at 20x and the PFC at 10x. Laser intensities were kept the same for each slices, enabling comparison of fluorescence intensities and therefore threshold settings in ImageJ for cFOS quantification could be kept the same across slices (see below).

2.12 Quantification and statistical analysis

2.12.1 Electrophysiological analysis

Electrophysiological recordings were analysed using AxographX. Response size of optogenetic stimulation was measured by subtracting the baseline and then measuring the peak amplitude in the second of the trace following the LED pulse. Neurons were classified by action potential firing patterns and cell morphology using post-hoc staining. Patched neurons with damaged dendrites due to tissue sectioning were excluded from data analysis.

For synaptic strength recordings in the RSC, a one-phase association exponential curve was fitted through response size averaged per cell per intensity using Graphpad.

For the pharmacology experiments, RMP, input resistance and firing frequency were extracted from the recordings. For the TCB-2 experiments only the IV recordings, but not spontaneous activity data, were analysed. The effect of TCB-2 on the RMP was determined by taking the average RMP of the IV recording at baseline and 10 minutes after drug application. The input resistance was calculated by the reduction in membrane potential in response to a -100 pA injection. The number of spikes per current injection was counted to calculate the spiking frequency for every 25 pA step of positive current injection to create an FI curve.

Regarding the 5-HT and ketanserin experiments, the resting membrane potential was determined for every trace within the 100 ms preceding the current injection, resulting in an RMP value for every 10 seconds of the recording. The first 4 minutes of the recording were used as a baseline since the drugs took about 2 minutes to reach the recording chamber. The effect of 5-HT on the RMP was determined by averaging the RMP values of one minute surrounding the peak of the 5-HT effect. The peak was defined as where the RMP was the highest, which was usually around 14 minutes into the recording. The RMP after ketanserin application was determined by taking the average of the RMP values from the last minute of the recording. The relative effects of 5-HT and ketanserin on RMP were calculated by taking the average RMP values after application and subtracting the average RMP baseline values for each cell.

2.12.2 Behavioural analysis

For the splash test, latency and duration were measured from the videos for grooming behaviour, rearing and climbing. DeepLabCut was used to analyse OFT, NOL and NOR data. The nose, ears and tail base was manually selected in 11

videos from several mice and conditions to train a network using the default network resnet_50. This network was then used to label the position of nose, ears and tail base of the mouse in each video. Subsequently, MATLAB was used to further analyse the position traces. The nose trace was used to analyse the position of the mouse in relation to the centre of the environment (OFT) or the two objects (NOL and NOR). A circle with a radius of 5 cm was drawn around each object. Whenever the nose of the mouse was within this circle this was assigned to exploration of that object. The preference for the novel object was calculated as exploration of object A divided by the sum of exploration of object A and exploration of object B, where object A is the novel object. The total exploration time is the exploration time of object A and object B combined.

2.12.3 Images

Confocal images were analysed using ImageJ. For cells recorded in the PFC, the location of biocytin-filled cells was measured by drawing a line between the soma of the cell and the brain surface or midline of the brain slice. The distribution and spread of the injection site were measured relative to the length of the subiculum since the size of the subiculum is different along the anterior-posterior axis. For cFOS experiments, the particle analyser tool in ImageJ was used to automate cell counting. The settings are described in Table 2.7.

Region	**cFOS**		**PV**	
	Size (μm^2)	**Circularity**	**Size (μm^2)**	**Circularity**
Subiculum	20-600	0.35-1.00	80-800	0.10-1.00
PFC	50-600	0.30-1.00	80-800	0.20-1.00

Table 2.7: Setting used for cFOS and PV quantification using the ImageJ Particle Analyser.

2.12.4 Sequencing data and statistical analysis

Sequencing data from the Allen Brain Institute was downloaded from their website. The gene expression by cluster, median was downloaded from the Whole cortex & hippocampus – 10x genomics (2020) with 10x-SMART-Seq taxonomy (2020) page on 2 June 2020. Matlab was subsequently used to extract and visualize the sequencing results in heatmaps.

Sample size for experiments was determined adapting the sample size from previous published papers investigating similar effects. For example, Lui and

Carter investigated projections from the ventral hippocampus to the prefrontal cortex and recorded from ~20 neurons per region and cell type (Liu and Carter, 2018). We have adapted sample size to our experimental design expecting a similar effect size. Additionally, post-hoc power calculations were performed to determine achieved power and calculate the needed sample size to achieve 80% power with the found effect size and a statistical threshold of 0.05.

Statistical analysis was performed in GraphPad Prism. Graphs were generated in GraphPad Prism. Statistical tests used were t-test, Fisher's exact test, one-way ANOVA followed by Tukey multiple comparison test, two-way ANOVA followed by Bonferroni or Sidak multiple comparison test. The threshold for statistical significance was set at $p < 0.05$. The following indications of statistical significance are used: * $p < 0.05$; ** $p < 0.01$; and *** $p < 0.001$.

Chapter 3: Probing subicular inputs to the medial prefrontal cortex

3.1 Introduction

As described in Chapter 1, the subiculum (SUB) is the main output structure of the hippocampus and a dichotomy in structure and function exists along the dorsal-ventral axis. The dorsal SUB (dSUB) is known to be involved in cognitive function and projects to regions that are also known to be important for cognitive processing like the retrosplenial cortex (RSC), medial entorhinal cortex and mammillary nuclei (MM). In contrast, the ventral SUB (vSUB) is involved in emotional processing and projects to limbic structures like the amygdala, nucleus accumbens (NAc) and lateral entorhinal cortex.

In this chapter, we are interested in the projection from the subiculum to the medial prefrontal cortex (mPFC). The ventral subiculum projects to the superficial layers of the infralimbic cortex. Additionally, it is thought that the dSUB projects to the mPFC. Recently, prelimbic (PL)-projecting dSUB neurons have been identified as S100b-expressing cells in the proximal dSUB (Cembrowski, Wang, *et al.*, 2018). This corresponds with tracer injections of the proximal SUB resulting in fibres in the prefrontal cortex (Bienkowski *et al.*, 2018). So far, the dSUB has only been shown to project to the IL and sparsely the PL (Witter, Ostendorf and Groenewegen, 1990; Bienkowski *et al.*, 2018), however, a recent tracing study raised the possibility of projections from the dSUB to the anterior cingulate cortex (ACC) as well (Bienkowski *et al.*, 2018). In addition to the anatomical experiments, electrical stimulation of dSUB neurons *in vivo* also elicited responses in the ACC and PL (Nakamura, Katayama and Kawakami, 2010), showing that the different regions of the mPFC and dSUB are somehow connected but evidence for a direct functional, monosynaptic connection is lacking. Therefore, in this chapter we studied the functional connectivity between the dSUB and the mPFC using channelrhodopsin-assisted circuit mapping (Petreanu et al, 2007).

It is thought that the border between the CA1 and SUB is not a very sharp border and a more gradual transition between the two regions exists (Yao *et al.*, 2021). Several markers to distinguish between the CA1 and SUB have been found. For example, selective markers for dCA1 pyramidal cells that have been identified are Wfs1, Calb1, Car2 and Enpp2 (Dong *et al.*, 2009; Cembrowski *et al.*, 2016; Yao *et al.*, 2021). Additionally, VGLUT2 was identified as a marker for dSUB output neurons which is not expressed in the CA1 (Wozny *et al.*, 2018). Therefore, in this study we used VGLUT2-Cre mice to specifically express ChR2 in the dSUB and

not the CA1. With this technique, we examined the location and identity of postsynaptic mPFC cells to obtain more information on the dSUB-mPFC projection. The research in this chapter has also been published (Beerens *et al.*, 2021).

3.2 Functional connectivity between the dorsal subiculum and the prefrontal cortex

A viral vector driving expression of Cre-dependent channelrhodopsin-2 (ChR2) and enhanced yellow fluorescent protein (eYFP) was injected into the dorsal subiculum (dSUB) of VGLUT2-IRES-Cre mice (N = 19 mice) to target excitatory subicular neurons (Figure 3.1A). Previous work has shown that VGLUT2 is selectively

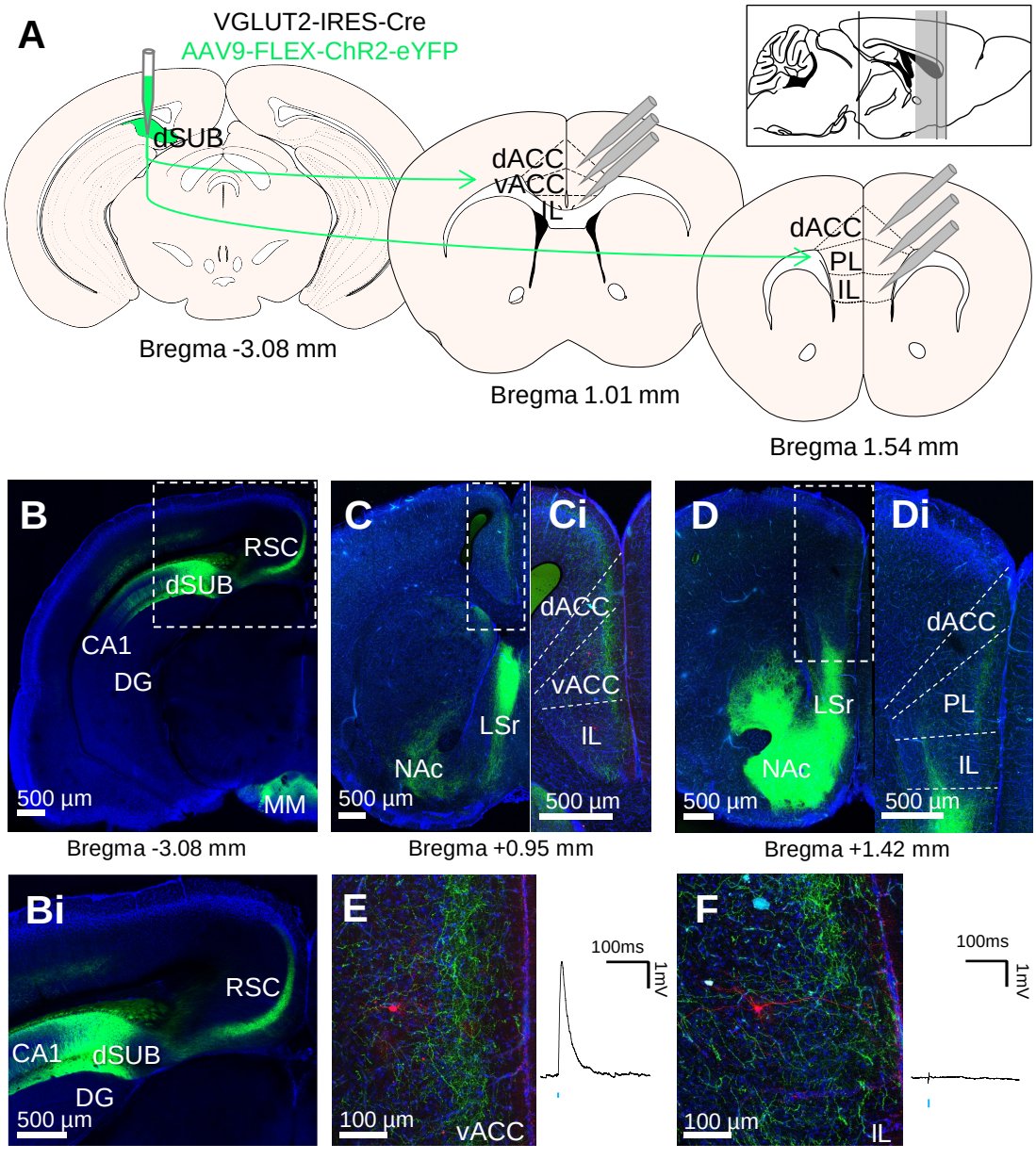

Figure 3.1 (see previous page): **Functional connectivity between the dorsal subiculum and the prefrontal cortex**

A) Overview of the experimental design. A viral vector containing ChR2 is injected into the dorsal subiculum (dSUB). Responses to light stimulation were recorded from cells in the dorsal anterior cingulate cortex (dACC), ventral ACC (vACC), pre- (PL) and infralimbic (IL) prefrontal cortex across different distances from bregma. B) Image of the injection site at bregma -3.08 mm. Fibres can be seen in the retrosplenial cortex (RSC) and the medial mammillary nucleus (MM). Bi) Enlargement of the region in B. C) Fibres in the prefrontal cortex at bregma +0.95 mm. Additionally, fibres are seen in the lateral septum (LSr) and the nucleus accumbens (NAc). Ci) Enlargement of the region in C showing fibres in the ACC, but not the IL. D) Fibres in the prefrontal cortex at bregma +1.42 mm. Additionally, fibres can be seen in the nucleus accumbens and lateral septum. Di) Enlargement of the region in D showing fibres in the superficial layers of the PL and the deep layers of the IL. E-F) A recorded neuron in the (E) vACC and the (F) IL on the left with the light-induced response on the right. Blue tick indicates the time point of LED stimulation. B-D) Scale bar 500 µm. E-F) Scale bar 100 µm. Green, eYFP; Blue, DAPI; Red, biocytin-streptavidin. Notably, all images are obtained from the same animal.

expressed in subicular output neurons (Wozny *et al.*, 2018) and not in surrounding brain regions like the CA1 and dentate gyrus (Lein *et al.*, 2007), therefore this approach allows specific manipulation of subicular output neurons (Figure 3.1B). Further evidence proving selective ChR2 expression is provided in section 3.3.

First, we validated our approach by scanning the brain for presence of ChR2-positive fibres to visualize projection sites. ChR2-positive fibres were observed in several different brain regions. The regions showing strongest innervation are the retrosplenial cortex (RSC), rostral part of the lateral septum (LSr), the nucleus accumbens (NAc) and the medial mammillary nucleus (MM) (Figure 3.1B-D). These regions are known projection sites from the dSUB and have been extensively studied before (Witter, Ostendorf and Groenewegen, 1990; Kim and Spruston, 2012; Bienkowski *et al.*, 2018; Cembrowski, Phillips, *et al.*, 2018; Cembrowski, Wang, *et al.*, 2018). Additionally, weak but substantial labelling was seen in the mPFC (Figure 1C,D). ChR2-positive fibres seem to be mainly confined to layer II-III of the prelimbic (PL) and anterior cingulate (ACC) cortex and deep layers for the infralimbic cortex (IL), but only in anterior parts of the mPFC (Figure 3.1Ci,Di). Interestingly, fibres were absent in the thalamus (data not shown), also a known projection site of the dorsal subiculum (Witter, Ostendorf and Groenewegen, 1990; Kitanishi, Umaba and Mizuseki, 2021), indicating that this

dSUB-thalamus projection is originating from non-VGLUT2 neurons. Indeed, scRNAseq data supports this; VGLUT2 is expressed in near-projecting (NP) but not intratelencephalic (IT) or corticothalamic (CT) projecting neurons (Yao *et al.*, 2021) (Figure 3.2A).

We next investigated the functional connectivity between the dSUB and mPFC by optogenetically stimulating VGLUT2-positive fibres in slices of mPFC. Postsynaptic activity upon stimulation was recorded using whole-cell patch-clamp recordings in four different regions of the mPFC, namely the IL, PL, dACC and vACC (Figure 3.1A). Cells were stimulated with a 2 ms pulse through a 60x objective for 5 times at an interval of 10 s. Light-induced excitatory postsynaptic potentials (EPSPs) were observed across multiple regions and cells conforming functional connectivity between the dSUB and mPFC. An example of a responsive

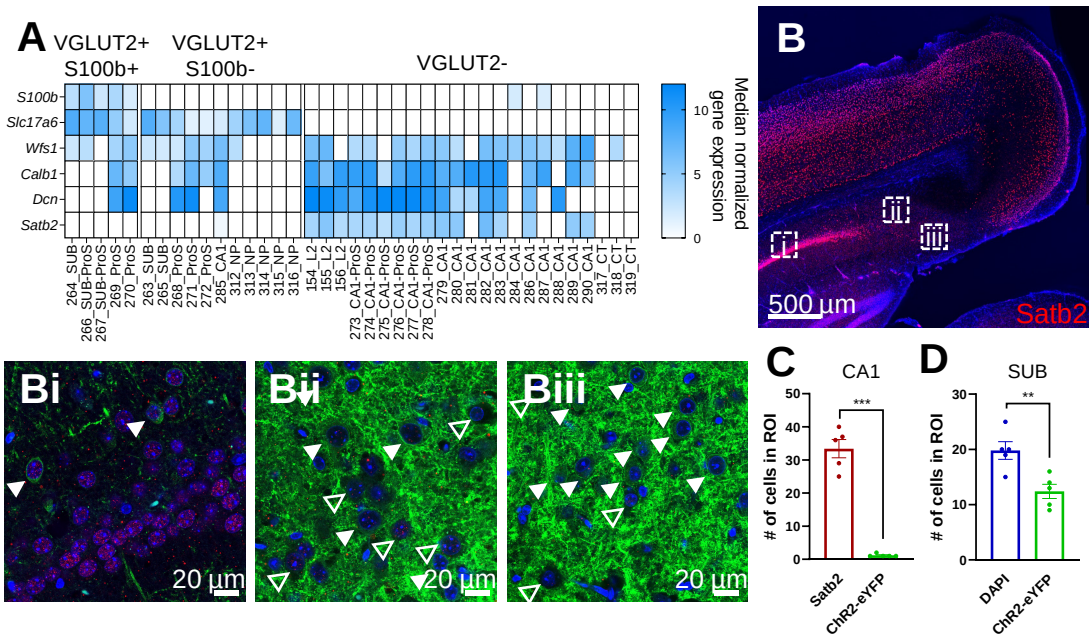

Figure 3.2: ChR2 is specifically expressed in the subiculum but not CA1 neurons

A) Gene expression in SUB and CA1 clusters as defined and provided by the Allen Brain institute. B) Satb2 staining of the injection site region with enlarged images of the CA1 (Bi), S100b-region of the SUB (Bii) and middle of the SUB (Biii). Enlarged images show Satb2-staining in red and ChR2-eYFP expression in green. The white arrows in Bi indicate neurons that are positive for Satb2 and ChR2-eYFP. The closed arrows in Bii & iii indicate ChR2-positive neurons, whereas the open arrows are ChR2-negative. C) Quantification of Satb2 and ChR2-expressing cells in the CA1. D) Number of DAPI cells and cells expressing ChR2 in the subiculum. ROI for both C and D is 184.7 x 184.7 µm in size.

neuron and a non-responsive neuron is shown in Figure 3.1E and Figure 3.1F, respectively.

3.3 Viral vector targets subiculum but not CA1 neurons

To demonstrate that specifically dSUB but not CA1 neurons are infected we looked into specific marker expression for CA1 neurons. We explored co-expression patterns for CA1 markers together with *Slc17a6* (encoding for VGLUT2) expression to see which markers are specifically expressed in CA1 and non-VGLUT2-expressing neurons. To do this, we have used publicly available single-cell RNA sequencing (scRNAseq) data (Tasic *et al.*, 2018). Hippocampal cells were clustered into different cell types, i.e. cell clusters, based on their gene expression. Here we used the median gene expression of those clusters originating from the SUB and CA1. The possible CA1 markers we selected were *Wfs1*, *Calb1*, *Dcn* and *Satb2*. Additionally, we looked at *S100b* expression, since it was suggested that this specific population of SUB neurons projects to the PFC (Cembrowski, Wang, *et al.*, 2018). *Wfs1*, *Calb1* and *Dcn* were enriched in both VGLUT2-positive and -negative neurons in the CA1 regions, as well as the SUB (Figure 3.2A) rendering them useless as a CA1 marker. However, only VGLUT2-negative neurons contain considerable mRNA levels of *Satb2* (Figure 3.2 A,B), therefore we decided to utilize *Satb2* expression as a marker for CA1 neurons to visualize the division of CA1 and SUB. Additionally, the sequencing data shows that *Slc17a6* is almost exclusively expressed in cell clusters derived from the subicular neurons and is not expressed in cell clusters shared between the CA1 and subiculum (i.e. CA1-SUB clusters), proving that VGLUT2 is a subiculum-specific marker.

Therefore, we next stained brain slices for Satb2, which shows expression in cortical regions and the CA1, but no signal in the SUB. Expression in the RSC and CA1 provides the exact borders of the SUB (Figure 3.2B). Quantification of ChR2-eYFP expression showed abundant expression of the virus in the SUB (Figure 3.2Bii,Biii,D), with 12.4 ± 1.3 out of 19.8 ± 1.6 DAPI cells expressing ChR2 (N = 5 animals; n = 5 sections). However, only very few cells in the CA1 region (1.2 ± 0.2 out of 33.4 ± 2.8 Satb2-positive cells) expressed ChR2 (Figure 3.2Bi,C). This low expression in the CA1 could possibly be explained by the sequencing data, which shows that cluster “285_CA1” also has minimal expression of *Satb2*, while also expressing *Slc17a6*. However, the number of infected CA1 neurons is not substantial enough to explain the dense projections seen in the mPFC. Therefore, we show that ChR2-eYFP is specifically expressed in the SUB and that mPFC-projecting neurons are originating in the SUB.

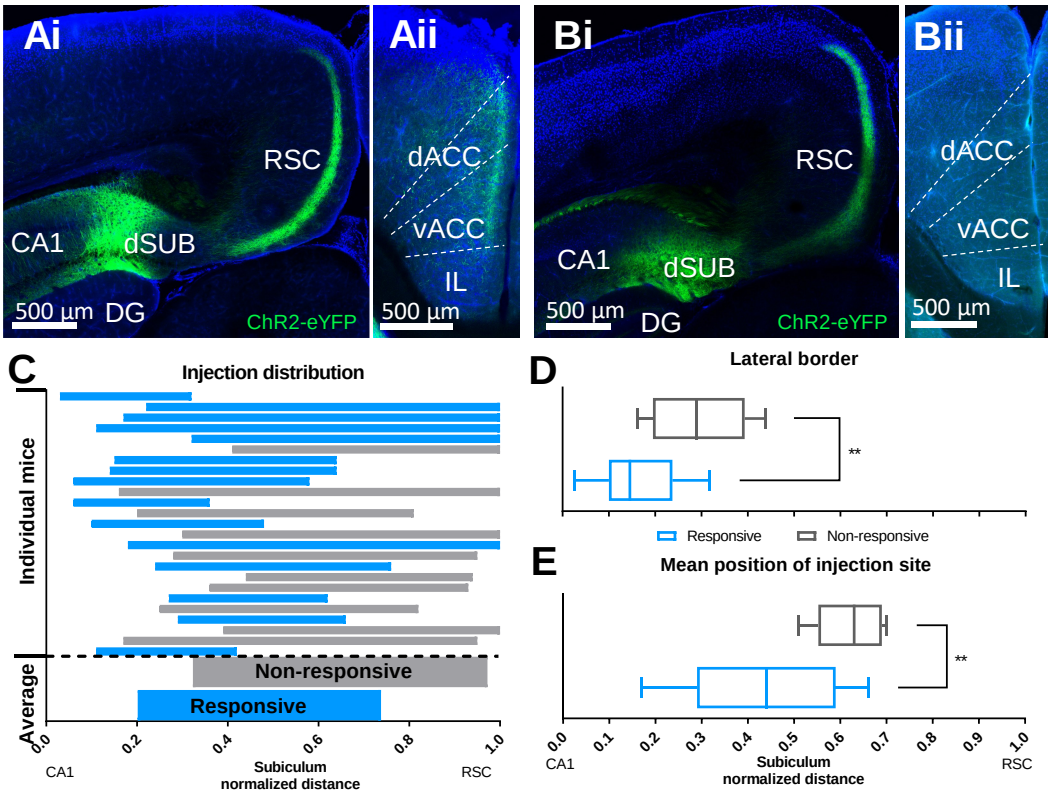

Figure 3.3: Prefrontal cortex projection originates from the proximal part of the dorsal subiculum.

Ai,Bi) Example of a (**Ai**) proximal and (**Bi)** distal injection site. Scale bar 500 µm. **Aii,Bii**) Prefrontal cortex images corresponding to either (**Aii**) proximal or (**Bii**) distal injection site. Images in Ai and Bi are from the same mice as Aii and Bii, respectively. **C**) Graph showing the distribution of injection sites. The upper part shows the distribution of injection sites for individual mice. Bars from mice that contained cells that were responsive to stimulation are blue, whereas bars from mice that showed no response to stimulation are grey. The bottom part of the graph displays the average injection site distribution for responsive and non-responsive mice. The width of the SUB is normalized to 1, with the border with the CA1 and the RSC being at 0 and 1, respectively. **D**) Mean normalized location of the lateral end of the injection site for responsive and non-responsive mice. **E**) Mean normalized position of the injection sites for responsive and non-responsive mice. Data in **D** and **E** are represented as boxplots with the box extending from the 25th to 75th percentiles, the middle line representing the median and the whiskers indicating the minimum and maximum values.

3.4 Prefrontal cortex projection originates from the proximal part of the dorsal subiculum

However, not all cells recorded in the mPFC showed a response to optogenetic stimulation. Only 39 out of 141 recorded neurons responded to stimulation with a response size of 1.83 ± 2.01 mV, which might suggest cell-type or region specificity. 46 of those 102 non-responsive cells came from mice that had no cells at all that responded to stimulation. The prefrontal cortex of these non-responsive mice also seems to contain fewer ChR2-positive fibres than mice that had at least one cell responding to stimulation. For mice that showed responses to stimulation, on average 56.8 ± 7.7 % of cells per mouse responded to stimulation. With the aim to explain these differences, we compared the precise injection sites of responsive (N = 15) and non-responsive (N = 10) mice. Indeed, some mice had an injection site that was centred in the proximal part of the dSUB (Figure 3.3Ai), whereas others showed an injection site more towards the distal part of the dSUB (Figure 3.3Bi). These different injection sites were also accompanied by differences in fibre presence in the prefrontal cortex: more proximal injection sites showed fibres in the prefrontal cortex (Figure 3.2Aii), whereas these were absent for injections in the distal part of the SUB (Figure 3.2Bii).

Quantifying the exact location and width of the injection site for each mouse also showed that mice that exhibited optogenetic responses had an injection site that was located closer to the CA1 than the RSC (Figure 3.3C). On average, the centre of the injection site was located significantly more towards the CA1 for responsive mice (0.43 ± 0.04) compared to the non-responsive mice (0.62 ± 0.02; t -test, p = 0.0016; Figure 3.3E). Additionally, the lateral edge of the injection site was located more towards the CA1 for responsive mice (t-test responsive vs nonresponsive, 0.16 ± 0.02 vs 0.30 ± 0.03, p = 0.0019; Figure 3.3D). This data are in line with previous research suggesting that prefrontal-projecting neurons are located in the proximal part of the dorsal SUB (Kim and Spruston, 2012; Bienkowski *et al.*, 2018; Cembrowski, Phillips, *et al.*, 2018; Cembrowski, Wang, *et al.*, 2018). Therefore, only the data from mice with an injection site in the proximal subiculum was analysed further. Of note, relative injection sites are overlapping between individual responsive and non-responsive mice (Figure 3.3C), presumably due to individual anatomical differences, and therefore an exact location of prefrontal-projecting neurons cannot be derived from our data.

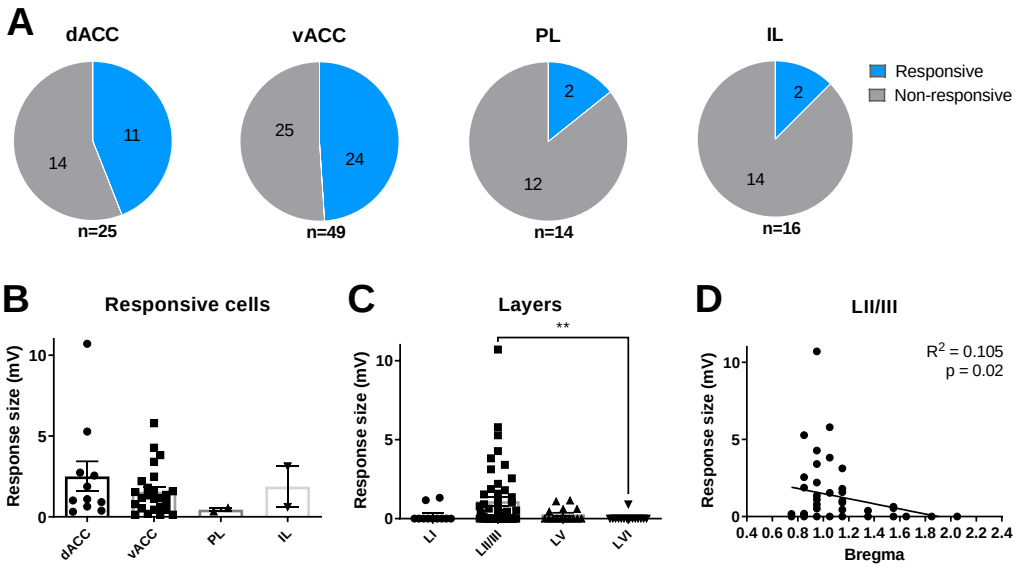

Figure 3.4: Proximal dorsal subiculum neurons project preferably to superficial layers of the anterior cingulate cortex in the posterior part of the prefrontal cortex

A) Proportion of recorded cells that were responsive or non-responsive to light stimulation in the dACC, vACC, PL and IL. B) Response size in responsive cells recorded from different regions of the mPFC. C) Response size of all neurons per layer. LI, n = 11; LII/III, n = 51; LV, n = 15; LVI, n = 15. D) Correlation between response size and distance from bregma for LII/III neurons (n = 51).

3.5 Proximal dorsal subiculum neurons project preferably to superficial layers of the anterior cingulate cortex in the posterior part of the prefrontal cortex

Neurons from proximal injected mice that showed a response to optogenetic stimulation (39 out of 103 recorded neurons) were found across all four regions of the mPFC. However, there was a significant difference in proportion of responsive cells between the regions (Chi-square test, p = 0.01; Figure 3.4A). The vACC had a higher proportion of responses than the IL and PL (Fisher's exact test, vACC vs IL, p = 0.017; vACC vs PL, p = 0.030), but there was no significant difference with the dACC (Fisher's exact test, p>0.999). This suggests that the subiculum has a preference of projecting to the ACC over other regions of the mPFC. However, the response sizes (EPSPs) did not differ between the subregions of the mPFC (Figure 3.4B). Nonetheless, it must be noted that there is a very small number of IL (n = 2) and PL (n = 2) responsive neurons, preventing any strong conclusions about response size for these regions.

The position of each postsynaptic neuron was also determined in relation to cortical layers. Comparing the response size for all recorded neurons per layer revealed a difference across layers (Kruskal-Wallis test, p = 0.007; Figure 3.4C). Posthoc comparison revealed a significant difference between LII/III and LVI (p = 0.005).

Since the vACC exhibited the most responses and this regions is only present in the posterior mPFC, whereas the IL and dACC are also present in the anterior PFC (Figure 3.1A), we wondered if the response size was stronger in the posterior vs anterior mPFC. To investigate this, we used a linear regression between response size and distance from bregma. Since LII/III harbours most of the responsive neurons, this analysis was only performed for LII/III neurons. The linear regression revealed a correlation, with higher responses being present in the posterior PFC (R^2 = 0.105, p = 0.02; Figure 3.4D), agreeing with the fact that the vACC is only present in the posterior mPFC. Together, this indicates that the SUB projects more strongly to superficial layers in both dorsal and posterior regions of the mPFC, and more specifically to the ACC.

3.6 Proximal dorsal subiculum drives activity of both inhibitory and excitatory neurons in the mPFC

Both inhibitory and excitatory neurons were recorded in the superficial layers of the mPFC (Figure 3.5A). Postsynaptic neurons were classified into different cell types based on firing pattern, hyperpolarisation and morphology. This resulted in four categories: pyramidal cells (n = 64), neurogliaform cells (n = 12), fast spiking interneurons (n = 7) and putative non-fast spiking interneurons (n = 8) (Figure 4B-F). Neurogliaform cells exhibited the well-described characteristic late-spiking phenotype (Kawaguchi, 1995; Schuman *et al.*, 2019), whereas all interneurons that did not fulfil the criteria of a fast-spiking or late-spiking cell were classified as non-fast spiking (putative) interneurons.

Interestingly, two types of LII/III pyramidal cells were identified using clustering analysis on pyramidal recordings from all mice, both responsive and non -responsive (Figure 3.6A). The pyramidal cells were clustered based on correlation of resting membrane potential (RMP), input resistance (Rinput) and firing frequency at different current injections (100 – 400 pA). Type II (n = 30) pyramidal cells often did not display a clear sag potential and had a higher firing frequency upon current injection than type I (n = 46) (Figure 3.5B,C). The electrophysiological characteristics were also significantly different between the two types of pyramidal

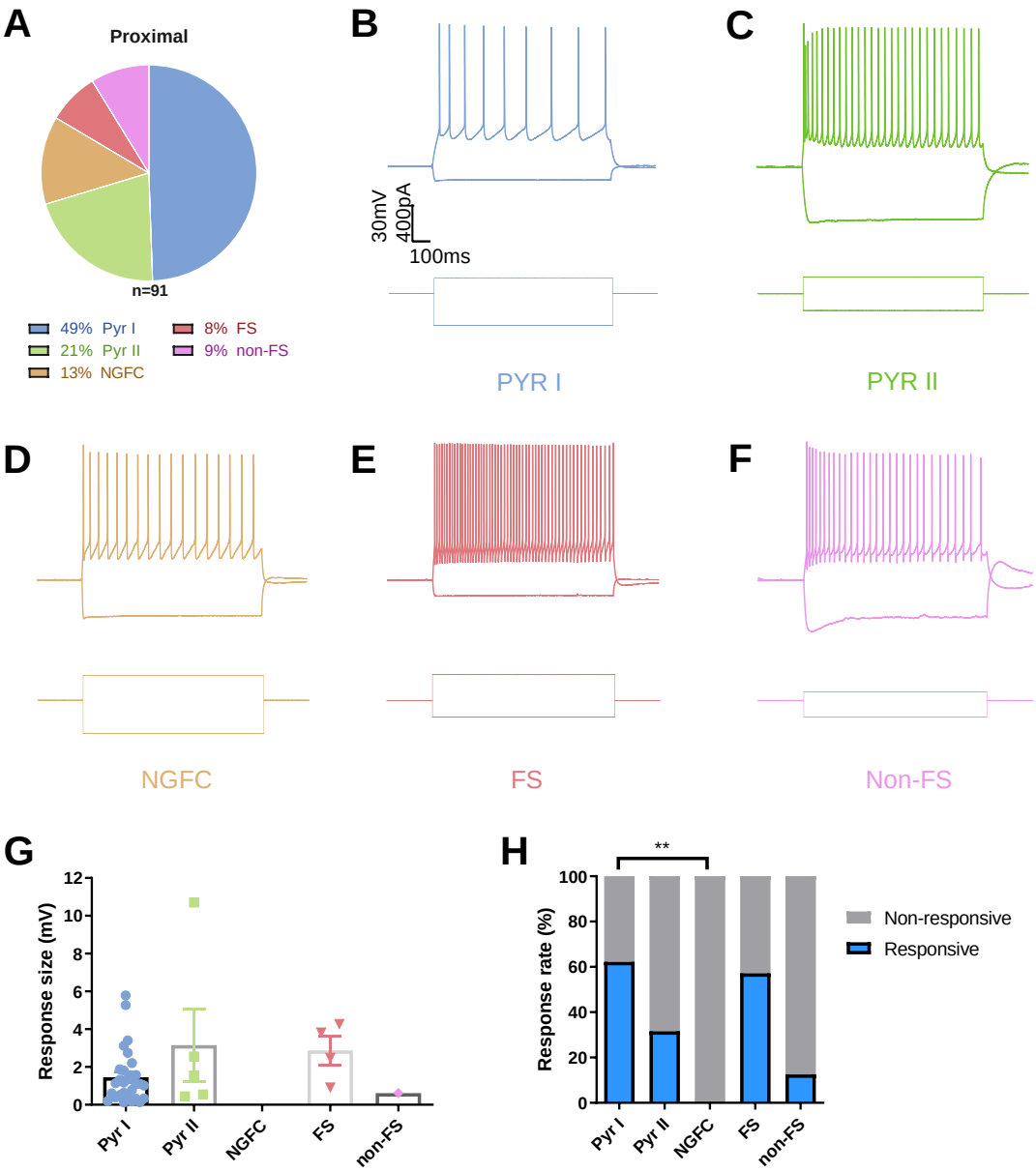

Figure 3.5: **Proximal dorsal subiculum drives activity of both inhibitory and excitatory neurons in the mPFC.**

A) Proportion of cell types recorded in layer II-III of proximally injected mice. B-F) Spiking pattern and hyperpolarization in response to current injection for (B) pyramidal type I cells, (C) pyramidal type II cells, (D) neurogliaform cells, (E) fast spiking interneurons and (F) non-fast spiking interneurons. G) Response size upon light stimulation per cell type. Data are represented as mean ± S.E.M. H) Proportion of cells responsive to optogenetic stimulation per cell type. Pyr I, n = 45; Pyr II, n = 19; NGFC, n = 12; FS, n = 7; non-FS, n = 8.

cells (Two-way ANOVA, P<0.001), but no clear differences in morphology are present (Figure 3.6B,C). Input resistance is higher in type II pyramidal cells, but the cell types did not differ in RMP (p = 0.7767; Figure 3). A difference in access resistance was not responsible for the difference in input resistance, since this was not significantly different between cell types (P>0.999; Figure 3.6H). Additionally, type II pyramidal neurons were firing at higher frequencies than type I cells at the same current injections, therefore exhibiting higher excitability than type I pyramidal cells (Two-way ANOVA, p<0.001; Figure 3.6D,E).

When comparing all five different cell types, the response size upon optogenetic stimulation did not differ between cells (Figure 3.5G). However, the proportion of responses was not uniform for the different cell types (Chi-square test, p<0.0001; Figure 3.5H), mainly driven by the result that none of the NGFC recorded neurons responded to stimulation (Pyr I vs NGFC, p = 0.001). Located superficially NGFCs only have short, stubby dendrites (Hestrin and Armstrong, 1996), which could possibly explain why none of the 12 recorded NGFCs showed responses to optogenetic stimulation as axonal fibres from the SUB and NGFC dendrites may simply not overlap. On the other hand, there were no differences between Pyr I, Pyr II, FS and non-FS neurons. Therefore, we concluded that the dSUB projects to both excitatory and inhibitory neurons in the mPFC.

3.7 Discussion

3.7.1 Summary of the results

We investigated and characterized neuronal connections of VGLUT2-positive neurons of the dSUB to specific subregions and different cell types in the mPFC. We found that proximal dSUB neurons mainly project to the superficial layers of both the dACC and vACC, but neuronal responses were also recorded in IL and PL neurons following optogenetic stimulation. Interestingly, both excitatory and inhibitory neurons were innervated, except for neurogliaform cells. Our detailed analysis of the viral injection sites revealed that dSUB neurons in the proximal part are more likely to project to the mPFC than neurons in the distal part of the dSUB (Figure 3.3). However, in a few mice we observed infected neurons in the proximal part, without finding responsive neurons or fluorescently labelled fibres in the mPFC. This suggests that connectivity patterns may be more variable, but the exact reason for that remains unclear.

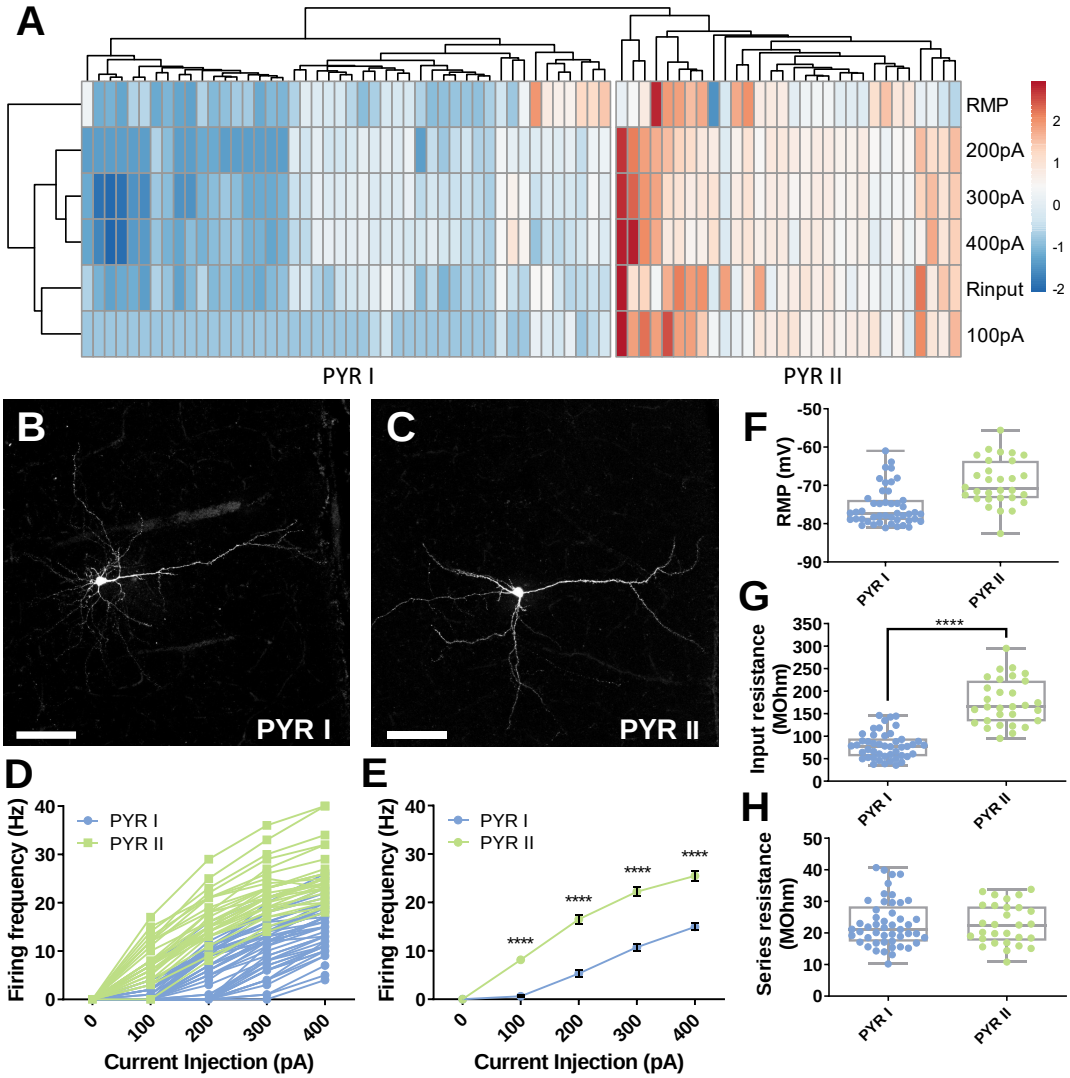

Figure 3.6: PYR II cells have higher excitability than PYR I cells.

A) Heatmap generated through ClustVis showing clustering of type I and type II pyramidal cells based on RMP, input resistance and firing frequency at current injections of 100-400 pA. Settings used are Euclidean distance as the similarity measure and hierarchical clustering with average linkage. B-C) Example Z-projection confocal images of a (B) type I and a (C) type II pyramidal cell. Scale bar 100 µm. D) Frequency-current curve for individual type I and type II pyramidal cells. Type I, n = 46; Type II, n = 30. E) Average frequency-current curve for type I and type II pyramidal cells. Data are presented as mean ± S.E.M. E-G) Passive characteristics of type I and type II pyramidal cells, comparing (F) resting membrane potential, (G) input resistance and (H) series resistance. Data are presented as boxplots with the box extending from the 25th to 75th percentiles, the middle line representing the median and the whiskers indicating the minimum and maximum values.

3.7.2 Circuitry dynamics

We found that the dSUB projects to both inhibitory and excitatory cells in the PFC. However, there are some slight differences in the proportion of each cell type that receives input from the dSUB. We found that both pyramidal type I and FS interneurons have the highest proportion of cells that receive input following light stimulation, followed by type II pyramidal cells and then non-FS interneurons. Since more type I cells than type II cells receive input from the dSUB, these cells might receive more excitatory stimulation upon dSUB activation. FS cells provide perisomatic inhibitory input to pyramidal cells and receive input from non-FS cells. Since type II pyramidal cells receive less input from the dSUB these cells might be more susceptible to inhibition from FS neurons by dSUB activation than type I pyramidal cells. Therefore, the stimulation of the PFC cells by the dSUB might result in stimulation in favour of the type I pyramidal cells.

If the type I and type II pyramidal cells also have distinct target cells and/or regions, this might also result in a shift in circuit activation. The role the dSUB-PFC projection might therefore be shifting activity to type I pyramidal cells and their projections. However, experiments have to be performed to confirm this hypothesis, for example by paired recordings to establish the effect of dSUB stimulation on the PFC network and tracing experiments to determine the position of type I and type II pyramidal cells within a network.

3.7.3 Hippocampal-cortical connectivity

In line with previous data for CA1 projections we found a gradient in subicular-cortical connectivity (Ferreira-Fernandes *et al.*, 2019). Ferreira-Fernandes and colleagues showed an increase in connectivity strength from the ACC to RSC implying that synaptic responses increase along the anterior-posterior axis of the brain. We found the same for dSUB to the mPFC, with an increase in synaptic strength more posterior in the brain (Figure 3.4D). However, we only tested the mPFC as data for the RSC already shows a robust connection (Kinnavane *et al.*, 2018; Yamawaki *et al.*, 2019).

The similarity in synaptic strength along the anterior-posterior axis for both CA1 and SUB projections seems surprising; however, one might speculate that the signal that arises from SUB neurons may function as an amplification signal. Hippocampal CA1 neurons project both to the ACC and the SUB (Ferreira-Fernandes *et al.*, 2019). SUB projection neurons similarly target ACC neurons to amplify the hippocampal signal that they received. Future opto-electrophysiological studies using two-colour optogenetic stimulation (Hooks, 2018) may therefore

investigate whether dorsal CA1 and dSUB neurons convergently target neurons located in the ACC and RSC.

3.7.4 mPFC-projecting dSUB neurons

A recent study showed that 5 out of 8 identified groups of subicular pyramidal neurons project to the PFC and express the following molecular markers: *S100b*, *Dlk1*, *Tpbg*, *Gpc3*, and *Cbln4*, respectively (Cembrowski, Wang, *et al.*, 2018). *S100b* is enriched in dSUB neurons whereas *Gpc3* is more specifically expressed in the ventral subiculum. *Dlk1*, *Tpbg* and *Cbln4* are all expressed along the entire dorsoventral axis. For these PFC-projecting markers, *Slc17a6* (encoding VGLUT2) expression is only seen in *S100b* neurons, indicating that this population of neurons are the PFC-projecting dSUB neurons studied in this chapter. A more detailed analysis of the publicly available scRNAseq data could elucidate if this projection contains other specifically expressed genes compared to other dSUB populations, for example receptors which might indicate specific modulation of the dSUB-PFC projection.

Based on the findings of Cembrowski and colleagues, *S100b* is a marker of PFC-projecting SUB neurons, but unfortunately, it has a major disadvantage for cell-specific virus expression. *S100b* expression is not specific to the subiculum but is also widely expressed in surrounding regions, which makes it more challenging to limit expression specifically to subicular neurons. A dual recombinase-mediated expression approach called INTRSECT combining VGLUT2- and S100b-specific expression might be a solution (Fenno *et al.*, 2014).

3.7.5 Two types of LII/III PFC pyramidal neurons

In this chapter, we present evidence for two types of LII/III pyramidal neurons in the mPFC. Powerful transcriptomics analyses have recently refined the grouping of subicular neurons (Cembrowski, Phillips, *et al.*, 2018; Cembrowski, Wang, *et al.*, 2018). Classical electrophysiological studies identified two major classes of pyramidal neurons (Staff *et al.*, 2000). However, in combination with retrograde tracing methods spatially-clustered neurons have indicated the existence of more than these two major classes (Kim and Spruston, 2012). Different subregions of the SUB, the proximal and distal part of either the dSUB, but also the vSUB, may comprise of up to over 20 different classes of neurons (Cembrowski, Phillips, *et al.*, 2018; Cembrowski, Wang, *et al.*, 2018; Ding *et al.*, 2020).

The clustering method that we have used in this study was hierarchical clustering with Euclidean distance and average linkage using ClustVis. We have used this clustering approach since it shows the hierarchical relation of individual

cells based on the measured parameters. This is also why we did not choose to use k-means clustering. For this clustering approach, a set number of groups is needed where the data is then divided into. Because we did not know how many groups our dataset consisted of we decided to use hierarchical clustering instead. Additionally, our dataset is small and therefore hierarchical clustering is also a good choice.

However, this method does not analyze if the clusters are indeed distinct. Other clustering methods or statistical analysis would have to be performed to show if these clusters are indeed distinct. Additionally, a combinatory approach of different techniques would have to show if the two types of pyramidal neurons are distinct in other perspectives than firing properties as well. For example, single cell RNA sequencing could elucidate if these two cell types also have different gene expression profiles, which would strengthen the findings in this chapter. However, differences in gene expression profile do not always reflect different cell types, since this classification can be even more refined using additional information like projection targets (Kim *et al.*, 2020; Peng *et al.*, 2021).

3.7.6 Limitations of the study

The main limitation of this study is the low number of recorded neurons for some cell-types. Since the IL and PL have a very low connectivity ratio, it is difficult to record from optogenetic stimulation responsive neurons within these regions. We only recorded from two responsive cells in both regions, which was only 14% (IL) and 12.5% (PL) of total recorded neurons in those regions. To increase this number to a more decent sample size (e.g. n = 10 per region), we would have to record many more cells from many more mice. In the trade-off between number of mice used and the value of information from these recordings, we decided to not increase the sample size there. Since the connectivity rate is already very low, this would not provide much more information about the dSUB-PFC connection.

However, when we performed a post-hoc power calculation, it revealed that our study is underpowered. The sample size would have to be increased to achieve a suitable power of 80%. Sample size calculations with power 80% and a statistical threshold (α) of 0.05 show that to be able to detect differences in response size between the different regions (ACCd, ACCv, IL and PL) the sample size would have to be increased to 67 cells per group. This would equal a total number of nearly 300 cells.

Ideally, we would have liked to look into cell-type specific input for each brain region, but unfortunately, the sample size was not big enough to achieve this. To

look at the connectivity of different cell types, we needed to group all brain regions together. However, a different experimental approach has to be taken to make it possible to look into interneuron connectivity for each brain region. In our experiments we used the VGLUT2-IRES-Cre mouse line to achieve brain region-specific ChR2 expression. This means that when recording from postsynaptic neurons the cell type recorded is largely left up to chance. This is also reflected in the distribution of cell types recorded (Figure 3.5A), which largely resembles the occurrence of each cell type in the brain. To specifically record from interneurons, or even specific types of interneurons, one would have to use a transgenic mouse line that labels these interneurons ,e.g. GAD2-Cre, PV-Cre or NPY-Cre crossed with a reporter line. Considering the time constrains of my PhD we have decided to opt out of this approach. Therefore, our study may pave the way for more refined analyses taking novel transgenic animal models in terms of their cell identity and their additional target regions into account. Combining these sophisticated methods will be key to unravel the details of the connectivity between the main hippocampal output region and the prefrontal cortex.

Chapter 4: The effect of maternal separation on structure and function of the subiculum

4.1 Introduction

Major depression is a prevalent mood disorder that presents itself with symptoms concerning mood and motivation, but it also affects cognitive functioning. However, cognitive deficits in major depressive disorder (MDD) and underlying mechanisms are understudied. It has been shown that the main cognitive functions that are affected are memory and spatial navigation (Ravnkilde *et al.*, 2002), reflected in poor performance in a virtual spatial navigation task for MDD patients (Gould *et al.*, 2007).

Additionally, research in animal models of depression have been performed to try and elucidate the underlying mechanisms. Reduced performance in several spatial and non-spatial memory tests have been observed, including the Morris water maze, novel object recognition, novel object location and working memory tests (Henningsen *et al.*, 2009; Yu *et al.*, 2011; Luo *et al.*, 2014; Rocha *et al.*, 2021; Olave *et al.*, 2022). Since the dorsal hippocampus plays a key role in spatial memory this implicates a role for this part of the hippocampus in at least the cognitive symptoms of depression.

As mentioned in Chapter 1, the hippocampus is proposed to have a dichotomy of function along the dorsoventral axis. In terms of pathology of depression, the ventral hippocampus has been implicated in the mood symptoms of depression, whereas the dorsal hippocampus could be responsible for the cognitive deficits. As the cognitive symptoms are often overlooked, the role of the dorsal hippocampus in depression has not been studied in detail. There are few studies focussing on the dorsal CA1. Chronic stress-induced increase in HCN channel expression has been shown specifically for dorsal but not ventral CA1, resulting in altered cellular properties and increased excitability in this region (Kim, Brager and Johnston, 2018). Additionally, downregulating these HCN channels in the dorsal CA1 before chronic stress prevented depressive-like behaviour as measured by the sucrose preference test (SPT) and open field test (OFT). This also indicates a potential role of the dorsal hippocampus not only in the cognitive deficits but also in mood symptoms of depression. Of note, memory performance was not tested in this study. Recently, expression of AMPA-receptor GluA1 has also been shown to be altered in susceptible mice, with a reduction in female but an increase in male mice, specifically for the dorsal but not ventral hippocampus

(Olave *et al.*, 2022).

Since the subiculum (SUB) and the CA1 are the main output structures of the hippocampus, a role of the SUB in depression could also be hypothesized. The role of the SUB in depression has been studied in humans, where it is shown that structure is altered in MDD patients (Cole *et al.*, 2010; Hao *et al.*, 2020; Schmaal *et al.*, 2020; Ho *et al.*, 2022). It should be stressed that even though the SUB and CA1 show similarities in terms of connectivity and functions, they also show marked differences in of structure and function. For example, transcriptomic profiling demonstrated different cell types between the SUB and CA1 (Yao *et al.*, 2021). Functionally, even though both regions are involved in spatial navigation, the SUB contains a cell type that is not present in the CA1, namely boundary vector cells (Lever *et al.*, 2009). This cell becomes active when the mouse approaches a boundary of the environment. Additionally, both regions contain place cells but differences between the two regions exist. Place cells in the SUB show a larger receptive field and fire consistently between different environments, compared to small receptive fields and environment-dependent place firing in the CA1 (Sharp, 1997). Therefore, a unique role for the dSUB in the pathology of depression might exist.

Whereas the SUB projects to various different brain regions, we were particularly interested in the projection to the retrosplenial cortex (RSC). The projection from the dorsal subiculum to the retrosplenial cortex is pivotal in the encoding and retrieval of a spatial memory like the novel object location test (de Landeta *et al.*, 2020; Opalka and Wang, 2020). Since object location memory has shown to be reduced in the maternal separation model of depression (Reincke and Hanganu-Opatz, 2017), and dSUB-RSC projection to be essential in the object location memory, this suggests that the dSUB-RSC projection might be affected. Additionally, object recognition memory, which is non-hippocampus dependent, has been shown to be intact when object location memory was affected, suggesting that it is specifically the dSUB to RSC projection that is affected and not the RSC in general (Olave *et al.*, 2022). However, it has to be noted that CA1-projecting SUB neurons have also been implicated in object location memory (Sun *et al.*, 2019), in addition to other subcortical structures like the thalamus (Jeffery *et al.*, 2019).

In addition to cognitive dysfunction and mood symptoms, it has also been suggested that early-life stress alters the sensitivity to acute stress (Qin *et al.*, 2019). However, not much is known about the acute stress response in the dorsal hippocampus and if this is affected by early-life stress. Additionally, hypoactivity of

the medial prefrontal cortex (mPFC) is associated with depression. How mPFC activity is modulated by acute stress and if this is affected by early-life stress has not been shown before.

Therefore, we wanted to investigate the structural and functional changes of the dorsal SUB in the maternal separation model of depression. First, we assessed behavioural impact of our model using several tests for depression-associated behaviour and memory function. Using these tests, we identified control, susceptible and resilient mice. Using patch-clamp recordings, we compared the electrophysiological properties of dorsal and ventral subicular neurons for these three groups of mice. We also investigated the dSUB-RSC connection after maternal separation using *in vitro* optogenetics. Additionally, we investigated acute stress-induced neuronal activation of the dSUB and the mPFC using cFOS expression.

4.2 Maternal separation induces in a mild behavioural phenotype

Maternal separation (MS) in combination with early weaning was used as a model of depression and early life stress. Half of the pups from each litter were removed from the dam for 6 hours a day between P6 and P16. Separated pups were weaned at P17 and control pups were weaned at the normal age of P21. During separation, pups were placed in a separated cage in a different room from the dam. This cage was divided in different compartments and pups were placed in individual compartments to prevent them from touching each other. Behavioural tests were performed in adult mice from P45 onwards.

Different behavioural paradigms were chosen to test for different aspects of depression-like behaviour: sucrose preference test for anhedonia, open field test for anxiety and splash test for grooming behaviour. During the splash test mice were sprayed with a sucrose solution to induce grooming behaviour. Grooming behaviour was analysed as the total time spent grooming and latency to groom. The total grooming duration seems to be slightly reduced in maternal separated (MS) mice but this was not significant (Ctrl: 82.45 s ± 9.22 s vs MS: 63.45 s ± 8.07 s, t-test, $p = 0.1305$). This effect seems to be mainly present in female MS mice (female Ctrl: 89.82 s ± 11.39 s vs MS: 58.82 s ± 15.36 s, Sidak post hoc test following two-way ANOVA, $p = 0.1359$) (Figure 4.1A). The latency to groom was not different between separated and control mice (t-test, $p = 0.7493$, Figure 4.1B).

Another type of behaviour that was observed during the splash test was rearing, during which mice stand on their hind legs for a short period of time. This behaviour could indicate increased exploration of the environment. Rearing was

increased to 33.44 s ± 3.28 s in MS mice compared to 27.35 s ± 5.05 s in control littermates and this seems to be mainly present in the female mice (female Ctrl 22.82 s ± 5.96 s vs MS 34.34 s ± 4.22 s, Figure 4.1C), however this was not significant (Ctrl vs MS; t-test, p = 0.3092; female Ctrl vs MS; Sidak, p = 0.2787). To summarize, we found no significant differences between MS and control mice for grooming behaviour.

We performed this test with a closed home cage to prevent the mice from

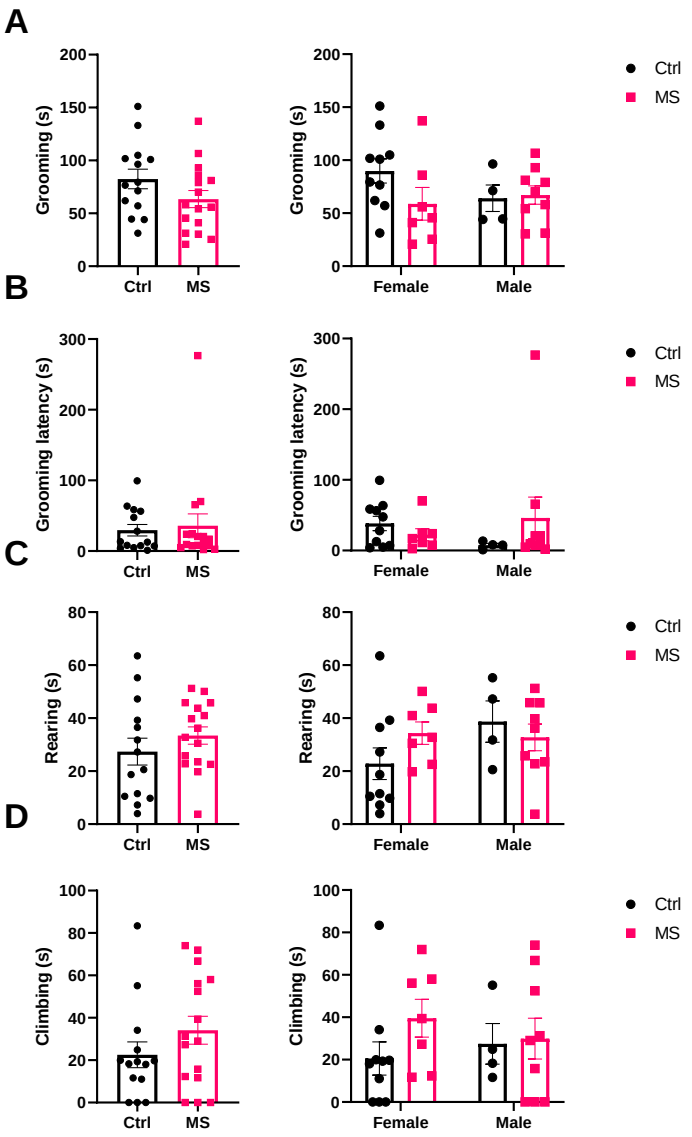

Figure 4.1: Grooming behaviour is not affected by maternal separation
A) Grooming duration, left: control (Ctrl, N = 14) against maternal separated mice (MS, N = 16), right: split according to sex (female N = 17, male N = 13); B) latency to groom and C) duration of rearing for control and separated mice (left) and the groups split into males and females (right). Data presented as mean ± S.E.M.

jumping out of the cage. However, mice were also able to climb on the cage lid. We quantified this behaviour, but there were no significant differences between control and separated mice (t-test, p = 0.2106, Figure 4.1D). Climbing duration also did not differ between males and females (two-way ANOVA, p = 0.8921, Figure 4.1D). MS mice show a slight reduction in time spent in the centre during the open field test compared to control mice, which is a measure of anxiety (Figure 4.2A). However, this was not significantly different from control mice (t-test, p = 0.3183). Interestingly, it seems that the MS mice can be split in two groups based on the time they spend in the centre of the box. There seems to be one group of three mice with more time in the centre, whereas the rest of the mice spends less time in the centre than the average of the controls. This might indicate resilience or susceptibility to the early life stress to result in anxiety-like behaviour. This effect

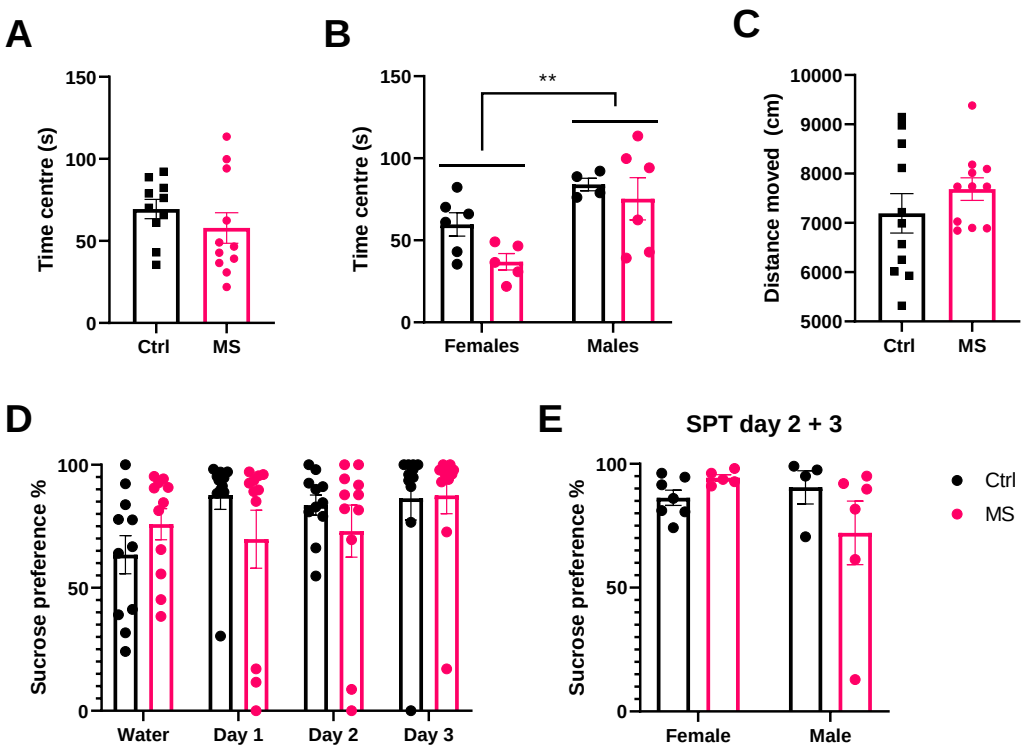

Figure 4.2: Maternal separation did not affect open field test and sucrose preference test

A-C) Open field test. A-B) Time spent in centre of the arena for A) control and separated mice and B) both groups split into males and females. D-E) Sucrose preference test D) Sucrose preference over the individual days of the test. During "water" mice were presented with two bottles containing water and the preference was calculated as a side preference. Day 1, 2 and 3 consisted of presenting one bottle with 1% sucrose and one bottle with water in alternating positions (left-right) over the individual days. Data presented as mean ± S.E.M.

seems to be more pronounced in female separated mice although not significant (Sidak, p = 0.1631), and overall males spend more time in the centre of the field (Figure 4.2B; Females 48.33 s ± 11.36 s vs males 79.67 s ± 4.35 s, two-way ANOVA, p = 0.0031), indicating that they are less anxious. This might also explain previous findings of increased susceptibility to stress for females (Dalla *et al.*, 2005; Guilloux *et al.*, 2011), although we do not find any significant differences between control and MS mice in terms of their sex. There was also no difference in distance moved during the open field test (Figure 4.2C; t-test, p = 0.3006).

Anhedonia, a reduced motivation or ability to experience pleasure, , is also a symptom of depression. We used the sucrose preference test to test for this depressive-like behaviour (Figure 4.2D,E). Mice were first presented with two bottles of water to test for side preferences. Both MS and control mice have a preference of 75.85 % ± 6.33 % and 63.47 % ± 7.77 % for one of the bottles containing water, indicating slight preference for one side of the cage (Figure 4.2D), but the difference between groups was not significant (two-way ANOVA, p = 0.7432). After this, one bottle of 1% sucrose solution and one bottle of water were presented to the mice for three consecutive days (Figure 4.2D). After every 24 hours the position of the bottles would be switched to correct for side preferences. It seems that the separated mice have the most reduced sucrose preference on day 1, although this was not significant (Sidak, p = 0.4124). Since this is the first day that the mice are presented with the sucrose solution a reduced consumption could also indicate neophobia. Neophobia means that mice are more anxious towards new foods and this is also the basis for the novelty supressed feeding test, which shows an increased latency in new food consumption in more anxious mice (Stedenfeld *et al.*, 2011). Therefore, the first day that the mice were presented with the sucrose solution was introduced as a habituation day. The average of day 2 and 3 with 1% sucrose were taken to get to the final sucrose preference percentage and is the actual test measure (Figure 4.2E). The reduction in sucrose preference seems to be highest in male separated mice (Ctrl 90.5 % ± 6.72 % vs MS 72.13 % ± 12.84 %), although this effect was not significant and may be mainly driven by one mouse with very low sucrose preference (Sidak, p = 0.2501). In summary, maternal separation might affect sucrose preference in male mice, but the effect is not significant.

4.3 Maternal separation results in susceptible and resilient mice

Overall, there only seem to be slight effects of maternal separation on individual tests and behaviours, but no significant difference between separated and control mice was observed. However, we noted that groups were heterogeneous, occasionally it even seems that there are subgroups in each main group. Therefore, we used z-score normalization to compare the results of individual tests in one score for each mouse (Figure 4.3A). Z-score normalization calculates how many standard deviations one mouse is deviated from the average of the control group for one particular test. In other words, it calculates how different the performance of individual mice is compared to the average control performance for one test. This can be calculated for each mouse for each test and is then averaged

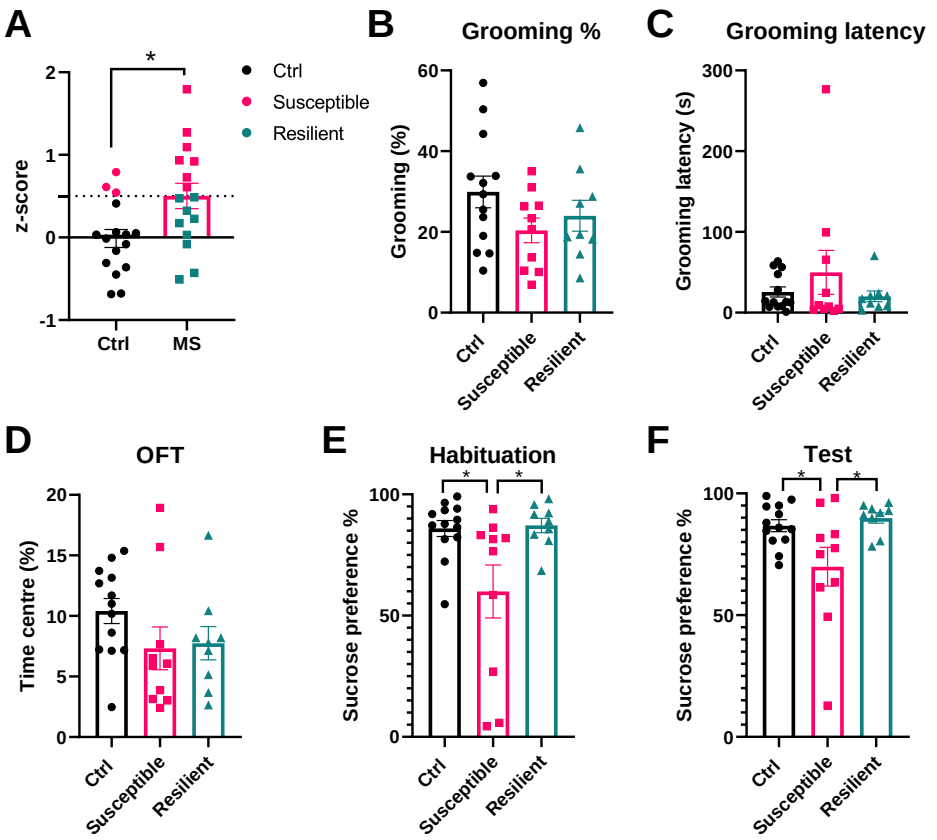

Figure 4.3: Maternal separation results in susceptible and resilient mice

A) Z-score normalization to compare performance in the splash test, open field test and sucrose preference test for individual mice. B) Time spent grooming during the splash test. C) Latency to groom during the splash test. C) Time spent in the centre during the open field test. D) Sucrose preference during the habituation day when the sucrose solution was presented to the mice for the first time. F) Sucrose preference as an average of day 2 and 3 to correct for side preference. Data presented as mean ± S.E.M.

to get one score for each mouse for all tests combined. We selected commonly used tests to identify depressive-like behaviour that have been shown to be affected by models of depression to calculate the z-score. The measures that we used were sucrose preference during habituation and test days, time spent grooming during splash test and time spent in the centre during the open field test. Therefore, this z-score could be seen as an emotionality score with a higher score representing worse performance on average for the tests and this indicates depressive-like behaviour (Guilloux *et al.*, 2011).

When comparing the z-score between control and separated mice it shows that the separated mice have a higher z-score, indicating altered behaviour compared to the control group (t-test, p = 0.0106) (Figure 4.3A). We used the mean of the MS group, in this case z = 0.5, to split the separated mice into two groups: all mice below the average were classified as resilient mice and all mice

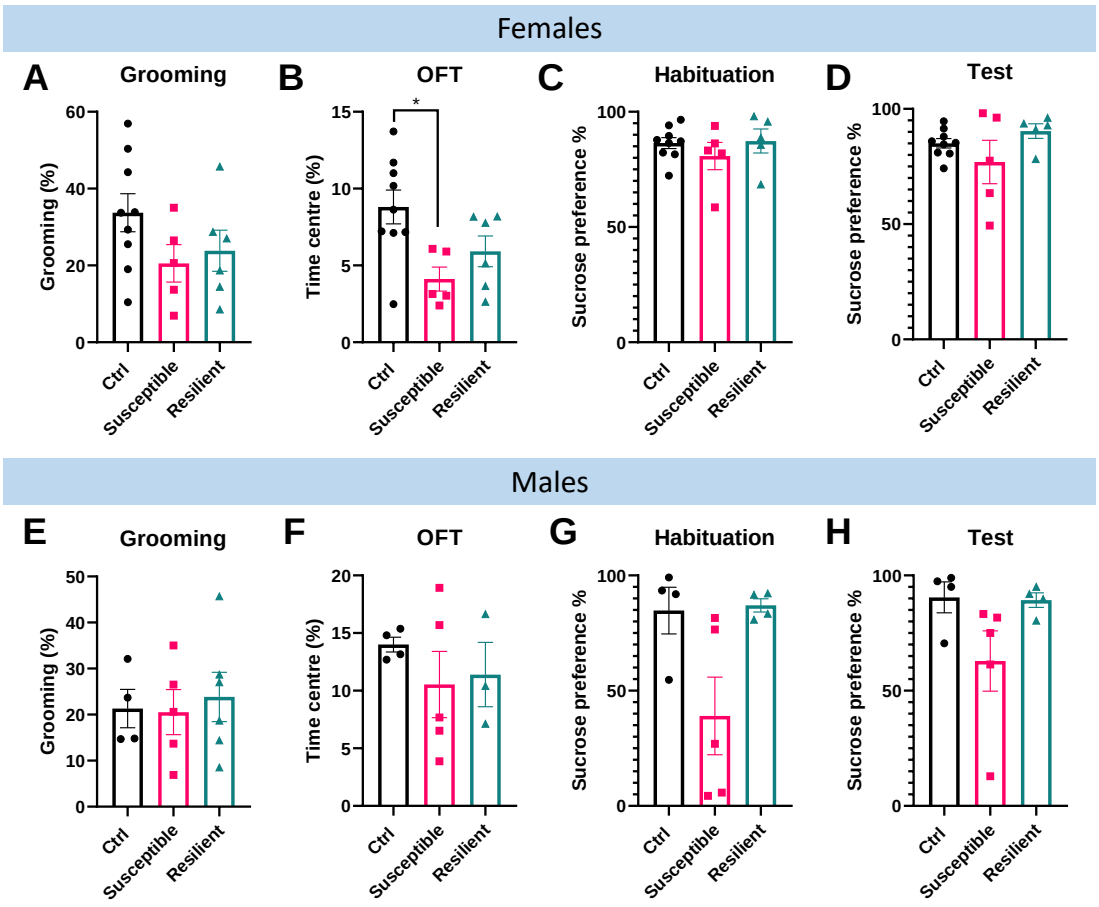

Figure 4.4: Susceptible and resilient mice split into females and males
Performance of control, susceptible and resilient mice split into females (A-D) and males (E-H) for the splash test (A,E), OFT (B,F), SPT habituation day (C,G) and SPT test days (D,H). Data presented as mean ± S.E.M.

above the average were susceptible to the maternal separation. The three mice from the control group that are also above this threshold were also classified as susceptible, since these also show a high z-score.

We next looked into the individual behavioural tests for these three groups to see if we would now identify significant differences in behaviour. While time spent grooming during the splash test and time spent in centre during the open field test are on average lowest, and latency to groom during the splash test are on average highest for the susceptible mice, there were no significant differences between control, susceptible and resilient mice for these behavioural measures (Figure 4.3B -D). However, sucrose preference seems to be only affected in susceptible mice (Figure 4.3E,F), meaning that this test mainly drives the difference in z-score for the resilient and susceptible mice. Sucrose preference is significantly reduced in susceptible mice compared to control (Tukey post hoc test following one-way ANOVA, $p = 0.0181$) and resilient mice (Tukey, $p = 0.0239$) during habituation. This might not be an accurate measure of anhedonia and could also indicate neophobia. However, the sucrose preference on the test days is also lower for susceptible compared to resilient mice (Tukey, $p = 0.0223$) and control mice (Tukey, $p = 0.0401$).

Unfortunately, splitting the individual groups into males and females results in low N-numbers with high variance which prevents a powerful comparison within groups for some tests and sexes. Splitting the groups into gender results in 4 males and 9 females for the control group, 5 males and 5 females for the susceptible group, and 4 males and 5 females for the resilient group. This analysis resulted in no significant differences between control, susceptible and resilient mice for both female and male mice, except for the OFT. Time spent in the centre was significantly reduced in susceptible mice for female mice only (Tukey, $p = 0.019$, Figure 4.4B). Even though the reduction in sucrose preference for susceptible mice was highly significant when males and females were combined (Figure 4.4E,F), splitting by sex abolished this effect due to increased variance and reduced sample size (Figure 4.4C,D,G,H).

4.4 Spatial memory function is affected in susceptible mice

Since memory function has been shown to be impaired in animal models of depression we wanted to test this for the control, susceptible and resilient groups of our animal model (Henningsen *et al.*, 2009; Yu *et al.*, 2011; Luo *et al.*, 2014; Rocha *et al.*, 2021; Olave *et al.*, 2022). To test memory function we used the novel object location (NOL) and novel object recognition (NOR) tests, since these two

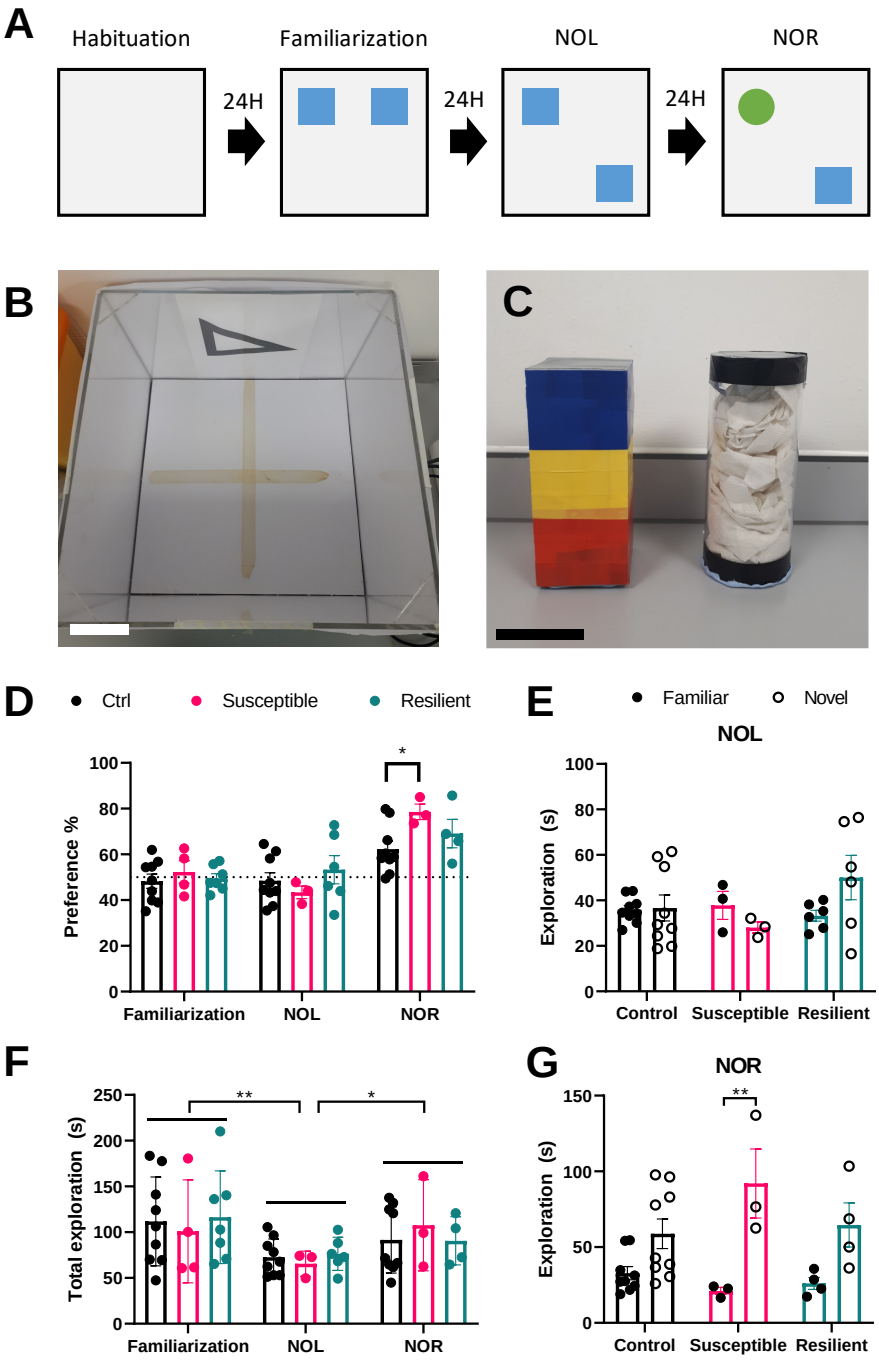

Figure 4.5: Object recognition memory might be affected in susceptible mice

A) Timeline of the novel object location and novel object recognition test. B) The arena with one of the wall labelled with a geometric shape. Scale bar 10 cm. C) Object used for the NOL and NOR. Scale bar 5 cm. D) Preference for the left side (familiarization), moved object (NOL) or novel object (NOR). E) Exploration in seconds for the familiar and moved object (novel) during NOL. F) Total exploration of both objects in seconds. G) Exploration in seconds for the familiar and novel object during NOR. Data presented as mean ± S.E.M.

types of memory have been shown to be differently affected by models of depression (Reincke and Hanganu-Opatz, 2017). These tests were performed on consecutive days. Habituation was performed on day 1 by allowing mice to freely move among the environment for 15 minutes (Figure 4.5A). Then, 24 hours later, two identical objects were placed in two aligned corners of the arena and the mouse was placed back and was allowed to explore the objects for 10 minutes (Figure 4.4A). This is the familiarization phase of the NOL. For the NOL test, 24 hours later one of the objects was moved to a corner diagonal from the familiar object (Figure 4.5A). The preference for the moved object was then calculated as a measure of object place memory. This object placement would then also serve as the familiar phase of the NOR. The next day during the NOR, the object that was not moved during the NOL was changed for another object (Figure 4.5A). The preference for the novel object as a percentage of the total exploration time was calculated as a measure of object recognition memory. The movement and replacement of the object was counterbalanced between sides and mice. The objects that were used are a transparent cylinder filled with paper and a rectangular tower wrapped in three colours of tape (Figure 4.5C). Climbing on the objects did not qualify as exploration and if a mouse presented that behaviour it would be excluded for that test and following tests to prevent bias towards one of the objects or locations. This resulted in the exclusion of 4 (1 Ctrl, 3 MS) out of 22 mice: two mice during familiarization and another two mice during the NOL.

The preference during familiarization shows the preference for one side of the environment for control, susceptible and resilient mice (Figure 4.5D). There are no differences between groups and the preference for one side is around 50% for all groups, meaning that the mice are not able to distinguish between the identical objects and that they do not present side preferences in the arena. During the NOL, the susceptible mice show a slight reduced preference for the moved object compared to control and resilient mice although this was not significant (two-way ANOVA, Ctrl vs Susceptible: $p = 0.5171$. Resilient vs Susceptible: $p = 0.3665$, Figure 4.5D). However, all groups spent around 50% of their total object exploration time in proximity of the moved object (Ctrl: 48.5 % ± 3.5 %, Sus: 43.4% ± 2.8 %, Res: 53.3 % ± 6.2 %), meaning that they spend equal time exploring both objects and that they do not recognise the moved object. There were also no differences in exploration time of the object in the novel and familiar location across all groups (two-way ANOVA, $p = 0.6147$, Figure 4.5E). The total exploration time of the objects was also reduced to 71.45 s ± 5.44 s during the NOL compared to the NOR (96.59 ± 9.55 s, two-way ANOVA, $p = 0.0237$) and familiarization (109.62 ±

7.94 s, two-way ANOVA, p = 0.0046), meaning that the mice might have lost interest in the objects due to both objects being perceived as familiar (Figure 4.5F).

In contrast, the total exploration time of the objects during familiarization and NOR were not different (two-way ANOVA, p = 0.3748), meaning that mice regained interest in the objects during the NOR to the same level as during the familiarization phase. Susceptible mice had a higher preference for the novel object (78.57 ± 3.41 %) in the NOR compared to the control mice (62.263 ± 3.56 %, Tukey, p = 0.0321), but do not differ significantly from the resilient mice (69.09 ± 6.19 %, Tukey, p = 0.4403, Figure 4.5D). This is also reflected in the exploration times of the familiar and novel object (Figure 4.5G). The susceptible mice spent more time exploring the novel object (Sidak, p = 0.0029), whereas there was only a trend towards significance for the control (Sidak, p = 0.0746) and resilient (Sidak, p = 0.0799) mice. All groups are showing a preference above 50% (Ctrl: 62.3 % ± 3.6 %, Sus: 78.6 % ± 3.4 %, Res: 69.1 % ± 6.2 %), meaning that they recognize the familiar object and explore the novel object.

In summary, our data shows that the susceptible mice may have enhanced object recognition memory but we are not able to draw any conclusions about the place memory. Place memory might not have been accurately assessed in our study since the control mice were not able to recognize the moved object. This might be because of insufficient spatial marking of the environment or other steps in the protocol that might have prevented accurate memory consolidation or retrieval. This topic is further explored in the discussion.

4.5 Electrophysiological characteristics of the dorsal and ventral subiculum are not affected by maternal separation

Since maternal separation resulted in a mild behavioural phenotype in susceptible mice, we next investigated if this was accompanied by changes in the SUB. Whereas the ventral SUB has been studied in relation to depression and stress, more recent studies have indicated that the dorsal SUB might be involved in the pathology of depression, especially concerning cognitive symptoms (Cole *et al.*, 2010; Li *et al.*, 2017). Therefore, we performed *in vitro* electrophysiological recordings in slices that were prepared 4-20 days after behavioural assessment and compared several active and passive properties of dorsal and ventral subicular neurons of control, susceptible and resilient mice.

Slices were split into dorsal and ventral hippocampus based on the ratio between the length and width of the hippocampus. A threshold ratio of 1.09 was

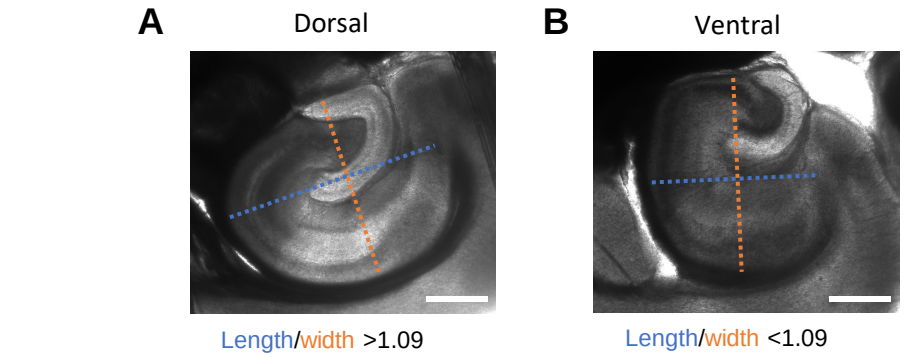

Dorsal

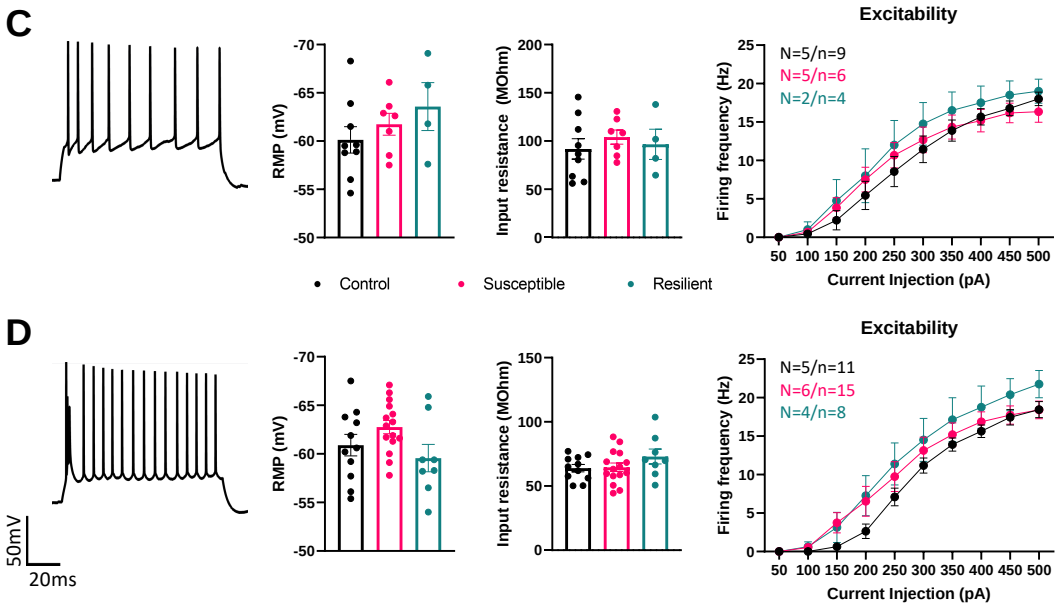

Ventral

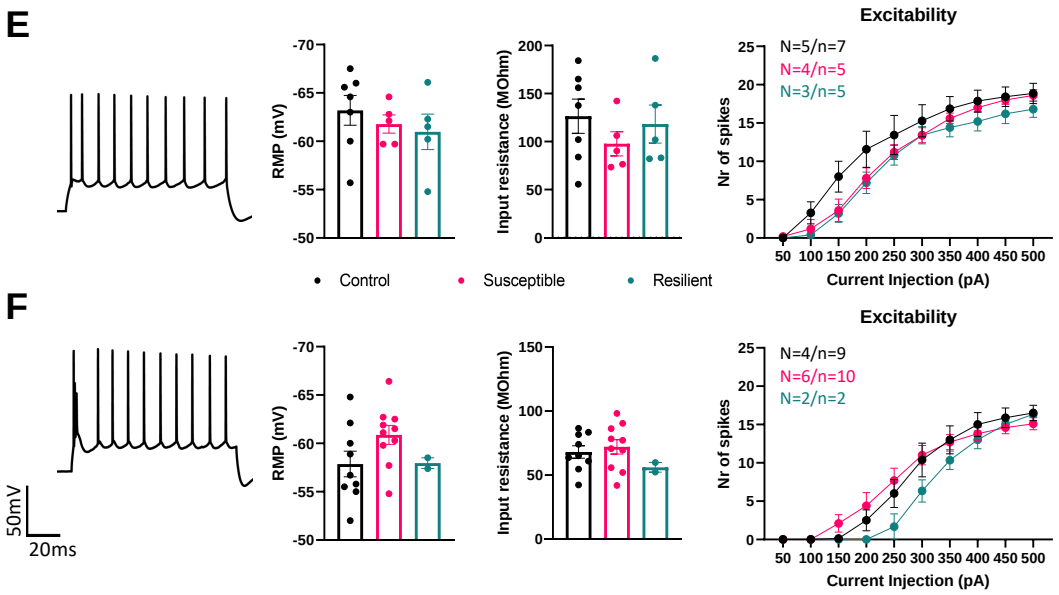

Figure 4.6: (see previous page) Electrophysiological characteristics of excitatory neurons in the dorsal and ventral subiculum

A,B) Images of dorsal and ventral hippocampal slices. The location was along the dorsal-ventral axis was determined by the length:width ratio of the hippocampus. Ratio >1.09 are dorsal slices and ratio <1.09 are ventral slices.C-F) From left to right: firing pattern, resting membrane potential, input resistance and excitability of regular and burst firing cells in the dorsal and ventral subiculum. C) Regular firing cells and D) burst firing cells in the dorsal subiculum. E) Regular firing cells and F) burst firing cells in the ventral subiculum. Scale bar is 1 mm. N/n = number of cells (n) recorded in number of mice (N) for each group and region. Data presented as mean ± S.E.M.

used since this was the middle point of the total range of ratios from selected slices (0.89 – 1.30) and this was found to reliably distinguish between dorsal and ventral hippocampal slices. The dorsal hippocampus has a more elongated shape (length-width ratio > 1.09) and the dentate gyrus has a sharper angle in these slices (Figure 4.6A). In contrast, the ventral hippocampus is more rounded (length-width ratio < 1.09) and the dentate gyrus also has a more rounded shape in the ventral hippocampus compared to the dorsal hippocampus (Figure 4.6B). Excitatory neurons of both the dorsal and ventral subiculum can be electrophysiologically divided into two different groups: regular firing and burst firing neurons (Cembrowski, Phillips, *et al.*, 2018; Simonnet and Brecht, 2019). Burst firing cells show a typical burst for the first action potentials (Figure4.6C,E), whereas this is absent for the regular firing cells (Figure 4.6E,F). For dorsal subicular regular firing cells, there were no significant differences in resting membrane potential (one-way ANOVA, $p = 0.3506$) and input resistance (one-way ANOVA, $p = 0.6916$) following maternal separation (Figure 4.6C). However, it has to be noted that n-numbers are relatively low with high variance for this cell type (Ctrl: 9 cells from 5 mice; Susceptible: 6 cells from 5 mice; Resilient: 4 cells from 2 mice). Mice were grouped into susceptible and resilient mice after the recordings were performed, meaning that cells were recorded blind for grouping. This also explains the imbalance of cells and mice between groups. There is a trend towards significance for the difference in RMP between the resilient and susceptible mice (one-way ANOVA, $p = 0.09$) for the bursting cells in the dorsal subiculum, but there are no differences in input resistance (one-way ANOVA, $p = 0.2592$, Figure 4.6B). In terms of firing frequency per current injection at a fixed membrane potential of -70 mV, there is no effect of group for dorsal regular firing cells (two-way ANOVA, $p = 0.6144$) and dorsal burst firing cells (two-way ANOVA, $p = 0.3440$), meaning that maternal

separation does not affect the excitability of the dorsal subiculum (Figure 4.6C,D).

For the ventral subiculum, there were also no significant differences between groups for RMP and input resistance for both regular (two-way ANOVA, RMP: $p = 0.5755$, input resistance: $p = 0.5091$) and burst firing cells (two-way ANOVA, RMP: $p = 0.1669$, input resistance: $p = 0.4434$, Figure4.6E,F). The excitability measured as f-I-curves was also not affected (two-way ANOVA, regular: $p = 0.3266$, burst: $p = 0.5561$). This means that the dorsal subiculum, but not the ventral subiculum, might be affected in susceptible mice, but only a trend for a potential difference in RMP was found. Please note that the n-number for ventral cells in some groups are low, also prohibiting accurate analysis for the ventral subiculum. N-numbers would have to be increased to make reliable conclusions.

We also looked into spontaneous activity of dorsal and ventral subiculum neurons and analysed the amplitude and number of spontaneous EPSCs and IPSCs. Cells were recorded in voltage clamp at -50 mV to allow simultaneous detection of EPSCs and IPSCs in the same recordings (Figure 4.7A,D). These recordings were performed in the same cells as recorded in Figure 4.6. If there were no IPSCs detected for a cell, this cell was excluded from the amplitude analysis, meaning that the amplitude graphs only contain cells for which at least one IPSC or EPSC was recorded.

For the dorsal regular firing cells, there are no differences in amplitude for both EPSCs and IPSCs for control, susceptible and resilient mice (two-way ANOVA, EPSC: $p = 0.3462$ IPSC: $p = 0.4533$, Figure 4.7B,C). However, whereas the frequency of IPSCs was not different among groups, the frequency of EPSCs was affected by maternal separation (one-way ANOVA, $p = 0.01$, Figure 4.7B). The frequency of EPSCs was significantly increased to 0.54 ± 0.30 Hz for resilient mice compared to control (0.039 ± 0.008 Hz) and susceptible mice (0.055 ± 0.012, Tukey, ctrl vs resilient: $p = 0.0120$, susceptible vs resilient, $p = 0.0194$). Regarding bursting cells in the dorsal SUB, there were no differences between groups in neither the amplitude nor the frequency for either EPSCs or IPSCs (Figure 4.7E,F).

In the ventral SUB, regular firing cells showed an increase of IPSC frequency (Susceptible 0.17 ± 0.13 Hz vs Ctrl 0.07 ± 0.04 Hz) and EPSC frequency (Susceptible 0.29 ± 0.11 Hz vs 0.1505 ± 0.05 Hz) in susceptible mice, but these effects were not significant (one-way ANOVA, IPSC: $p = 0.4366$, EPSC: $p = 0.3671$, Figure 4.8B,C). There were also no changes in spontaneous activity amplitude (one-way ANOVA, IPSC: $p = 0.4275$, EPSC: $p = 0.9751$, Figure 4.8B,C). Additionally, there were also no significant differences in excitatory and inhibitory current amplitude and frequency for burst-firing cells (Figure 4.8E,F).

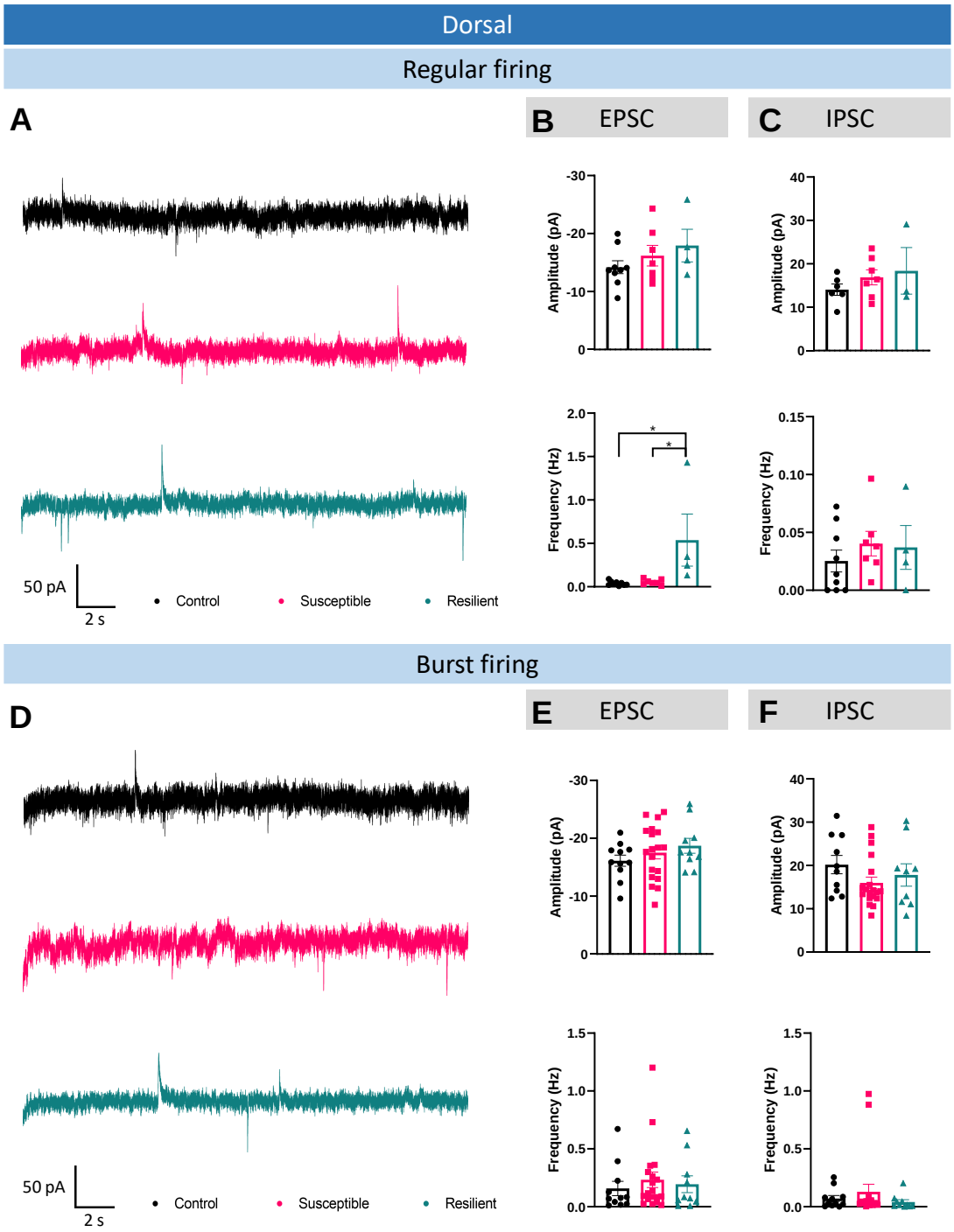

Figure 4.7: Spontaneous activity in the dorsal subiculum was not affected by maternal separation

A-C) Regular firing neurons. A) Example traces of spontaneous activity recorded for control (black), susceptible (pink) and resilient (green) mice. Both EPSCs and IPSCs were analysed from the same traces. Cells were recorded from 5 control, 5 susceptible and 2 resilient mice. B) EPSC amplitude (top) and frequency (bottom). C) IPSC amplitude (top) and frequency (bottom). D-F) Same as A-C but then for burst firing cells. Cells were recorded from 5 control, 6 susceptible and 4 resilient mice. Data presented as mean ± S.E.M.

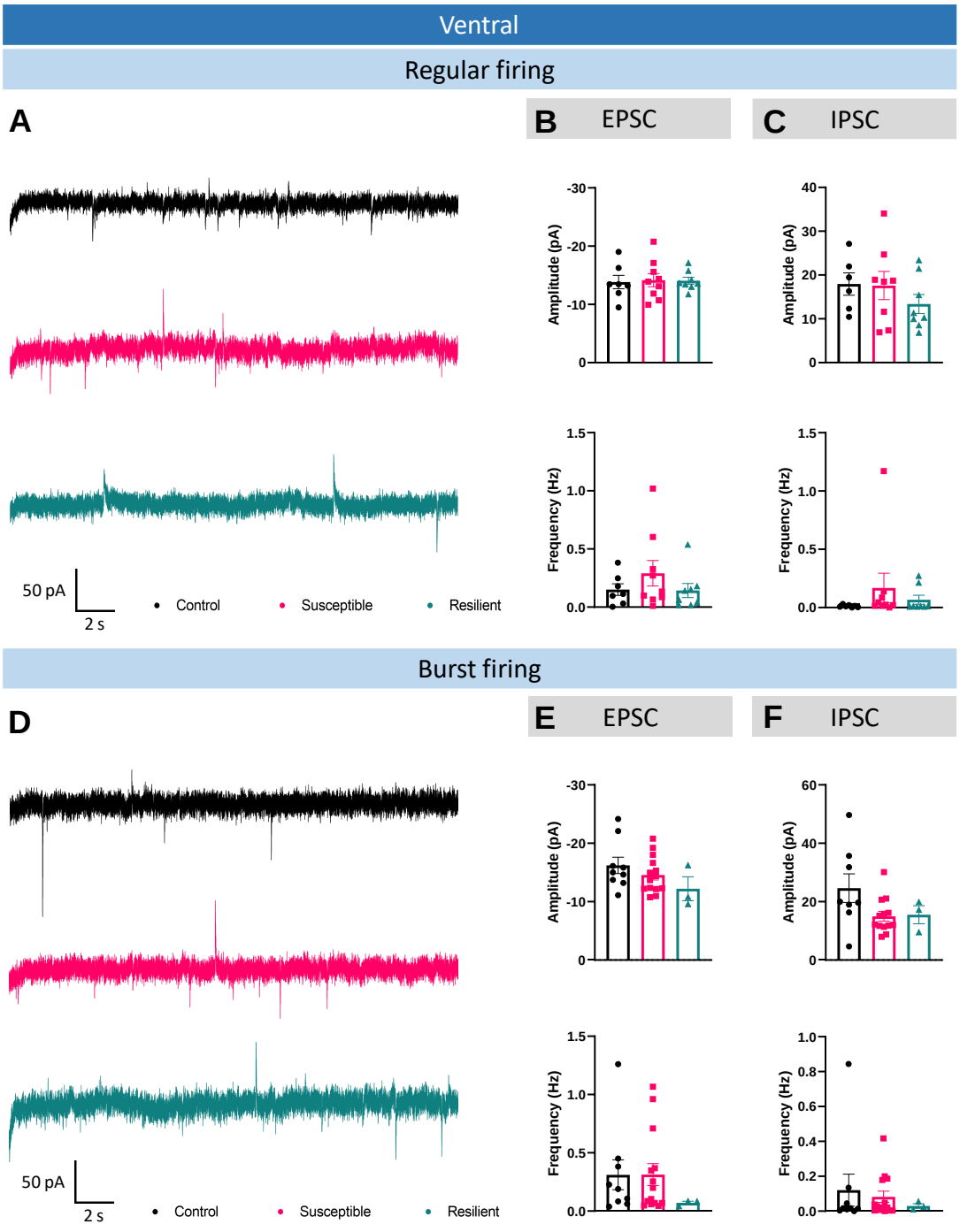

Figure 4.8: Spontaneous activity in the ventral subiculum was not affected by maternal separation

A-C) Regular firing neurons. A) Example traces of spontaneous activity recorded for control (black), susceptible (pink) and resilient (green) mice. Both EPSCs and IPSCs were analysed from the same traces. Cells were recorded from 5 control, 5 susceptible and 4 resilient mice. B) EPSC amplitude (top) and frequency (bottom). C) IPSC amplitude (top) and frequency (bottom). D-F) Same as A-C but then for burst firing cells. Cells were recorded from 4 control, 6 susceptible and 3 resilient mice. Data presented as mean ± S.E.M.

In summary, we only found subtle differences in electrophysiological characteristics and spontaneous activity of dorsal and ventral subiculum neurons. However, it has to be noted that n-numbers are on the low side for some cell types and regions.

4.6 Maternal separation increases subicular excitatory input of PV interneurons in the retrosplenial cortex

Previous research has indicated that spatial memory is affected in animal models of depression. The dorsal hippocampus plays an essential role in object location memory and therefore we investigated if this region was affected in our animal model of depression. It has also been shown that the connection of the dorsal SUB to the retrosplenial cortex (RSC) is essential in object location memory but that this connection is not involved in object recognition memory (de Landeta *et al.*, 2020). We hypothesized that the dSUB-RSC cortex connection was affected along with the object location memory. Interestingly, we observed an increase in exploration time for the novel object in the NOR indicating that susceptible mice might have improved object recognition memory. As mentioned earlier, we did not detect changes in the NOL, which means that the mice were not able to encode or retrieve spatial memory. Even though we were not able to assess object location memory properly, we were still interested if maternal separation resulted in functional differences for the dSUB-RSC projection

In order to study the functional connection from the dSUB to the RSC we injected an AAV-virus containing ChR2 in the dSUB of VGLUT2-Cre mice to selectively express ChR2 in the dSUB. This resulted in a strong band of fibres in the superficial layers of the RSC (Figure 4.9A,B). Next, we performed patch-clamp recordings in slices that were prepared 4-20 days after behavioural assessment. We recorded in the superficial layers of the RSC and illuminated the slices with a blue LED to investigate connectivity. Cells were filled with biocytin and stained post -hoc to visualize the morphology. The RSC consist of three major cell types: Low rheobase (LR) pyramidal cells, regular spiking (RS) pyramidal cells and fast-spiking (FS) interneurons. These cells can be distinguished in terms of input resistance and spike halfwidth (Brennan *et al.*, 2020). Therefore, we plotted the input resistance against the spike halfwidth for all recorded cells and this resulted in three clusters (Figure 4.9C). We checked the firing pattern of all cells to see if this matched the typical firing pattern of the cell types and this shows that the clusters corresponded with LR, RS and FS neurons (Figure 4.9D-F), demonstrating

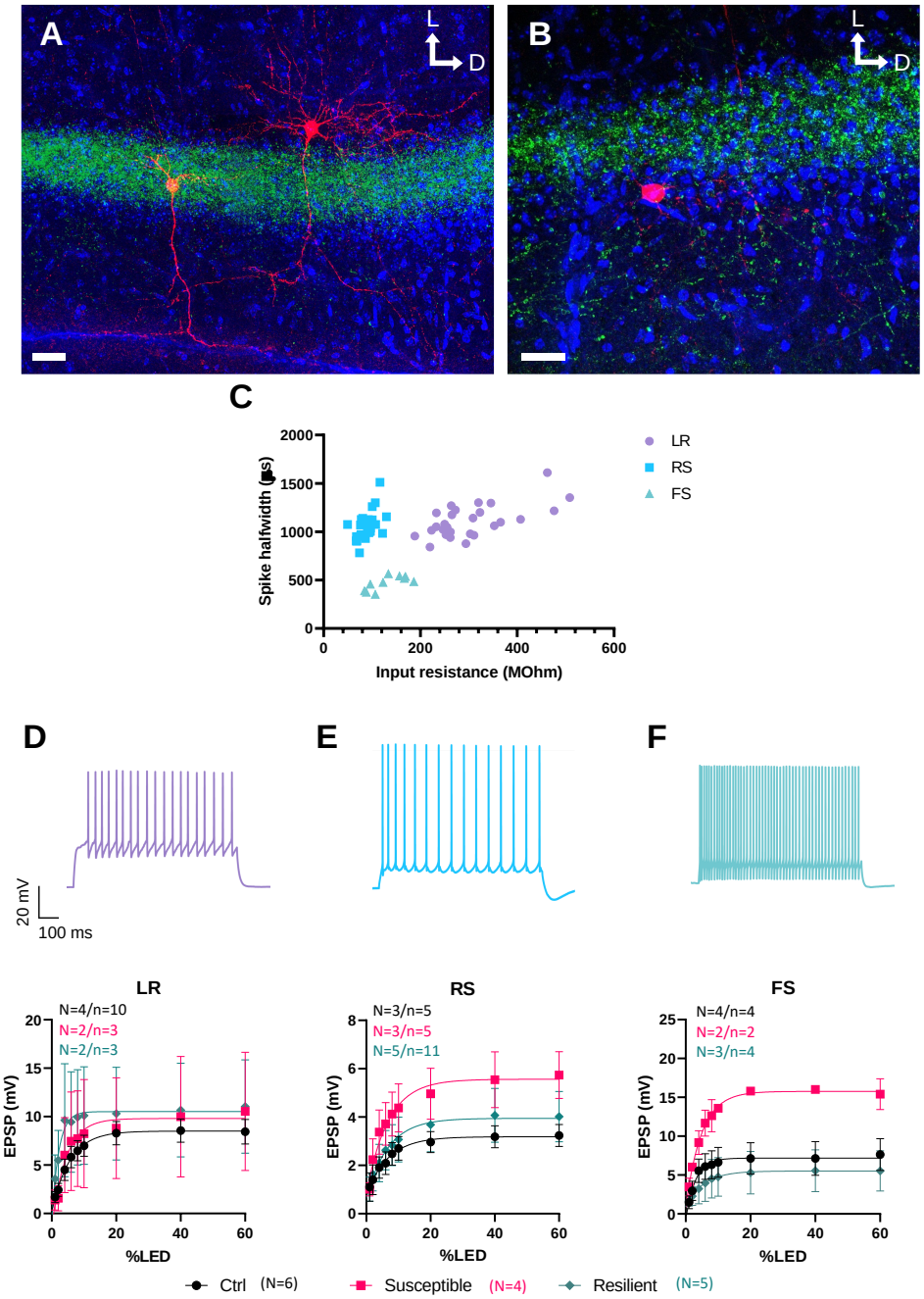

Figure 4.9: Synaptic strength in postsynaptic dSUB-RSC neurons

A) Reconstructed LR (left) and RS (right) neuron recorded in the RSC. B) Reconstructed FS interneuron in the RSC. A-B) Arrows indicate dorsal-ventral and medial-lateral orientation. Scale bar 30 µm. C) Spike halfwidth plotted against input resistance for all recorded neurons resulted in three clusters which correspond to LR, RS and FS neurons. D-F) Firing pattern (top) and synaptic strength recordings of of D) LR, E) RS and F) FS neurons. EPSPs were averaged for mice and then for groups. The solid line is a fitted exponential curve through the average values of the groups. N/n = number of cells (n) recorded from number of mice (N). Data presented as mean ± S.E.M.

that we recorded from all three types of neurons. The combination of morphology and electrophysiological characteristics was used to classify the neurons as LR, RS or FS.

To investigate the strength of the synaptic connection between the dSUB and RSC we stimulated the cells with different light intensities. The synaptic strength can be analysed by fitting an exponential curve through the data points. Changes in the slope (K) of the curve would indicates presynaptic alterations whereas differences in the plateau are indicative of postsynaptic changes. Analysing the fitted curves between the groups revealed no differences in K and plateau for LR and RS cells, but there was a difference in plateau for FS cells (Best-fit values plateau Ctrl: 7.18, Susceptible: 15.76, Resilient: 5.517, $p = 0.0121$, Figure 4.9F).

These results may suggest that that the projection from the dSUB to excitatory neurons in the RSC was not affected by maternal separation, but there could potentially be an increased excitatory drive onto FS interneurons in mice that were susceptible to maternal separation. Since the effect was only present in the plateau but not the rise of the curve, the effects could be interpreted as postsynaptic changes in the RSC and most likely not by presynaptic changes in the dSUB.

Of note, posthoc imaging revealed that virus expression in RSC slices of injected mice was heterogeneous, not all mice had a similar strong band in the RSC, as can be seen in Figure 4.9A and B. However, all recorded cells from all mice responded to optogenetic stimulation. Since a reduced expression of virus in dSUB neurons might affect the response size of dSUB-RSC connections, we compared the response size for all neurons between mice. In Figure 4.10A-D are example images from mice that show either stronger or slightly weaker labelling in the RSC. When looking at the response size from these mice (2 and 14 for weaker labelling and 6 and 13 for stronger labelling) we see that weak labelling does not result in solely low amplitude responses, or vice versa. Therefore, we believe that the subtle differences in injection site and amount of viral particles and thus labelled fibres in the RSC, which are inevitable to this methods, did not influence the synaptic strength recorded for the different groups of mice, and that the differences seen are a true effect and not caused by differences in injection sites.

4.7 Acute restraint-induced cFOS expression

Our data shows that there are no striking differences in electrophysiological characteristics and spontaneous activity of the dorsal subiculum. Next, we wanted to test if maternal separation affected neuronal activity levels in the dorsal SUB.

Additionally, it has been suggested that this animal model has different stress coping mechanisms, and that behavioural consequences might be more pronounced after stress exposure later in life (Bian *et al.*, 2021; Knox *et al.*, 2021). Therefore, we decided to investigate the activation level of the dSUB using cFOS expression in control and separated mice while being in their home cage or after acute stress. Restraint was used as an acute stressor where mice were placed in a small handling tube that could be temporarily closed (Figure 4.11A). In order to determine the optimal timing of cFOS expression during restraint we tested

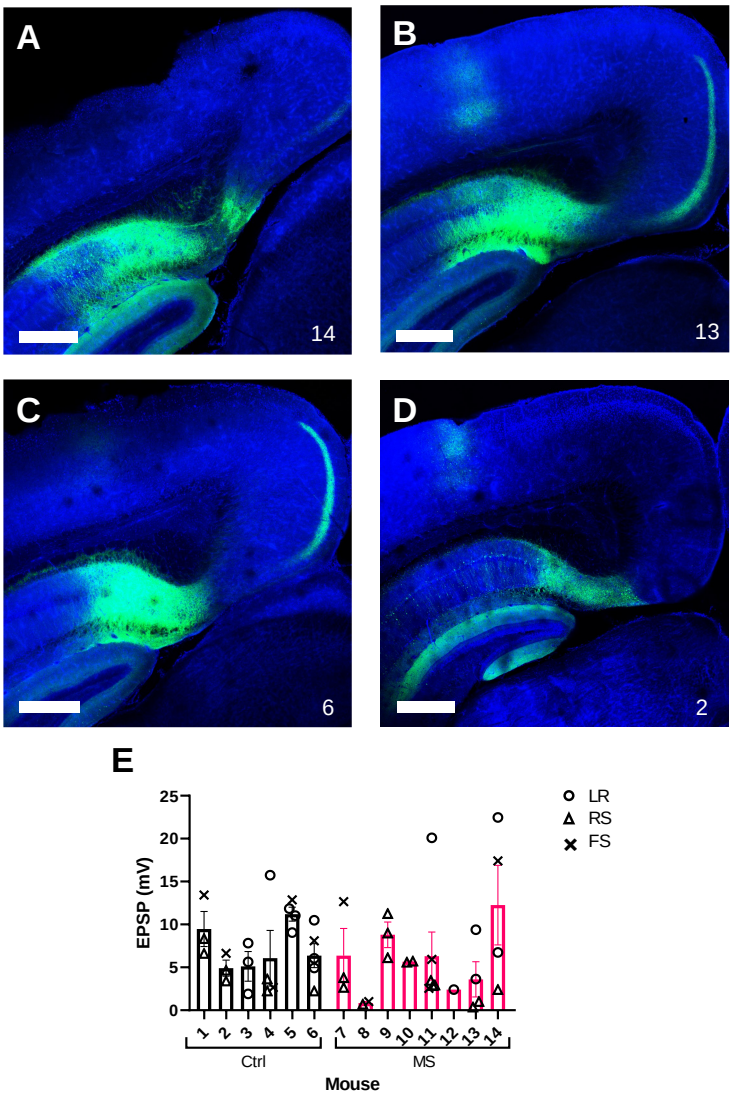

Figure 4.10: ChR2 was unevenly expressed in the RSC across mice

A-D) Example images of injection sites with (A,D) weak and (B,C) strong expression in the RSC. Numbers in the right bottom corner correspond with the mouse number in figure E. Scale bar 500 µm. E) LED-induced EPSP per cell per mouse. Symbols correspond to average response per cell, distinguishing between cell types. Data presented as mean ± S.E.M.

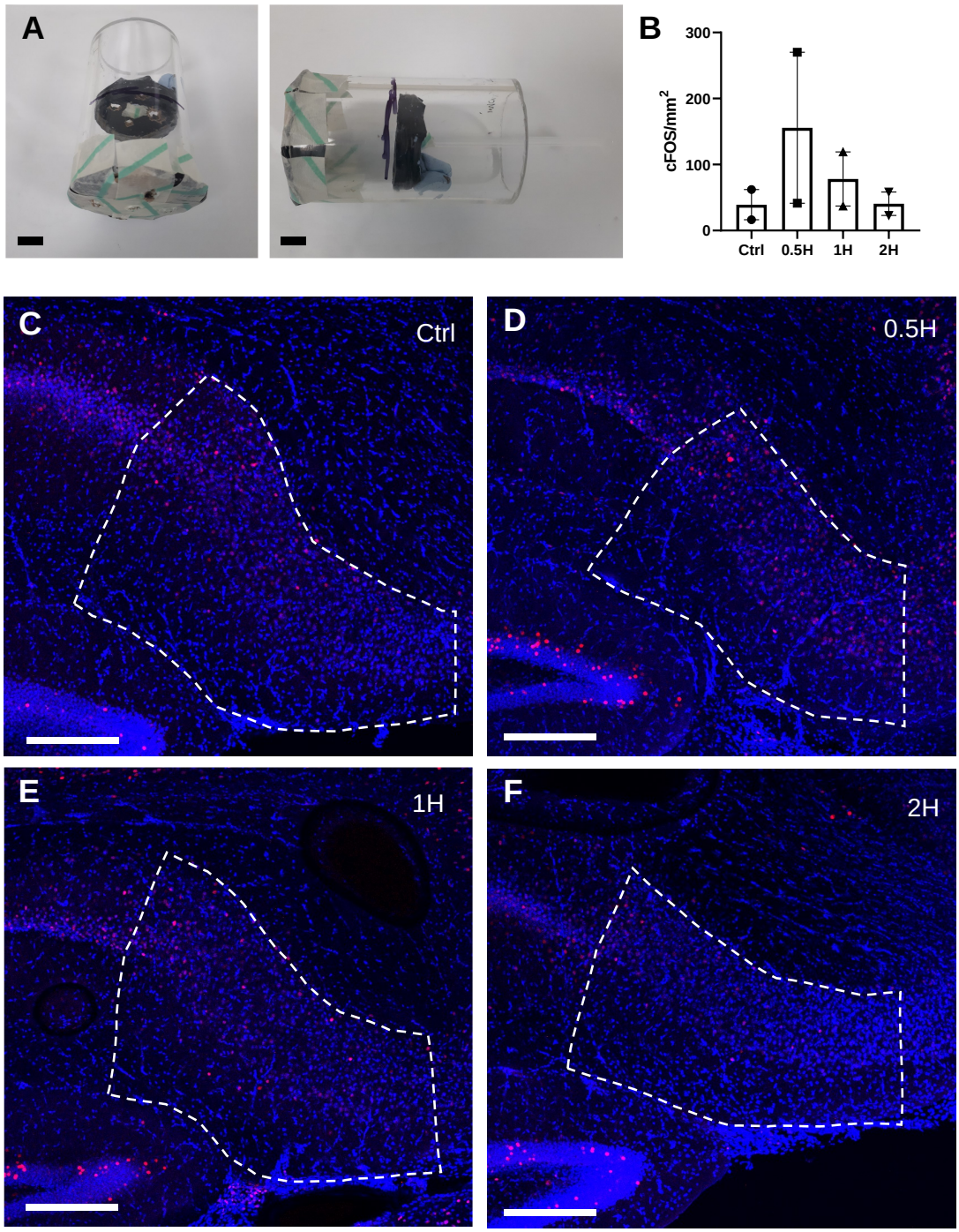

Figure 4.11: Optimization of restraint protocol for cFOS analysis

A) Modified handling tube used for restraint. Bottom and top lid contained holes for air flow. Scale bar 1cm. B) Quantification of cFOS expression in the subiculum for homecage control, 30 minutes, 1 hour and 2 hour after the restraint period of 1 hour. C-F) Example images of cFOS expression (red) for C) control, D) 30 minutes, E) 1 hour and F) 2 hours after restraint. DAPI in blue. Scale bar 250 µm. Data presented as mean ± S.E.M.

different time points: cFOS expression was analysed for home cage control, 30 minutes, 1 hour and 2 hours of restraint. Mice were perfused 1 hour after the end of restraint. The results show that cFOS expression was increased for 30 minutes (155.7 ± 114.3) and 1 hour (78.11 ± 41.07) of restraint compared to home cage controls (39.24 ± 22.88, Figure 4.11B,D,E). This was returned back to levels of home cage control for 2 hours of restraint (40.61 ± 17.70, Figure 4.11B,F). This indicates that the mice might accommodate to the acute stress when exposed to it for longer than one hour.

4.7.1 Maternal separation increases acute stressor-induced dSUB activation

Based on the results for the optimization of the restraint protocol we decided to implement restraint for 1 hour for optimal cFOS expression. Since PV neurons have also been implicated in the pathology of depression, we also stained for PV neurons in the SUB and prefrontal cortex. Another advantage was that the PV staining made it easier to distinguish between the CA1 and the SUB. PV was more abundantly and diffusely expressed in the SUB, whereas this was more confined to the pyramidal layer for the CA1 (Figure 4.12).

For now, we have not analysed cFOS expression in the RSC since the RSC had not be shown to be involved or affected by non-hippocampus dependent acute stress. Instead, the RSC is associated with posttraumatic stress disorder (PTSD) and involved in context-dependent fear memory encoding and retrieval during fear conditioning (Corcoran *et al.*, 2018). However, based the results presented in section 4.6 it would have been interesting to analyse cFOS expression in the RSC as well.

The cFOS stain implies that SUB neurons were active during home cage

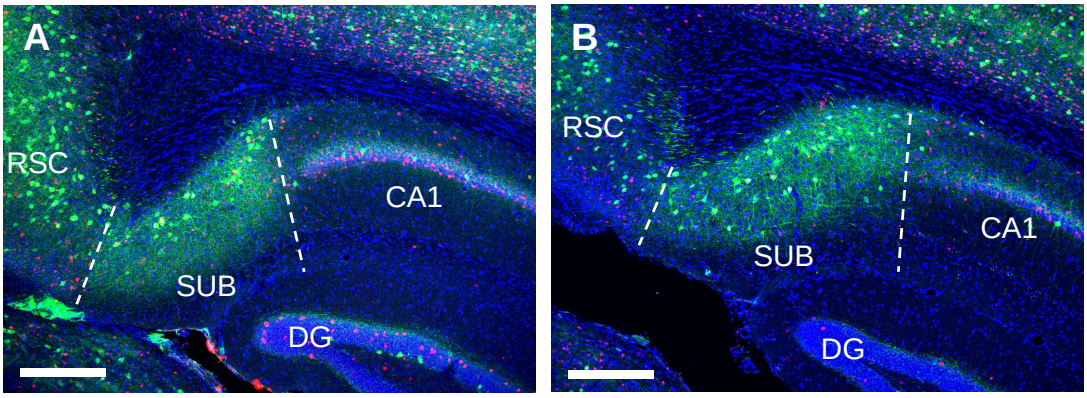

Figure 4.12: PV expression in the hippocampus

Example images of PV expression in the hippocampus of A) control and B) maternal separated mice. Scale bar 250 µm. Green = PV, Red = cFOS, Blue = DAPI.

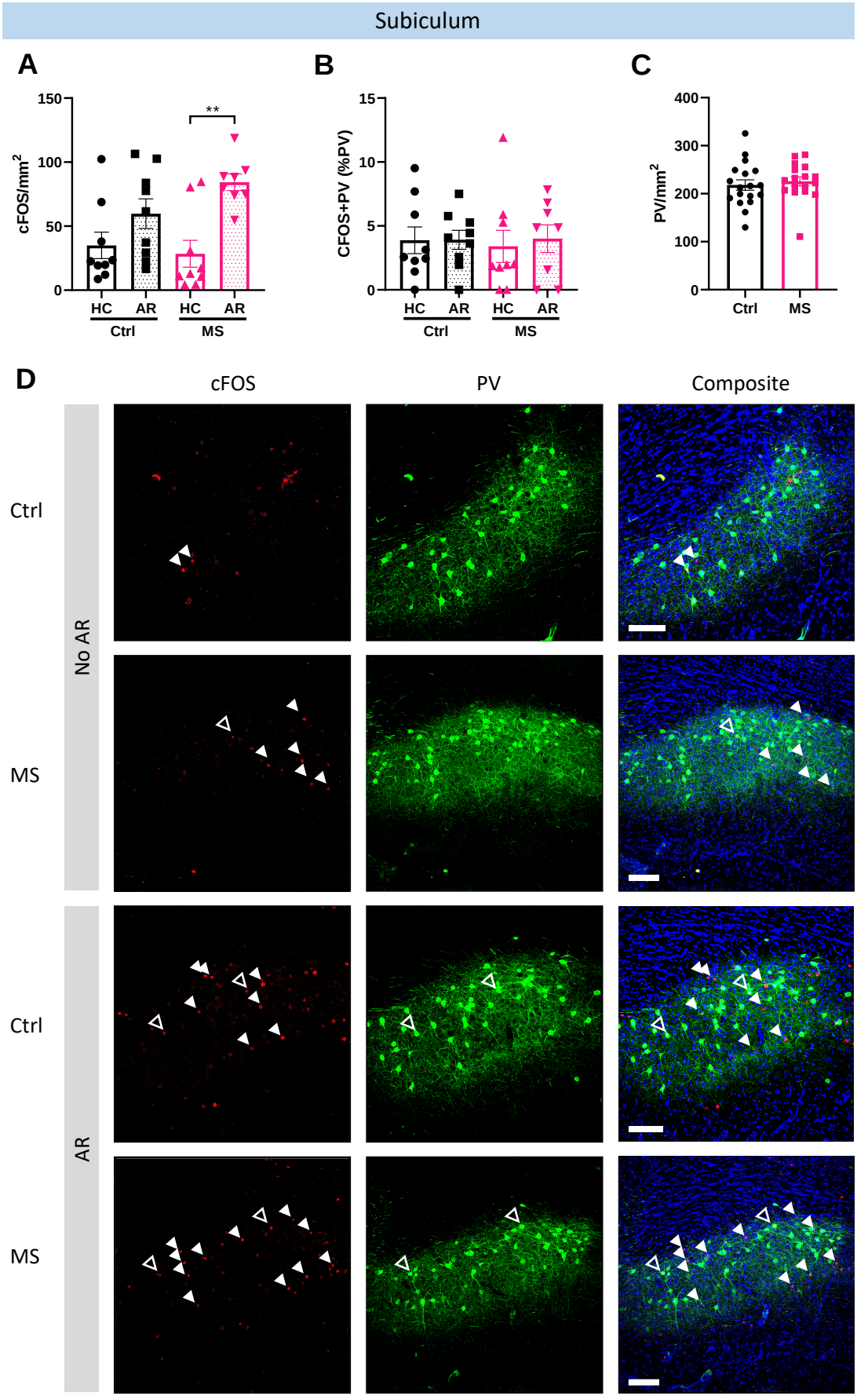
Subiculum
A
B
C
cFOS/mm2
CFOS+PV (%PV)
PV/mm2
HC
AR
Ctrl
MS
**
D
cFOS
PV
Composite
Ctrl
MS
No AR
AR

Figure 4.13: (see previous page) Acute stress induced cFOS expression in the dSUB

A) cFOS expression per mm^2 in control or MS mice in home cage conditions or after acute restraint stress. B) cFOS expression in PV neurons as a percentage of total number PV neurons. C) Number of PV cells per mm^2. D) Example images of cFOS (red) and PV (green) expression and composite images combined with DAPI (blue). HC = home cage, AR = acute restraint. Closed arrows indicate cFOS-positive neurons and open arrows indicate PV- and cFOS -positive neurons. Scale bar 100 µm. Data presented as mean ± S.E.M.

conditions as indicated by 35 ± 10 and 28 ± 11 neurons expressing cFOS per mm^2 in control and MS mice, respectively (Figure 4.12A,D). We did not observe an increase in cFOS after acute stress for control mice (59.75 ± 11.56 cFOS/mm^2, Sidak, p = 0.3106), but we found a highly significant increase in active cells in the dSUB of maternal separated mice indicating that the dSUB is affected by MS and it does show an increased response to acute stress (84.36 ± 6.52 cFOS/mm^2, Sidak, p = 0.0022) (Figure 4.13A,D). Intriguingly, the proportion of cFOS-positive PV cells was not affected by acute stress for both groups (two-way ANOVA, p = 0.9772, Figure 4.13B). Additionally, the number of PV cells was also not different between control and separated mice (t-test, p = 0.5990, Figure 4.13C). This shows that non-PV neurons in the dorsal subiculum are activated by acute stress only after maternal separation and this indicates a potential role for the dorsal SUB in early-life stress-affected stress coping.

4.7.2 Acute restraint increases cFOS expression in the PFC, but this is not modulated by maternal separation

As discussed in Chapter 1, the PFC has also been implicated to be involved in depression. Therefore, we also investigated acute restraint-induced cFOS expression in the PFC for control and maternal separated mice. For this, we analysed the IL, PL and ACC together as one region, as indicated in the outline in Figure 4.14D. Restraint-induced cFOS expression was significantly increased for both control (401 ± 64 cFOS/mm^2, Sidak, p<0.0001) and separated mice (392.8 ± 45.64 cFOS/mm^2, Sidak, p<0.001) compared to home cage conditions (control: 29.21 ± 8.40 cFOS/mm^2, MS: 23.27 ± 5.91 cFOS/mm^2, Figure 4.14A,D). Additionally, the percentage of activated PV neurons was also increased after acute stress (Ctrl: 5.23 ± 1.11 %, p = 0.006, MS: 3.22 ± 0.62 %, p = 0.0354) compared to home cage conditions (Ctrl: 1.01 ± 1.48 %, MS: 0.41 ± 0.29 %) (Figure 4.14B,D). However, there were no differences between control and

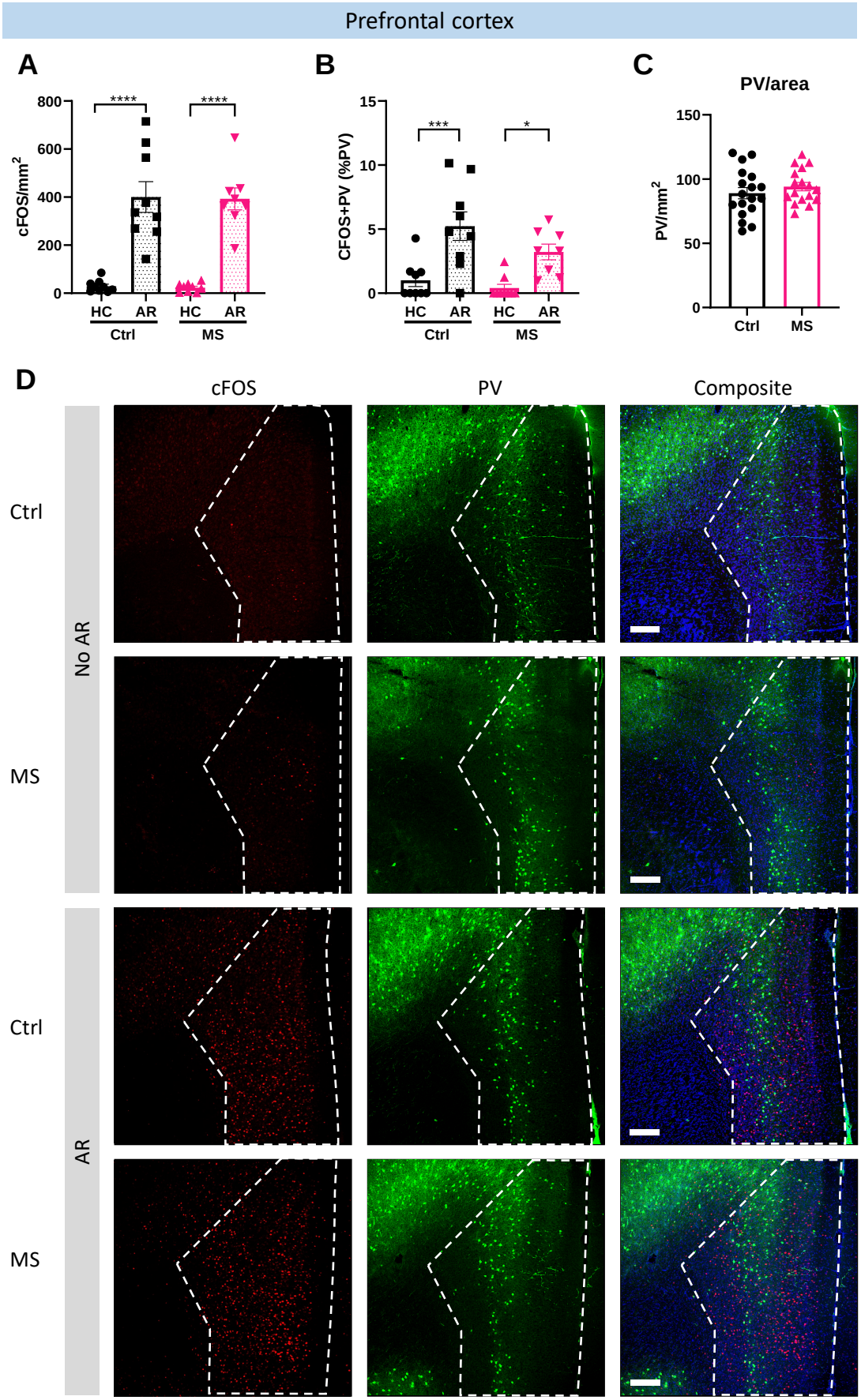
Prefrontal cortex
A
cFOS/mm2
800
600
400
200
0
****
****
HC
AR
HC
AR
Ctrl
MS
B
CFOS+PV (%PV)
15
10
5
0
***
*
HC
AR
HC
AR
Ctrl
MS
C
PV/area
PV/mm2
150
100
50
0
Ctrl
MS
D
cFOS
PV
Composite
Ctrl
MS
No AR
Ctrl
MS
AR

Figure 4.14: (see previous page) Acute stress induced cFOS expression in the PFC

A) cFOS expression per mm^2 in control or MS mice in home cage conditions or after acute restraint stress. B) cFOS expression in PV neurons as a percentage of total number PV neurons. C) Number of PV cells per mm^2. D) Example images of cFOS (red) and PV (green) expression and composite images combined with DAPI (blue). HC = home cage, AR = acute restraint. Scale bar 200 µm. Data presented as mean ± S.E.M.

separated mice for overall cFOS expression (two-way ANOVA, p = 0.8052) and only a trend for PV activation (two-way ANOVA, p = 0.0725). Overall the number of PV cells per mm^2 did not differ between control and separated mice (Ctrl: 89 ± 4, MS 94 ± 3, t-test, p = 0.3512, Figure 4.14C,D). Taken together, these results show that although mPFC neurons are highly activated after acute stress, this response is not modulated by early-life stress.

4.8 Discussion

4.8.1 Behaviour

In this chapter, we investigated the effects of maternal separation on depressive-like behaviour, memory performance and subiculum and PFC function. We divided maternal separated mice into susceptible and resilient mice based on overall performance in tests detecting depressive-like behaviour. When comparing these groups for individual tests, it shows that only sucrose preference was significantly affected in susceptible but not resilient mice. The behavioural effects after maternal separation are variable. Some studies find that anxiety is affected, whereas this is not present in other studies (Shalev and Kafkafi, 2002; Romeo *et al.*, 2003; Tan *et al.*, 2017; Tchenio *et al.*, 2017). This might be dependent on the exact model used or the age of the mouse at the time of testing. In a recent study, adolescent mice that have been subjected to MS showed increased anxiety-like behaviour, whereas this was absent in adult mice (Chen *et al.*, 2022). In contrast, differences in the forced swim test were only found in adult but not adolescent mice (Chen *et al.*, 2022). The forced swim test is very commonly used to test for depressive-like behaviour. Considering our effects of acute stress on cFOS activation, this test might have provided us with more insight into behavioural differences of stress coping; however, the test is controversial (Gorman-Sandler and Hollis, 2022). Interestingly, a reduced sucrose preference is present in both adolescent and adult mice (Chen *et al.*, 2022). The mice in this chapter were tested between P45 and

P60, which means that they were adult. Additionally, the behavioural effects vary greatly per animal model of depression or protocol that is used (Tractenberg *et al.*, 2016). Therefore, the limited behavioural effects we have found might be different from other studies dependent on the protocol and age of the mice that were used.

We also tested for memory performance in a novel object location and novel object recognition test. Altered cognitive function has been demonstrated in several animal models of depression using different cognitive tests including object location and recognition test, Morris water maze and alternating y-maze test (Yu *et al.*, 2011). Overall, studies report a reduced memory function, but again, results are variable between studies and animal models (Darcet *et al.*, 2016; Moreira *et al.*, 2016; Tractenberg *et al.*, 2016; Zhang *et al.*, 2020). In this chapter, we were not able to detect object location memory. There are several factors that could have prevented memory formation or retrieval. One of them is insufficient labelling of the arena to provide the mouse with a sense of direction. Possibly, labelling of more walls would have facilitated memory formation. Additionally, a longer period of habituation or a shorter period between familiarization and test could have improved the test. However, it has been shown that mice are able to perform well in the object recognition test without habituation and that it does not affect performance significantly (Leger *et al.*, 2013). Although it has to be noted that this might differ between mouse strains, with more anxious mice like BALB/c needing more habituation than C57BL/6 mice which are considered less anxious mice. Regarding the interval between familiarization and testing, studies have shown memory retrieval was no longer possible 24 hours after familiarization with the objects (Akkerman *et al.*, 2012). On the other hand, our results show that object recognition memory was successful with a 24 hour interval.

Here, we found significant improvement of novel object recognition memory in susceptible mice compared to control and resilient mice. The protocol that we used was slightly adapted from the typical object location memory test and this protocol has been used before (Denninger, Smith and Kirby, 2018). However, since the object location test served as the familiarization phase of the object recognition test, this might be a test of recency memory instead (Kinnavane, Albasser and Aggleton, 2015). Two different sets of objects are used for familiarization 24 hours apart. Again 24 hours later, mice were allowed to explore one object of both sets and usually explore the object they were less recently exposed to more. This shows that they remember the more recent object better. It is also shown that this type of memory is also hippocampus-dependent (Albasser *et al.*, 2012). However, in our case we used altered location and not a different set

of objects, therefore it is not certain that the NOL test phase resembles a recency memory test. Nonetheless, there are not many studies looking at recency recognition memory in animal models of depression, making it difficult to compare our findings to previous findings. One study found impaired recognition memory at juvenile age (P18) after maternal separation in rats (Reincke and Hanganu-Opatz, 2017). We have tested memory function in adult mice (P45-60) and behavioural effects might vary and sometimes be opposing depending on the age of the animals subjected to the tests.

4.8.2 Electrophysiology

In terms of the electrophysiological effects of maternal separation on subicular neurons, we found no significant differences for both active and passive properties of neurons in the dorsal and ventral SUB. There are not many studies looking at changes in the dorsal hippocampus in models of depression, but one of them showed changes in input resistance and I_h as a consequence of increased HCN1 expression in the dorsal but not ventral CA1 (Reincke and Hanganu-Opatz, 2017). We did not observe the same effects in the subiculum. This could be due to differences in brain regions or differences in animal model used, as Kim et al used chronic unpredicted stress in mice.

Additionally, spontaneous activity was also not affected by maternal separation. The only significant difference that was found was an increase in EPSC frequency for regular firing dorsal neurons in resilient mice. This has not been studied before in the dorsal subiculum, but EPSC frequency is shown to be affected after maternal separation in the prefrontal cortex (Chen *et al.*, 2022). They found a decrease in spontaneous EPSC frequency but not amplitude for adolescent mice that were subjected to maternal separation. Interestingly, this effect was the other way around for adult mice, with a decrease in spontaneous EPSC frequency. However, they did not separate the mice into susceptible and resilient mice, making it difficult to compare our results. The change of EPSC frequency but not amplitude would point towards a presynaptic mechanism. Changes in glutamate release after maternal separation have been suggested (Chen *et al.*, 2022).

Since the RSC and SUB are both essential in spatial memory and more specifically object location memory (de Landeta *et al.*, 2020), we investigated this projection in more detail. We show potential increase in synaptic strength for subicular neurons projecting onto fast-spiking interneurons in the RSC for susceptible but not resilient mice. Fast-spiking interneurons are most likely

parvalbumin-positive interneurons. These have been implicated to play an important role in the pathology of depression in several brain regions in both humans and animal models (Perlman, Tanti and Mechawar, 2021). We are not able to relate the physiological changes to memory function since we were not able to assess location memory. However, our data suggests that the projection from the SUB might result in an enhanced inhibition within the RSC as an increased excitation onto PV interneurons is evident. Since activity of the RSC is found to be essential for the retrieval of object location memories (de Landeta *et al.*, 2020), this might suggest changes in spatial memory but more research has to be performed to confirm this.

To further investigate this, *in vivo* experiments using electrophysiology and chemo- or optogenetics would provide valuable information. For example, electrophysiological recordings during object memory tests would show if the increased excitation of PV neurons by the dSUB as observed *in vitro* holds true *in vivo* by showing an increased level of PV activity during object location memory. Additionally, inhibiting PV neurons in susceptible maternal separated mice would show if reducing PV activity would rescue stress-induced cognitive impairment. Performing an experiment with stimulation PV neurons during memory consolidation or retrieval would elucidate if increased PV neuron activity is indeed disrupting spatial memory function. These experiments would increase our knowledge on the role of RSC PV interneurons during spatial memory and how this is affected by early-life stress.

4.8.3 cFOS expression

Electrophysiological recordings showed no major changes in dSUB properties and activity, but we were interested to see if there were any changes in brain region activity after acute stress. To see how our animal model would impact general neuronal activity we looked at cFOS expression after maternal separation. To facilitate cFOS expression we used acute restraint stress, since stress coping after maternal separation is also shown to be affected (Qin *et al.*, 2019). Therefore, we investigated stress-induced cFOS expression in maternally separated and control mice. Dorsal subicular neuron were indeed activated by acute stress, specifically in separated mice. This indicates that the dSUB is involved in stress coping. However, since the restraint protocol also introduced the mice to a different environment, we cannot exclude that this cFOS activation is induced by a change in environment. On the other hand, the dorsal CA1, which shares seminal functions with the SUB and is also highly implicated in spatial memory but not stress per se,

has also been shown to be affected by acute stress (Yu *et al.*, 2018). Additionally, downregulation of HCN channels in the dCA1 increased active coping strategies, whereas chronic mild stress increased HCN expression and these mice also showed increased passive stress coping strategies (Fisher *et al.*, 2018; Kim, Brager and Johnston, 2018), further implicating a role for the dorsal hippocampus in stress coping. Interestingly, an overactivation of interneurons but not pyramidal cells in the dCA1 after acute restraint has been shown and this was accompanied by a reduction in memory function (Yu *et al.*, 2018). Additionally, activating interneurons in the dCA1 affected spatial memory but not behavioural measures of anxiety (Yu *et al.*, 2018). This indicates that dorsal CA1 neural activity, and based on our data also activity in the dSUB, is affected by acute stress. However, in order to fully understand if cFOS expression in the dSUB is reflecting stress or environment processing, a group of mice that is subjected to the novel environment but no stressor is needed. If this group would also show increased cFOS expression, especially in separated mice, this would favour the explanation that altered environmental processing might be causative for our observations. If the cFOS expression would reflect environment processing instead of stress coping, the increased activation for separated mice might also contribute to different memory formation or retrieval. If cFOS expression is not modulated by novel environment exposure, this would indicate that the effect seen in our data is caused by the stressor.

Additionally, altered synaptic plasticity has been observed in the dSUB after acute stress, with differential effects from the CA1 (Macdougall and Howland, 2013). Nonetheless, our data shows that the dSUB is differentially activated after maternal separation, highlighting a potential role for the dSUB in depression and more specifically stress coping.

The PFC has also been shown to be involved in depression (Schmaal *et al.*, 2020; Pizzagalli and Roberts, 2022). We show that the PFC is highly activated by acute stress, although maternal separation did not affect the level of activation. Additionally, we show that PV neurons are also activated by acute stress, but again this was not affected by maternal separation. Previous studies have shown increased number of PV neurons in the PFC after stress and increased activation during stress exposure (Shepard and Coutellier, 2018; Page *et al.*, 2019). The reason that we do not see the same effect in our data could be due to a different model that was used, or a different region of interest. We analysed the PFC as one region, but it could be that there would be differentially affected regions within the PFC, e.g. the IL or PL, since these regions have been found to have opposing

functions. The behavioural data from the mice that were used for cFOS experiments is not available, therefore we are not able to distinguish between resilient and susceptible mice. This might also mask some differences between control and MS mice. For example, we have found a trend in reduced stress-induced activation of PV cells after maternal separation. This might be significantly different between either susceptible and control or resilient and control mice.

To summarize, our animal model shows limited changes in behaviour, accompanied with possible changes in projections to the RSC from the dSUB. The dSUB might be affected after maternal separation and involved in stress coping, however, how the dSUB contributes to this process still needs to be investigated. Behavioural tests examining stress coping in combination with dSUB manipulations might provide more insight into this. Additionally, a role for the dSUB projection onto RSC PV neurons in MS-induced cognitive impairment is suggested. How this projection and these interneurons are involved in the spatial memory impairment is still an open question and could be investigated with the experiments suggested above. Altogether, this study provides insight into the effect of early-life stress on the structure and function of the dorsal hippocampus.

4.8.4 Sample size limitations and statistics

Unfortunately, sample size was low for these experiments. For the behavioural experiments, calculations show that the power is now around 30%. In order achieve 80% power and detect differences between control and separated mice the groups should be about N=50. However, since the maternal separation group consists of both susceptible and resilient mice, this can explain the high N-number that is needed to achieve significance. When looking at the behavioural differences between susceptible and control mice, the power is around 40%, which is still underpowered. There, sample size calculations show a sample size of 25 per group. Because the proportion of susceptible and resilient mice in the separated group might differ between litters it might be more difficult to achieve a pre-set sample size for these groups.

In terms of cellular recordings, some experiments here were also underpowered. For example, optogenetic recordings of RSC cells had a low n-number. Power calculations reveals a power of 7.8%, 16% and 55% for plateau values for LR, RS and FS cells, respectively. To detect any significant differences in plateau values with a power of 80%, the recordings of RS and FS cells has to be increased to n=18 and n=5 per group, respectively.

These calculations are done for either number of mice or number of cells.

However, since the manipulation is done on the level of litter, different litters might respond differently to the treatment and therefore the n-number of litters might be more relevant. The current study was performed with three litters. Due to time constraints and the COVID-19 restrictions, it was not possible to include additional litters in this study, and comparison between litters is therefore not possible.

Furthermore, other statistical approaches might have suited our experimental design better. The aim of the study is to investigate if maternal separation affects behavioural and electrophysiological measurements. However, the measured outcome might also be affected by other factors than the maternal separation model, including sex, susceptibility of individual mice, litter, maternal care provided by the dam, the effect of the model on the dam and age of the mouse at time of recording. These random effects induce variation in the data and might therefore mask the effect of the fixed effect, our maternal separation model, on the measurements. The mixed model statistical approach takes all these factors in consideration and could therefore be considered as a good statistical method to analyse the effect of the different factors on the behavioural and electrophysiological outcome.

4.8.5 Animal models of early life stress

The main types of early life stress (ELS) models of depression are maternal separation (MS), maternal deprivation (MD) and limited nesting and bedding material (LNBM), all aimed at reducing maternal care that the pups receive. Within the MS models, many different protocols exist in term of duration of separation per day, the number of days that the pups are separated and if the pups are weaned early or at the regular age (Tractenberg *et al.*, 2016). However, usually the pups are removed for several hours a day over a period of the first three postnatal weeks. The MD model has increased separation periods. With this model, pups are removed from the dam for a period of at least 24 hours, but differences in exact duration are also variable between studies. For LNBM model, pups and dam are provided with sparse cage enrichment for example by removing nesting material and only adding a small amount of sawdust to the cage. Even though the pups are staying with the dam during their early life, the reduced cage enrichment reduces the quality of maternal care provided by the dam.

Whereas the MS model has been proven successful at inducing depressive-like behaviour in mice, it has shown to be more powerful in rats (George *et al.*, 2010; Bonapersona *et al.*, 2019). In agreement with this, we only found a mild behavioural phenotype with our MS model. Additionally, we have not demonstrated

that the separate pups are more stressed than their littermate controls during the separation period. Several test could have been included to characterize the model and show that the model works as intended. For example, measuring the cortisol levels during separation from separated pups and controls could indicate how stressed the pups are. Another often-found effect of depression models is decreased neurogenesis in the dentate gyrus (Stuart, Hinchcliffe and Robinson, 2019). Measuring this could also have been included to validate our maternal separation model.

Since we have not validated our model and our protocol only results in a mild behavioural phenotype, other ELS models as mentioned above might have been more effective in inducing more significant changes in behaviour, and potentially also electrophysiological measurements.

Chapter 5: Serotonin receptor expression in cortical and hippocampal NPY interneurons

5.1 Introduction

In this chapter, we are interested in a specific type of GABAergic inhibitory interneuron called neurogliaform cells (NGFC). Because their dendrites have a web-like structure, neurogliaform cells were first named spiderweb cells by Ramón y Cajal. The current name derives from the resemblance in morphology to glia cells, with shorter dendrites arranged in a stellate fashion and a smaller soma than other interneurons (Kawaguchi, 1995). This cell type has mostly been studied in the CA1 region of the hippocampus and in superficial layers of sensory cortical regions. A recent study by Tasic and colleagues has shed light on transcriptomic subclasses of NGFCs (Tasic *et al.*, 2018). However, the study also showed that excitatory neurons differ between brain regions, whereas inhibitory neurons are more consistent between regions. Inhibitory neurons for different brain regions are derived from different structures during development, i.e. caudal ganglionic eminence vs medial ganglionic eminence, which might contribute to the different transcriptomic classes. In this chapter, we look more into transcriptomic, electrophysiological and pharmacological differences of NGFCs in the auditory cortex (AUD) and CA3 region of the hippocampus. The results of this chapter are published (Beerens *et al.*, 2022).

5.2 Previous work

The pharmacological experiments performed in this chapter are based on the findings of work performed by Dr. Jochen Winterer and Prof. Christian Wozny in collaboration with Prof. Csaba Földy from the University of Zürich, Switzerland. All the data shown in this section has been collected by them. To study the diversity of NGFCs in two different cortical regions, NGFCs were patch-clamped to study electrophysiological characteristics and subsequently prepared for single-cell RNA sequencing. A schematic of the timeline of these experiments is visualised in Figure 5.1. NPY expression is thought to be one of the main characteristics of NGFCs, in addition to its very distinctive electrophysiological characteristics (Kawaguchi, 1995; Overstreet-Wadiche and McBain, 2015; Schuman *et al.*, 2019). By using an NPY-GFP mouse these cells can be visualized for patch-clamping. Recordings of NPY-GFP positive cells in the stratum lacunosum-moleculare of the CA3 (n = 20) and superficial layers of the AUD (n = 10 cells) were performed by Dr.

Jochen Winterer and Prof. Christian Wozny. NGFCs exhibited the characteristic firing pattern and action potential shape as previously described (Kawaguchi, 1995; Schuman *et al.*, 2019). Electrophysiological characteristics including resting membrane potential, maximal action potential frequency, action potential threshold, input resistance, action potential halfwidth, action potential peak amplitude, sag potential, attenuation of action potential firing and latency to fire were determined for cells from both the CA3 and auditory cortex (Figure 5.2). None of these characteristics was different for cells from the two regions, except for the latency to fire (Two-way ANOVA, p = 0.187; Bonferroni, p = 0.0003; Figure 5.2). This is also visible in the spiking pattern in response to increasing steps of current injection as depicted in Figure 5.2A,B. Broadly speaking, this means that cells from these two structures are not different in their intrinsic electrophysiological characteristics.

Subsequently, these cells were prepared for single-cell RNA sequencing. All recorded neurons indeed expressed *Npy*, confirming that NPY-GFP was a good marker. Together with *Npy*, NGFC marker gene *Reln* was more highly expressed in AUD than CA3 neurons. In line with previous studies, *Ndnf* and *Car4* were expressed in half of AUD neurons but only two CA3 neurons (Schuman et al., 2019; Tasic et al., 2018). The other NGFC markers *Lamp5* and *Nos1* were

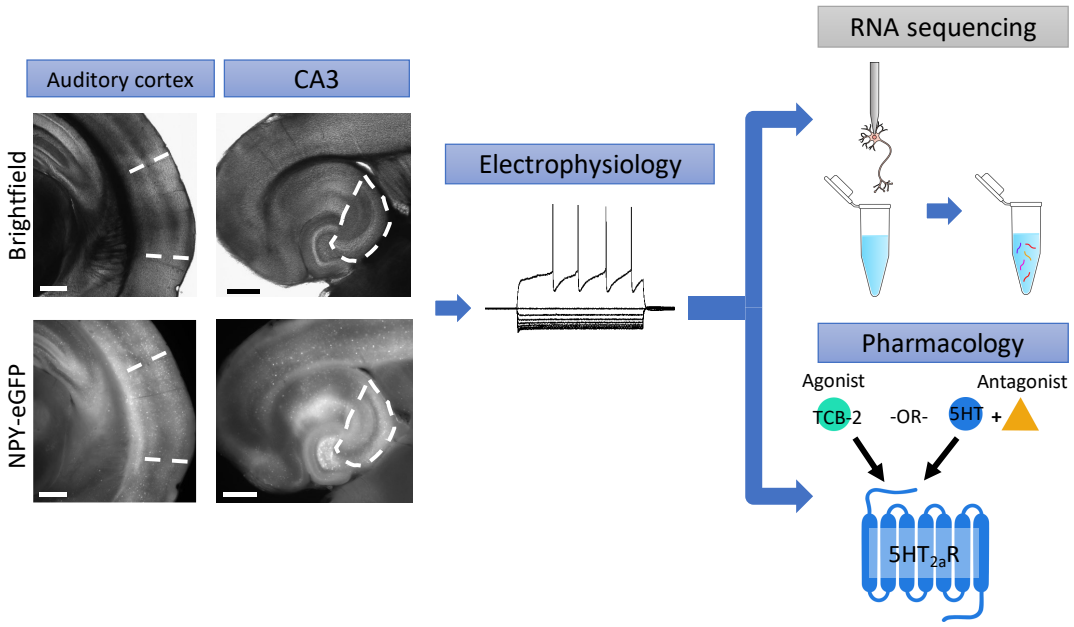

Figure 5.1: Experimental timeline

NPY neurons from the auditory cortex and CA3 were visualized using NPY-eGFP mice. Electrophysiological characteristics were recorded, after which the cells were extracted for scRNA sequencing or recordings were continued for pharmacological experiments. For the latter, either an agonist or a combination of 5-HT and an antagonist were applied. Scalebar: 1 mm.

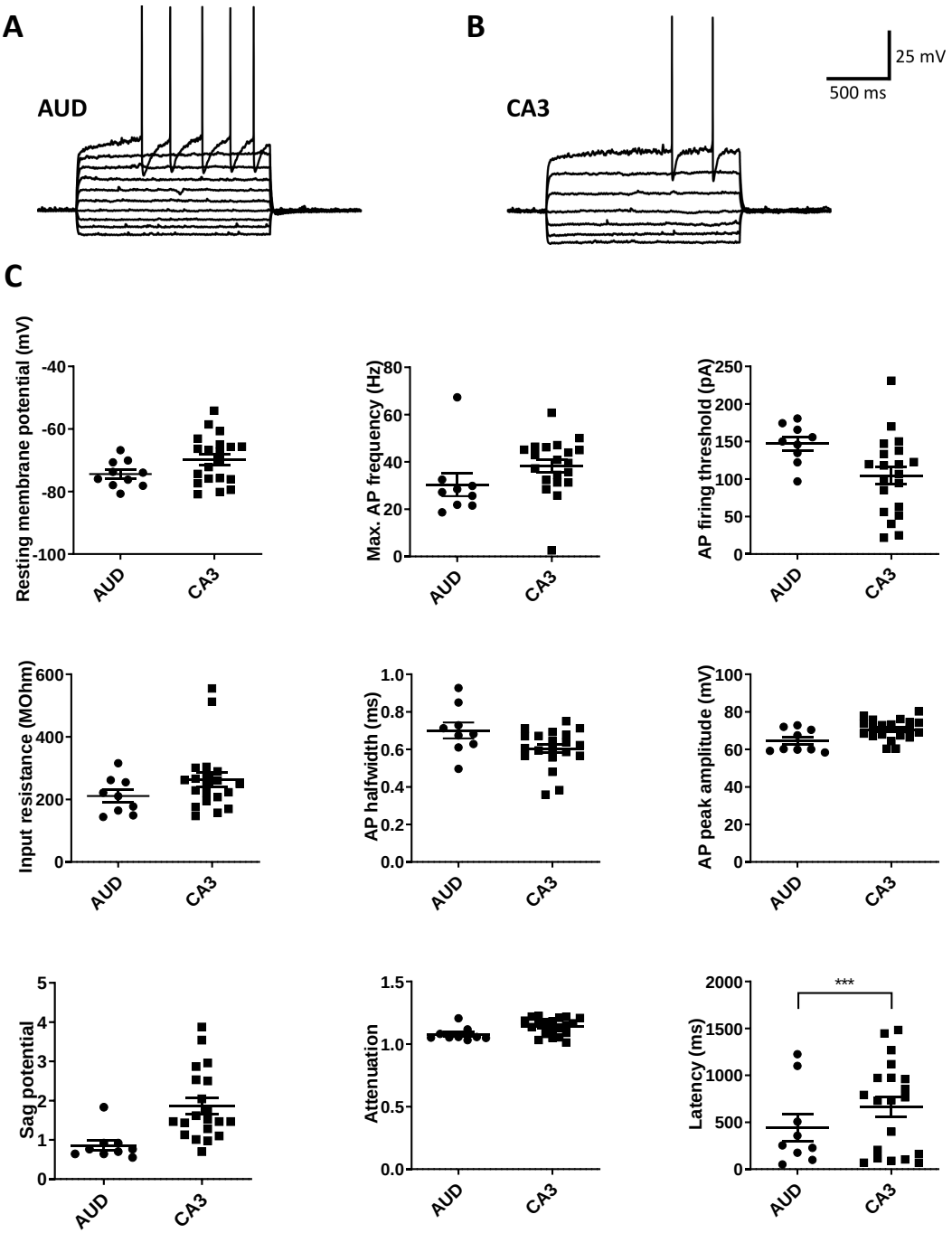

Figure 5.2: Electrophysiological characterization of CA3 and auditory cortex NGFCs

A-B) IV profile for NPY neurons from the A) auditory cortex and B) CA3. C) Different electrophysiological characteristics were determined for NPY+ cells in the CA3 (n = 20) and auditory cortex (n = 10). Data presented as mean ± S.E.M.

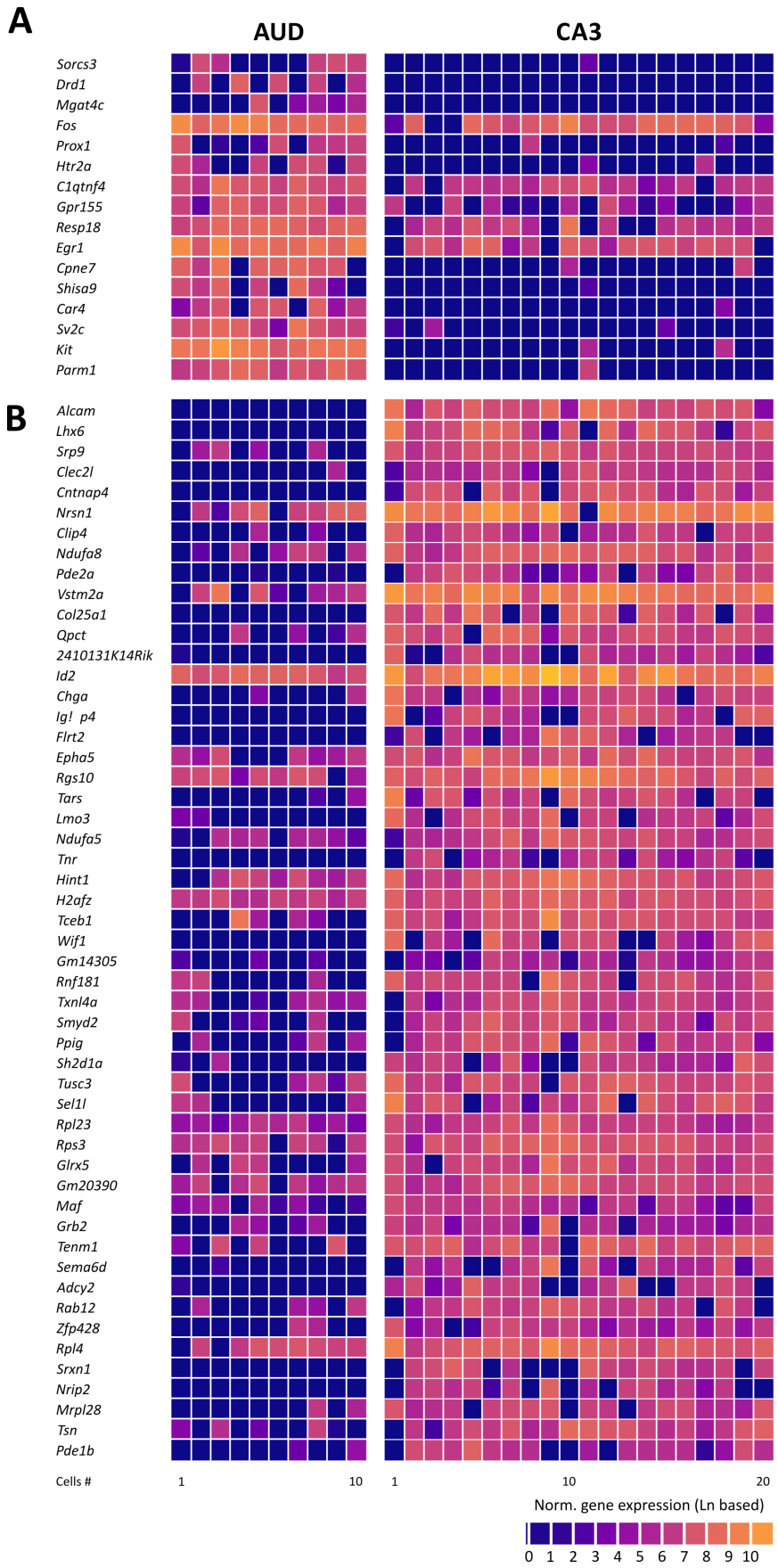

Figure 5.3: Differentially expressed genes in CA3 and AUD NPY-positive cells

A) Genes with higher expression in the AUD than CA3 with a p-value < 0.001.

B) Genes with higher expression in the CA3 than AUD with a p-value < 0.001 .

expressed in almost all AUD and CA3 neurons and the expression level did not differ between both regions. All recorded neurons expressed GABAergic markers *Gad1* and *Gad2*, no cells expressed the glutamatergic marker *Slc17a6* and only very few cells expressed *Slc17a7* in addition to GABAergic markers, confirming that the NPY-positive cells are all inhibitory neurons.

The expression of origin-dependent transcription factors confirms that AUD and CA3 NPY interneurons are partially originating from different regions. AUD NPY-expressing interneurons express transcription factors *Prox1*, *Nr2f1* and *Sox6*, suggesting CGE origin. However, in addition to these CGE markers, CA3 NPY neurons also express MGE-associated transcription factors, like *Lhx6*, *Satb1* and *Nkx2-1*. This suggests that AUD NGFCs are derived from the CGE, whereas the CA3 NGFCs have a mixed origin from both the CGE and MGE, which might also indicate other genes expression differences.

Despite the fact that the intrinsic parameters are broadly the same between CA3 and AUD NPY-positive cells, synaptic receptors do show differences in expression level. More than 300 differentially expressed genes (p-value < 0.01) for CA3 and AUD NPY-expressing interneurons were detected, some (76 out of 367 genes) higher expressed in the AUD but the majority showing higher expression in the CA3 (300 out of 367 genes) (Figure 5.3). These differentially expressed genes included the 5-HT receptors. Both the *Htr1b* and *Htr2a* receptor were more highly expressed in the AUD than CA3, with *Htr2a* having the highest expression of the two. Interestingly, *Htr3a*, which is shown to be expressed in PV- and SST-negative interneurons in the superficial neocortex, was minimally expressed in these neurons (Lee *et al.*, 2010; Rudy *et al.*, 2011).

5.3 Results

The data in this section has been collected by Sanne Beerens under supervision of Prof. Christian Wozny. The 5-HT_{2A} receptor is targeted by hallucinogenic substances and considered as a therapeutic target in schizophrenia (López-Giménez and González-Maeso, 2017; Kantrowitz, 2020). Serotonin receptors play an important role in depression but are also involved in hallucinations. Therefore, this can also be an explanation for hallucinogenic side-effect of anti-depressants (Cancelli, Marcon and Balestrieri, 2004) and targeting of specific cells and brain regions could therefore improve medicinal therapy. Differential expression of especially *Htr2a* in the CA3 and AUD is therefore interesting to study further. Whether the difference in *Htr2a* mRNA expression also results in differences in expression of the receptor is not clear from these scRNA sequencing results.

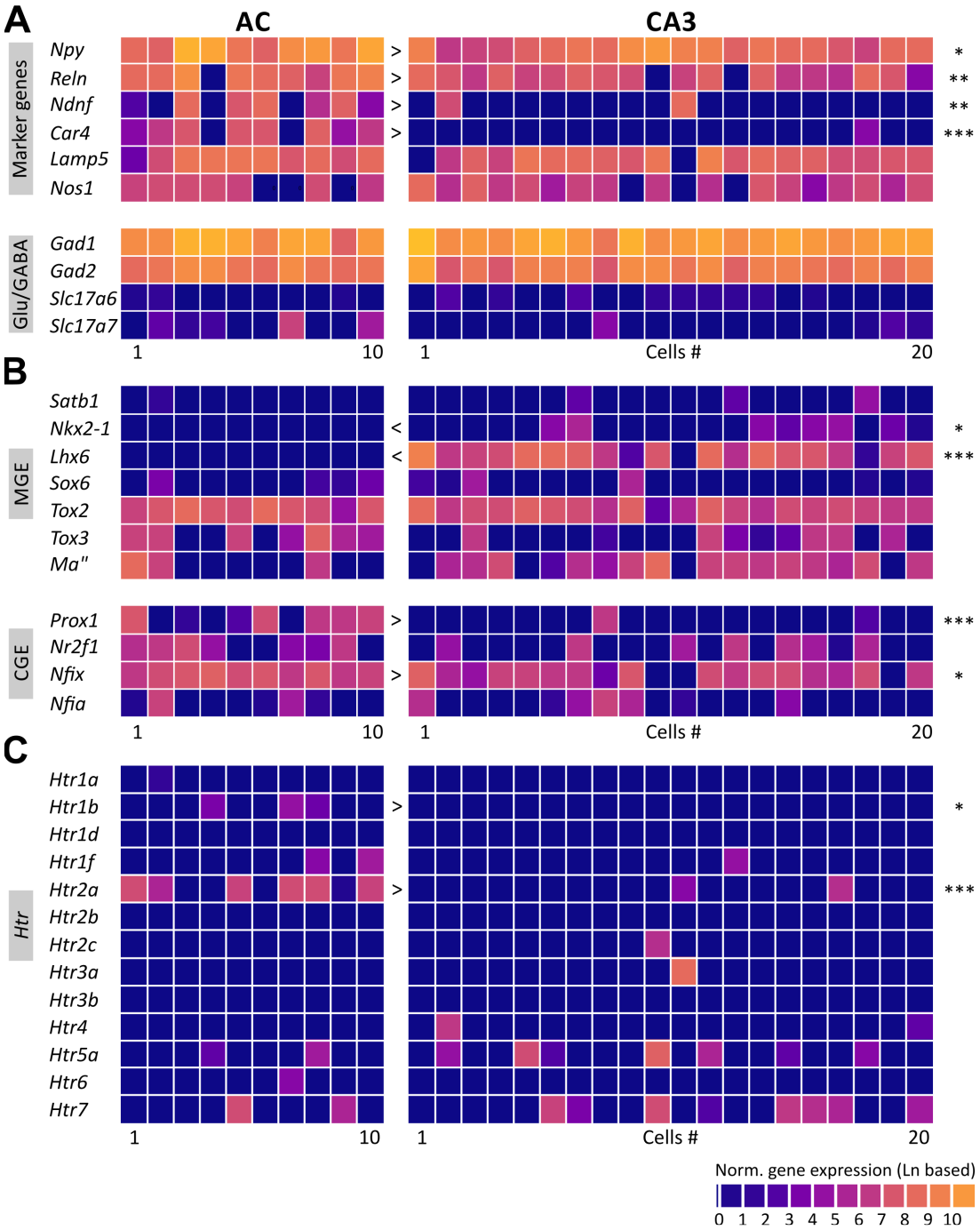

Figure 5.4: Gene expression profile of NGFCs in the CA3 and auditory cortex

A) Differentially expressed genes in CA3 vs AC NPY+ neurons, as well as the expression profile of inhibitory (*Gad1*, *Gad2*) and excitatory (*Slc17a6*, *Slc17a7*) neurons. B) Expression profile of MGE and CGE enriched genes to determine the origin of NGFCs cells in both regions. C) 5-HT receptor expression in CA3 and AC NPY+ neurons, showing significantly differential expression of *Htr1b* and *Htr2a*.

Therefore, we aimed to confirm the sequencing results by using pharmacological experiments. In order to do this, we performed slice patch-clamp recordings from NPY-GFP mice and used two different approaches: a 5-HT_{2A} receptor agonist (TCB-2), and 5-HT in combination with a 5-HT_{2A} antagonist (ketanserin).

5.3.1 The $5HT_{2A}$ agonist, TCB-2, did not affect AUD NGFCs and PFC pyramidal neurons

We chose TCB-2 as it has a high affinity for the 5-HT_{2A} receptor and is known as a potent and selective 5-HT_{2A} receptor agonist (McLean *et al.*, 2006; Fox *et al.*, 2010). We started to record from the AC, since we expected 5-HT_{2A} receptor expression in these cells based on the scRNA sequencing results (Figure 5.4C). After 2 minutes of baseline recording, the agonist TCB-2 (10 µM) was added to the perfusion solution and cells were recorded for 10 minutes. The application of TCB-

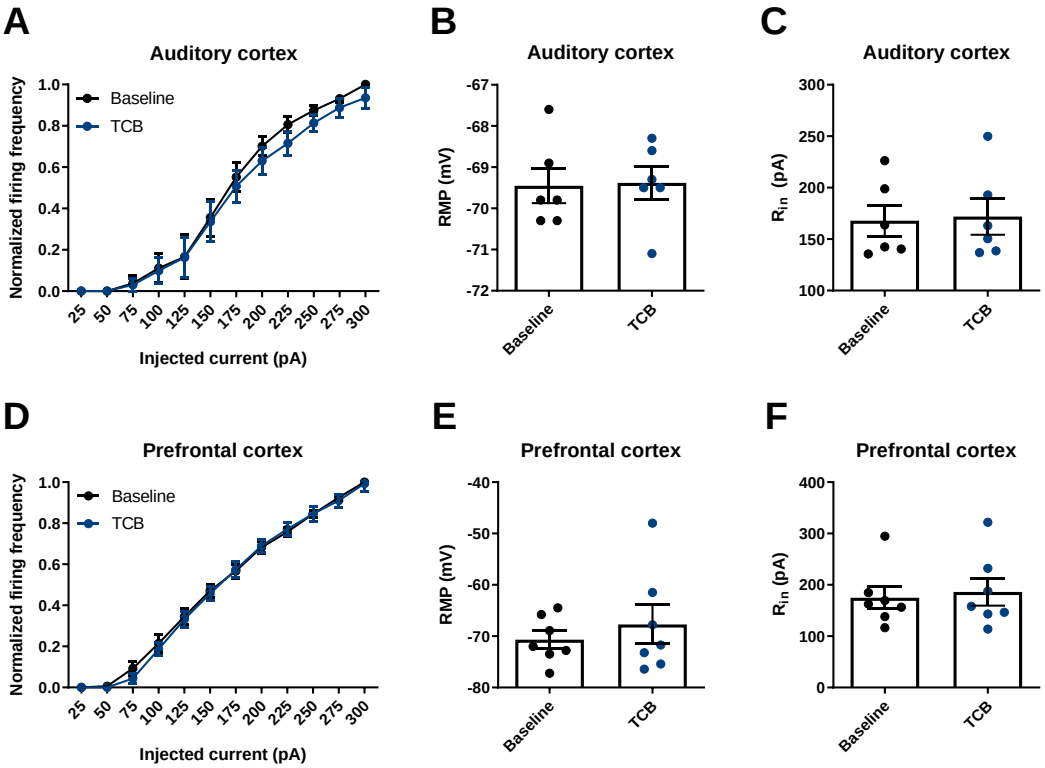

Figure 5.5: Application of a 5-HT_{2A} agonist does not induce changes in AUD and PFC NPY+ neurons

A) FI curve of NPY+ AC neurons during baseline recording and after application of TCB-2. Membrane potential was kept at -70mV. B) Resting membrane potential and C) input resistance before and after application of TCB-2. Input resistance was measured at resting membrane potential. D-F) Same as A-B but then for PFC L5 pyramidal cells, with the only difference that the MP was kept at -75mV in D. AC: n = 6; PFC: n = 7. Data presented as mean ± S.E.M.

2 did not result in any significant changes in membrane potential or input resistance (n = 6; t-test; RMP: p = 0.930, Input resistance: p = 0.421; Figure 5.5B,C). The frequency per current injection from the FI curve was not changed after TCB-2 application (two-way ANOVA, p = 0.540; Figure 5.5A).

Since the agonist did not result in any changes, we wanted to validate the working of TCB-2. Tian and colleagues previously published the effect of TCB-2 in prefrontal cortex layer 6 pyramidal cells (Tian, Schmidt and Lambe, 2016). They show a reduction in excitability of L6 pyramidal neurons after application of TCB-2. We decided to validate the working of TCB-2 by recording from layer 6 pyramidal neurons in the same way as Tian and colleagues did. Unfortunately, we were not able to replicate these results as the application of TCB-2 neither affected the firing frequency (n = 7; two-way ANOVA, p = 0.801), nor the RMP (t-test, p = 0.293) or the input resistance (t-test, p = 0.188; Figure 5.5B,C). The previous study had also shown a reduced excitability after TCB-2 application, which was not replicated by our results (Figure 5.5A). Possible explanations would be that the previous results are not reliable or that TCB-2 was not able to reach or activate the target. Since we have only used one batch of TCB-2 we can not exclude that another batch might have worked.

5.3.2 Application of the $5HT_{2A}$ antagonist, ketanserin, depolarizes AUD but not CA3 NGFCs

Since the application of an agonist did not show any effects, we tried a different approach. We decided to use 5-HT to activate all 5-HT receptors followed by the 5-HT_{2A}-specific antagonist ketanserin tartrate. After 2 minutes of baseline recording, 5-HT (30 µM) was added to the perfusion system and 10 minutes later ketanserin (10 µM) was added. The recording continued until t = 30 minutes. This antagonist is highly selective for the 5-HT_{2A}, although it also has affinity to the 5-HT_{1D} receptor. However, based on the scRNA-seq data, this receptor is neither expressed in AUD nor in CA3 NPY-positive neurons. In the AC, application of 5-HT increased RMP by 1.61 ± 0.65 mV, although not significantly (Figure 5.6A; n = 11; Tukey, p = 0.078), and application of ketanserin reduced this back to baseline levels (Figure 5.6A; Tukey; 5-HT vs ketanserin, p = 0.0063; Baseline vs ketanserin, p = 0.838). Change in RMP from baseline was significantly higher for 5-HT compared to ketanserin (t-test, p = 0.0032; Figure 5.6B), showing that ketanserin effectively counteracted the effect of 5-HT. When the same was repeated for the CA3, 5-HT was able to increase RMP by 1.72 ± 0.36 mV (n = 7; Tukey, p = 0.0051; Figure 5.6C) but this was not affected by the additional application of ketanserin

(Tukey, ketanserin vs 5-HT, p = 0.7812; Figure 5.6C). The change in RMP from baseline was also the same for 5-HT and ketanserin (t-test, p = 0.5173; Figure 5.6D), showing that the 5-HT_{2A} receptor antagonist was not effective in reducing the 5-HT effect. When plotting the time course of the RMP for both CA3 and AUD together, this also shows that cells from both regions depolarized after 5-HT reached the recording chamber at around 4 minutes, but only the AUD shows a decrease in RMP after ketanserin reached the bath after 14 minutes (Figure 5.6E). However, when looking at the FI curves, ketanserin seems to affect excitability only in the AUD for low current injections but this effect was not significant. On the other hand, ketanserin affected the excitability of neurons in both the AUD and CA3 for high current injections (Figure 5.6F,G). This could possibly be an effect of the long recording time instead of an effect of the drug per se, since the quality of the cell or seal might reduce with the recording time. To rule this out, a long recording without drug applications could be performed as a control. In conclusion, the pharmacological recordings were able to replicate the scRNA sequencing results,

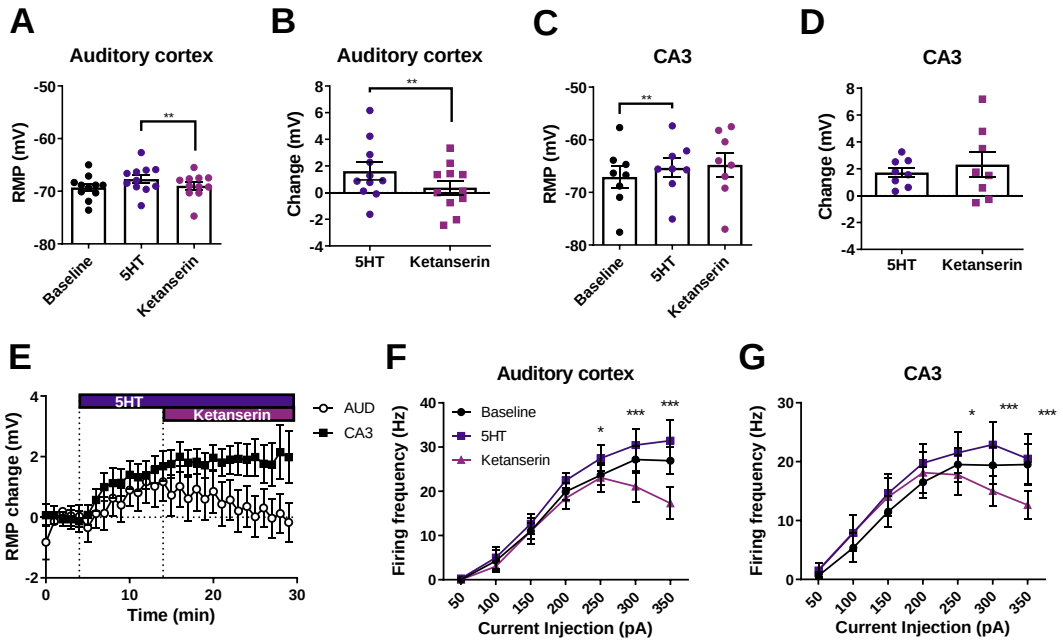

Figure 5.6: The 5-HT_{2A} antagonist, ketanserin, restores resting membrane potential in AUD, but not CA3, NGFCs.

A,C) Resting membrane potential during baseline, 5-HT and ketanserin application. B,D) Change of resting membrane potential compared to baseline after 5-HT and ketanserin application. E) Resting membrane potential over time for both CA3 and AC neurons. F,G) FI curve during baseline, 5-HT and ketanserin for F) AC and G) CA3. AC: n = 11; CA3: n = 7. Data presented as mean ± S.E.M.

proving that the change in RNA expression of *Htr2a* also resulted in changes in 5-HT_{2A} protein expression.

5.4 Discussion

Work from our collaboration showed that NPY neurons from AUD and CA3 are derived from different parts of the ganglionic eminence. The neurons from these regions also have differentially expressed genes, including *Htr2a*. We provide pharmacological experiments to examine if pharmacology would confirm the sequencing results, and to investigate if differential gene expression also resulted in differential protein expression. By applying the 5-HT_{2A} selective antagonist ketanserin in addition to 5-HT we show that indeed the 5-HT_{2A} receptor is selectively expressed in the AUD but not CA3 NPY-expressing interneurons.

5.4.1 Differences in gene expression

The scRNA-sequencing revealed more than 300 differentially expressed genes between AUD and CA3 NPY-expressing cells. This is about 6% of the total number of genes expressed in these cells. When comparing this to other sequencing studies, they show larger difference between cell types, but about a similar difference between cell types of different brain regions. For example, sequencing studies form the Allen Brain Institute found an average of about 4,000 differentially expressed genes (DEGs) between individual cell types (Tasic *et al.*, 2018). On the other hand, they found about 100-200 DEGs for corresponding cell types between cortical regions or cortex and hippocampus (Tasic *et al.*, 2018; Yao *et al.*, 2021). With a total of 9,500 genes per cell this is about 42% between individual cell types but only 1-2% for cell types between brain regions. Our data is thus in agreement with this finding and corresponds to differences between brain regions but not cell types. Therefore, the NPY-positive cells in our study might be different cell types but still very similar and possibly a continuum from the same cell type.

In terms of marker genes, NGFCs are usually identified by the expression of a combination of genes, like *Reln*, *Ndnf* and *Car4*. One gene that all NGFCs have in common is NPY. Nonetheless, not all NPY+ cells are NGFCs. For example, Ivy cells in the CA1 also express NPY but are a different class of interneurons (Fuentealba *et al.*, 2008). Therefore, NPY+ cells are best identified as NGFCs in combination with either electrophysiology or morphology or other marker genes. Recently, *Lamp5* has been identified as a marker for NGFCs (Yuste *et al.*, 2020), however, this marker has previously been shown to only be expressed in CGE-derived interneurons (Tasic *et al.*, 2018). On the other hand, Tasic and colleagues

mention a MGE-derived *Lamp5*-positive cell type, which might be a type of neurogliaform cell that was previously identified as a chandelier cell. In addition to this finding, our scRNA-seq results also show expression of *Lamp5* in combination with MGE-markers as *Lhx6*. Although Lamp5 was expressed in 100% of the NPY-cells in the auditory cortex, this was 90% for NPY-positive cells derived from the CA3. The cells not expressing *Lamp5* were positive for *Reln* and exhibited the classical neurogliaform late-spiking phenotype. Additionally, other markers like *Ndnf* and *Car4* were only partially expressed. This variation among marker expression might reflect different NGFC cell types (Overstreet-Wadiche and McBain, 2015; Webster *et al.*, 2021). Different types of NGFCs have been suggested, like nNOS+ and nNOS- cells, which might also be reflecting differential ganglionic eminence origin (Tricoire *et al.*, 2010). Based on the scRNA results presented in this chapter, the markers for NGFCs might be origin and/or brain region-specific, as *Car4* and *Ndnf* are expressed more in the AUD than the CA3.

5.4.2 Serotonin and excitability: intracellular signalling pathways

The two main types of serotonin receptors that have been studied in relation to neuronal excitability are 5-HT_{1A} and 5-$HT_{2A/C}$. It has been shown that 5-HT_{1A} stimulation increases K^+ currents through activation of GIRK channels and reduces calcium currents through inhibition of T-type Ca2+ channels leading to reduced excitability. In contrast, 5-HT_{2A} activation reduces K^+ currents resulting in increased excitation (Di Giovanni *et al.*, 2020).

It has also been shown that 5-HT-receptor activation affects NMDA-receptor trafficking to the membrane by affecting microtubule function (Yuen and Yan, 2007). Stimulation of 5-HT_{1A} receptors results in inhibition of protein kinase A (PKA) through $G_{i/o}$, which leads to reduced extracellular signal–regulated kinase (ERK) activation and thereby reduced microtubule-associated protein 2 (MAP2) phosphorylation. MAP2 binds and stabilizes microtubules in its phosphorylated form, meaning that 5-HT_{1A} stimulation reduces microtubule stability and NMDA trafficking, which results in less NMDA receptors present at the membrane. In contrast, 5-HT_{2A} activation stimulates beta-arrestin, which enhances PKA activity and thereby MAP2 phosphorylation through the same downstream pathway as 5-HT_{1A} receptors. Since 5-HT_{1A} is absent and 5-HT_{2A} is minimally expressed in CA3 NPY-positive neurons, this could explain why there is no effect of 5-HT on excitability. On the other hand, both 5-HT_{1A} is also absent from NPY-positive neurons in the AUD, which does not explain why there is also no effect of 5-HT on excitability in those neurons.

5.4.3 Limitations

A post-hoc power calculation shows that the ketanserin experiments are underpowered. For AUD recordings, a power of 28% in the change of RMP was achieved, whereas the number of cells per group would have to be increased to n = 42 to achieve a power of 80%.

Overall, we believe that this study is a good example for the use of combined transcriptomics and electrophysiological approaches. Unfortunately, morphological data is missing from out data set since cells cannot be reconstructed when performing single-cell RNA sequencing. Solely looking at either electrophysiology, morphology or transcriptomics might overlook different subclasses of neurons (Kim *et al.*, 2020). Neurons with the same transcriptomics profile might have different electrophysiological characteristics, or vice versa. Therefore, a combinatory approach is needed to discover and accurately classify neurons.

Chapter 6: Discussion

6.1 Summary of findings

The hippocampus is one of the main regions involved in learning and memory. Additionally, it has also been shown to be involved in a variety of disorders. In this thesis, three different projects have been presented centred on cellular diversity and hippocampal information processing in health and disease. In summary, in Chapter 3 we characterized the projection from the dSUB to the mPFC in detail. We showed that the dSUB mainly projects to the dorsal regions of the mPFC more posterior in this brain region. In terms of cell-type specificity, the dSUB projects to both excitatory and inhibitory neurons in the mPFC, but not neurogliaform cells.

In Chapter 4 we continued to investigate the dSUB but in relation to depressive-like behaviour. We show that our maternal separation model of depression results in mild phenotype of depressive-like behaviour. Mice could be grouped into being resilient or susceptible to early-life stress based on their overall behavioural z-score. One of the main findings from this chapter is an increase in stress-induced cFOS expression of the dSUB after maternal separation, indicating a possible role for the dSUB in stress coping which is sensitive to early-life stress. Additionally, we showed increased excitation of fast-spiking interneurons in the RSC by the dSUB after maternal separation, which could point towards an increase in feedforward inhibition to the RSC

Chapter 5 investigated the transcriptomic, electrophysiological and pharmacological differences between NPY-positive interneurons in the auditory cortex (AUD) and CA3 region of the hippocampus. This chapter provides a proof of concept to combine the transcriptomic and electrophysiological data derived from patch-seq experiments with results from pharmacological experiments to further characterize specific cell types. The example used in this chapter shows differences in *Htr2a* expression, encoding the 5-HT_{2A} receptor, in AUD- and CA3-derived NPY-positive interneurons. The respective absence or presence of this receptor was confirmed by pharmacological experiments when applying the 5-HT_{2A} antagonist ketanserin. Transcriptomic data shows that NPY-positive interneurons are probably derived from different parts of the ganglionic eminence during development, possibly explaining their differences in gene expression. Importantly, these results also challenge the finding that individual interneuron cell types as defined by transcriptomics are largely similar and shared between different brain regions, at least for NPY-positive interneurons, and indicates that region-specific subtypes of interneurons might exist.

There are several overall themes important in cell-type specific investigations that will be discussed below.

6.2 Cellular diversity: How much detail in cell type classification is needed?

Transcriptomic profiling of neurons has led to increased knowledge on developmental origin of neurons and the composition of the brain. The discovery of marker genes for subtypes of cells also enabled cell-type specific investigations of different cell types using Cre-specific expression of tools for visualization or manipulation. However, this approach also has some downsides.

One of these limitations is that the number of clusters after RNA sequencing and clustering analysis is determined by the sample size. A greater sample size allows for a higher resolution and the discovery of smaller clusters. For example, a previous study analysing the cell types in the visual cortex sequenced 1,600 cells and revealed the existence of 49 clusters containing 19 glutamatergic and 23 GABAergic clusters (Tasic *et al.*, 2016). However, a more recent study by the same group performed scRNA sequencing on the visual cortex and the motor cortex. They collected 23,822 single-cell transcriptomes and found 133 clusters containing 56 glutamatergic and 61 GABAergic cell types (Tasic *et al.*, 2018). Whereas glutamatergic clusters were mostly derived from only one of the two regions, the GABAergic clusters were almost exclusively shared between the regions, meaning that this increase in clusters was not caused by sampling from an additional cortical region. Therefore, researchers are looking into automatic classification of neurons to overcome some limitations of clustering that is currently used (Armañanzas and Ascoli, 2015).

An even more recent study by the Allen Institute for Brain Science sequenced the whole neocortex and revealed an even more detailed taxonomy (Yao *et al.*, 2021). This study also reveals that, in contrast to what Tasic and colleagues found in 2018, glutamatergic cell types are not highly distinct between regions, but rather form a gradient across multiple cortical regions. Since the motor cortex and visual cortex are not neighbouring regions this explains why they found distinct cell types in their earlier study. This also stresses the point that this clustering analysis is a great tool to group cells based on gene expression within a study, but that this might not add up to other studies based on the exact sample used. This gradient is not only reflected in the gene expression profile but also in morphology. It has been shown that the dendritic length and morphological

complexity of layer 2/3 pyramidal cells varies gradually along the rostrocaudal axis (Benavides-Piccione *et al.*, 2006). This also emphasizes that clustering is a mathematical approach to group neurons, but that this might not always be functionally relevant.

It also has to be considered until what level of detail this cell type classification is still informative. In other words, how fine should cell types be distinguished to be useful for understanding circuit function. The biological relevance of the gene clustering and taxonomy has also been studied, at least for interneurons (Paul *et al.*, 2017). It was shown that ~40 gene families are contributing to the distinction between cell types. These gene families are involved in biological processes of cell-adhesion molecules, neurotransmitter and modulator receptors, ion channels, membrane signalling pathways, neuropeptides and vesicular release and transcription factors, contributing to presynaptic and postsynaptic properties (Paul *et al.*, 2017; Huang and Paul, 2019). These findings indicate that clusters would also reflect functional differences between cell types. However, as mentioned in Chapter 1, cell types are often determined by the expression of multiple marker genes, making it difficult to apply the current cell-type specific techniques, for example, using Cre-dependent expression. The combination of Cre- and Flp-dependent expression using INRSECT specifies this a little further by being able to select cell types based on the expression of two genes, but it is still limited to this number of genes. Most cells might be explored with this technique, as estimated by Huang (Huang, 2014), but very specific cells characterized by the expression of more than two genes might be overlooked. Further specification of cell types incorporating more marker genes might increase knowledge on the existence of these cell types but current techniques might not be sufficient to study these very specific cell types.

Increased knowledge on cell type function is also relevant to understand circuit mechanisms of behaviour. To elucidate projection-specific cell types, combination of transcriptomic profiling and retrograde tracing have been used (Cembrowski, Wang, *et al.*, 2018; Tasic *et al.*, 2018). However, cells projecting to a region might still be a heterogeneous class, and cell types can project to multiple regions (Cembrowski, Phillips, *et al.*, 2018; Cembrowski, Wang, *et al.*, 2018), therefore this approach might not result in the most complete picture. Recent studies are trying to construct whole axons of neurons to show their projection targets, as demonstrated in a study by Peng and colleagues. They show distinct projection patterns for layer-specific intratelencephalic-projecting (IT) neurons (Peng *et al.*, 2021). Layer-specific projections for cortical layers have been shown

before, but this was not demonstrated for individual cell types within these layers before. This shows that even though IT neurons are considered somewhat a continuous class of neurons in terms of transcriptomic data (Tasic *et al.*, 2018), differences in terms of circuitries and projection patterns exist. Combining the discovery of markers for projection-defined subtypes of cells with *in vivo* techniques like chemo- or optogenetics or calcium imaging can then be used to study the role of these cell-specific projections in behaviour. An example of this is a recent study by Sánchez-Bellot and colleagues (Sánchez-Bellot *et al.*, 2022). They show that the ventral CA1-PFC projection consist of superficial- and deep-layer ventral CA1 neurons exhibiting opposing behavioural function. Simultaneous expression of different calcium indicators in superficial and deep neurons reveals differential activation during behaviour and subsequent optogenetic experiments confirmed contribution of these two classes of neurons to opposing behaviours. This study did not use transcriptomics but a known marker to distinguish between superficial and deep cells in the pyramidal layer of the ventral CA1. However, combining this with retrograde tracing and transcriptomics could provide more information on cell-type diversity for this projection.

A combination of transcriptomic cell type definition and behavioural involvement has to be applied to reveal functional relevant information on cell types. Electrophysiology, morphology, transcriptomics, connectivity and neural activity are necessary to elucidate behavioural relevance of cell-type classification. In perspective to psychiatric disorders, discovering affected cell types and corresponding circuitries for maladaptive behaviours might elucidate circuitry mechanisms for these disorders.

6.3 Optogenetics: an artificial approach

One of main technique that is used throughout this thesis is *in vitro* optogenetics. However, it has to be taken in mind that optogenetics is an artificial method to induce neuronal activity and study connectivity. Light-induced action potentials are accompanied by a larger calcium influx than electrically induced action potentials (Zhang and Oertner, 2007). This is most likely caused by activation of voltage-gated calcium channels during the after-depolarization following light stimulation, as photostimulation below the threshold for action potential generation did not result in Ca^{2+} influx (Zhang and Oertner, 2007). Additionally, increased release probability with light stimulation compared to electric stimulation is seen in paired recordings (Zhang and Oertner, 2007). This indicates that optogenetics does not completely resemble the endogenous situation in terms of current flow, but it is still

a valuable method to study connectivity.

When not using a transgenic line to express ChR2, this technique is also dependent on viral expression. Whereas the discovery of Cre-mediated virus expression has led to great discoveries in terms of cell-type specific function, viral expression is not always straight forward. For example, different viruses exist and are more or less selective for certain cells. There are different serotypes of AAV viruses, which are better at infecting certain cells or brain regions than others. For example, AAV6, AAV8 and AAV9 show best tropism for neurons in the cortex, whereas only transduction with AAV9 shows optimal expression the hippocampus (S. H. Chen *et al.*, 2019). AAVs viruses are used for their anterograde expression to visualize projection regions, however, some AAV serotypes have also been shown to have some retrograde properties or even trans-synaptic expression. AAV1 and 9 have been shown to facilitate expression in post-synaptic cells as demonstrated for injections in the visual cortex (Zingg *et al.*, 2019). Besides, serotypes 1 and 5 have been shown to travel retrogradely (Rotherme *et al.*, 2013). However, retrograde or trans-synaptic expression might be dependent on brain region or cell types that are targeted. For example, AAV5 has been shown to travel in a retrograde manner specifically for injections in the dentate gyrus, resulting in expression in the entorhinal cortex (Aschauer, Kreuz and Rumpel, 2013). All in all, AAV-mediated transgene expression is a great tool to visualize and manipulate projections but experiments have to be designed carefully by taking into account tropism and transport of the viral vector used.

In these experiments we have used a serotype 9 AAV virus, because this serotype has great tropism for cortical neurons (Aschauer, Kreuz and Rumpel, 2013). However, we used two different viral vectors in Chapter 3 and 4. This is also reflected in differential expression profiles of both injections (Figure 3.1B and Figure 4.10). The virus used in Chapter 3 is a virus containing a switch vector that is designed to express ChR2 in the presence of Cre, and mCherry in the absence of Cre. The virus from Chapter 4 also expressed ChR2 in the presence of Cre, but did not express anything in absence of Cre. Additionally, the Chapter 4 virus contained a WPRE sequence, which was absent in the switch vector virus. This sequence allows for more efficient transgene expression (Zufferey *et al.*, 1999), meaning that the switch vector might have been less efficient in expression. However, the titre of the virus also plays a role and it is difficult to say if the presence of the WPRE sequence is responsible for the different viral spread seen in Chapter 4.

Cre-mediated expression is a great tool for cell-specific expression but it has

been shown that it is not always very specific. It is shown that Cre-independent reproduction takes place during production of viral vectors, resulting in off-target expression of the transgene (Matsushita *et al.*, 2022). This also causes transgene expression from Cre-dependent viral vectors without the presence of Cre in wildtype mice (Botterill *et al.*, 2021). Recently, Matsushita and colleagues have designed a sequence, a unilateral spacer sequence (USS), that prevents this Cre-independent recombination when added to a viral construct (Matsushita *et al.*, 2022). This virus containing the USS was first design to express a fluorophore in Cre-negative cells, similar to the switch vector we used in Chapter 3. The design of this USS-containing virus is also similar to the switch vector design, where the Cre-independent mRuby sequence acts as the USS. This might indicate reduced Cre-independent recombination, which is also reflected in the specific expression of the vector in our experiments. In Chapter 3 we have characterized that ChR2 is indeed expressed in our target cells and not in surrounding regions, meaning that the Cre-mediated expression in our study was selective for the intended cells. Therefore, the virus might be less efficient because of the lacking WPRE sequence, but more specific because of the switch design.

Altogether, the research presented in this thesis has provided knowledge on cell specific processing in the hippocampus and cortex in wildtype mice and a mouse model of depression. The finding that the dorsal subiculum might play a role in stress coping after early-life stress is important for understanding brain circuitries involved in depression-affected stress sensitivity. Additionally, the projection from the dorsal subiculum to the prefrontal cortex that is characterized in this thesis might also play a role in depression, since both regions are implicated in depression. Further research would show if and how this projection contributes to depressive-like behaviour. Additionally, we have provided proof of concept for the combinatory use of electrophysiology, transcriptomics and pharmacology which showed differential gene expression and pharmacological responses within one type of interneuron. This technique might discover cell-type specific sensitivity to drugs or contribute to the development of drugs selective to certain cell types. The focus might be shifting from disorder-specific treatments to the design of symptom or brain-circuitry specific treatments. Therefore, this research might implicate a novel or more selective target for treatments for depression-associated cognitive deficits. Additionally, it stresses the point that cell type classification is essential for improvement of cell-type specific investigations, which provides more insight into the pathology of disorders on a cellular and circuitry level. This research is

essential for the development or more selective and specific treatments of disorders.

Bibliography

Aggleton, J. P. and Christiansen, K. (2015) 'The subiculum: The heart of the extended hippocampal system', *Progress in Brain Research*, 219, pp. 65–82. doi: 10.1016/bs.pbr.2015.03.003.

Akkerman, S. *et al.* (2012) 'Object recognition testing: Statistical considerations', *Behavioural Brain Research*, 232(2), pp. 317–322. doi: 10.1016/J.BBR.2012.03.024.

Albasser, M. M. *et al.* (2012) 'Evidence that the rat hippocampus has contrasting roles in object recognition memory and object recency memory.', *Behavioral Neuroscience*, 126(5), p. 659. doi: 10.1037/A0029754.

Alexander, W. H. and Brown, J. W. (2019) 'The Role of the Anterior Cingulate Cortex in Prediction Error and Signaling Surprise', *Topics in Cognitive Science*, 11(1), pp. 119–135. doi: 10.1111/tops.12307.

de Andrade, J. S. *et al.* (2013) 'Chronic unpredictable mild stress alters an anxiety-related defensive response, Fos immunoreactivity and hippocampal adult neurogenesis', *Behavioural Brain Research*, 250, pp. 81–90. doi: 10.1016/j.bbr.2013.04.031.

Armañanzas, R. and Ascoli, G. A. (2015) 'Towards Automatic Classification of Neurons', *Trends in neurosciences*, 38(5), p. 307. doi: 10.1016/J.TINS.2015.02.004.

Aschauer, D. F., Kreuz, S. and Rumpel, S. (2013) 'Analysis of Transduction Efficiency, Tropism and Axonal Transport of AAV Serotypes 1, 2, 5, 6, 8 and 9 in the Mouse Brain', *PLoS ONE*. Edited by J. Qiu, 8(9), p. e76310. doi: 10.1371/journal.pone.0076310.

Ascoli, G. A. *et al.* (2008) 'Petilla terminology: Nomenclature of features of GABAergic interneurons of the cerebral cortex', *Nature Reviews Neuroscience*, pp. 557–568. doi: 10.1038/nrn2402.

Beerens, S. *et al.* (2021) 'Probing subicular inputs to the medial prefrontal cortex', *iScience*, 24(8), p. 102856. doi: 10.1016/j.isci.2021.102856.

Beerens, S. *et al.* (2022) 'Transcriptomically-Guided Pharmacological Experiments in Neocortical and Hippocampal NPY-Positive GABAergic Interneurons', *eNeuro*, 9(2), p. ENEURO.0005-22.2022. doi: 10.1523/ENEURO.0005-

22.2022.

Benavides-Piccione, R. *et al.* (2006) 'Dendritic Size of Pyramidal Neurons Differs among Mouse Cortical Regions', *Cerebral Cortex*, 16(7), pp. 990–1001. doi: 10.1093/CERCOR/BHJ041.

Bian, Y. *et al.* (2021) 'Prolonged Maternal Separation Induces the Depression-Like Behavior Susceptibility to Chronic Unpredictable Mild Stress Exposure in Mice', *BioMed Research International*, 2021. doi: 10.1155/2021/6681397.

Bienkowski, M. S. *et al.* (2018) 'Integration of gene expression and brain-wide connectivity reveals the multiscale organization of mouse hippocampal networks', *Nature Neuroscience*, 21(November), pp. 1628–1643. doi: 10.1038/s41593-018-0241-y.

Biselli, T. *et al.* (2019) 'Optogenetic and chemogenetic insights into the neurocircuitry of depression-like behaviour: A systematic review', *European Journal of Neuroscience*, (November 2018), pp. 1–30. doi: 10.1111/ ejn.14603.

Böhm, C. *et al.* (2015) 'Functional diversity of subicular principal cells during hippocampal ripples', *Journal of Neuroscience*, 35(40), pp. 13608–13618. doi: 10.1523/JNEUROSCI.5034-14.2015.

Boldrini, M. *et al.* (2009) 'Antidepressants increase neural progenitor cells in the human hippocampus', *Neuropsychopharmacology*, 34(11), pp. 2376–2389. doi: 10.1038/npp.2009.75.

Bonapersona, V. *et al.* (2019) 'The behavioral phenotype of early life adversity: A 3 -level meta-analysis of rodent studies', *Neuroscience & Biobehavioral Reviews*, 102, pp. 299–307. doi: 10.1016/J.NEUBIOREV.2019.04.021.

Booeshaghi, A. S. *et al.* (2021) 'Isoform cell-type specificity in the mouse primary motor cortex', *Nature*, 598(7879), pp. 195–199. doi: 10.1038/s41586-021-03969-3.

Botterill, J. J. *et al.* (2021) 'Off-Target Expression of Cre-Dependent Adeno-Associated Viruses in Wild-Type C57BL/6J Mice', *eNeuro*, 8(6), pp. 363–384. doi: 10.1523/ENEURO.0363-21.2021.

Boyden, E. S. *et al.* (2005) 'Millisecond-timescale, genetically targeted optical control of neural activity', *Nature Neuroscience*, 8(9), pp. 1263–1268. doi:

10.1038/NN1525.

Brennan, E. K. W. *et al.* (2020) 'Hyperexcitable Neurons Enable Precise and Persistent Information Encoding in the Superficial Retrosplenial Cortex', *Cell Reports*, 30(5), pp. 1598-1612.e8. doi: 10.1016/J.CELREP.2019.12.093.

Butt, S. J. B. *et al.* (2005) 'The temporal and spatial origins of cortical interneurons predict their physiological subtype', *Neuron*, 48(4), pp. 591–604. doi: 10.1016/J.NEURON.2005.09.034/ATTACHMENT/9FD0147B-EC74-4EB5-A758-B052EE746203/MMC1.PDF.

Cadwell, C. R. *et al.* (2016) 'Electrophysiological, transcriptomic and morphologic profiling of single neurons using Patch-seq', *Nature biotechnology*, 34(2), pp. 199–203. doi: 10.1038/NBT.3445.

Cancelli, I., Marcon, G. and Balestrieri, M. (2004) 'Factors associated with complex visual hallucinations during antidepressant treatment', *Human Psychopharmacology*. Hum Psychopharmacol, pp. 577–584. doi: 10.1002/hup.640.

Cembrowski, M. S. *et al.* (2016) 'Spatial Gene-Expression Gradients Underlie Prominent Heterogeneity of CA1 Pyramidal Neurons', *Neuron*, 89(2), pp. 351–368. doi: 10.1016/j.neuron.2015.12.013.

Cembrowski, M. S., Phillips, M. G., *et al.* (2018) 'Dissociable Structural and Functional Hippocampal Outputs via Distinct Subiculum Cell Classes', *Cell*, 173(5), pp. 1280-1292.e18. doi: 10.1016/j.cell.2018.03.031.

Cembrowski, M. S., Wang, L., *et al.* (2018) 'The subiculum is a patchwork of discrete subregions', *eLife*, 7, p. e37701. doi: 10.7554/eLife.37701.

Chaudhury, D., Liu, H. and Han, M. H. (2015) 'Neuronal correlates of depression', *Cellular and Molecular Life Sciences*. Birkhauser Verlag AG, pp. 4825–4848. doi: 10.1007/s00018-015-2044-6.

Chen, B. *et al.* (2001) 'Increased hippocampal bdnf immunoreactivity in subjects treated with antidepressant medication', *Biological Psychiatry*, 50(4), pp. 260–265. doi: 10.1016/S0006-3223(01)01083-6.

Chen, K. H. *et al.* (2015) 'Spatially resolved, highly multiplexed RNA profiling in single cells', *Science*, 348(6233), p. 412. doi: 10.1126/science.aaa6090.

Chen, S. H. *et al.* (2019) 'Overview: Recombinant Viral Vectors as Neuroscience

Tools', *Current protocols in neuroscience*, 87(1), p. e67. doi: 10.1002/CPNS.67.

Chen, X. *et al.* (2019) 'High-Throughput Mapping of Long-Range Neuronal Projection Using In Situ Sequencing', *Cell*, 179(3), pp. 772-786.e19. doi: 10.1016/J.CELL.2019.09.023.

Chen, Yiwen *et al.* (2022) 'Early Life Stress Induces Different Behaviors in Adolescence and Adulthood May Related With Abnormal Medial Prefrontal Cortex Excitation/Inhibition Balance', *Frontiers in Neuroscience*, 15, p. 1771. doi: 10.3389/FNINS.2021.720286/BIBTEX.

Cole, J. *et al.* (2010) 'Subregional hippocampal deformations in major depressive disorder', *Journal of Affective Disorders*, 126(1–2), pp. 272–277. doi: 10.1016/j.jad.2010.03.004.

Commons, K. G. *et al.* (2017) 'The Rodent Forced Swim Test Measures Stress-Coping Strategy, Not Depression-like Behavior', *ACS Chemical Neuroscience*. American Chemical Society, pp. 955–960. doi: 10.1021/acschemneuro.7b00042.

Corcoran, K. A. *et al.* (2018) 'Role of Retrosplenial Cortex in Processing Stress-Related Context Memories', *Behavioral neuroscience*, 132(5), p. 388. doi: 10.1037/BNE0000223.

Covington, H. E. *et al.* (2010) 'Antidepressant effect of optogenetic stimulation of the medial prefrontal cortex.', *The Journal of neuroscience : the official journal of the Society for Neuroscience*, 30(48), pp. 16082–90. doi: 10.1523/JNEUROSCI.1731-10.2010.

Cryan, J. F., Hoyer, D. and Markou, A. (2003) 'Withdrawal from chronic amphetamine induces Depressive-Like behavioral effects in rodents', *Biological Psychiatry*, 54(1), pp. 49–58. doi: 10.1016/S0006-3223(02)01730-4.

Dalla, C. *et al.* (2005) 'Chronic mild stress impact: are females more vulnerable?', *Neuroscience*, 135(3), pp. 703–714. doi: 10.1016/J.NEUROSCIENCE.2005.06.068.

Darcet, F. *et al.* (2016) 'Cognitive Dysfunction in Major Depressive Disorder. A Translational Review in Animal Models of the Disease', *Pharmaceuticals*, 9 (1), p. 9. doi: 10.3390/ph9010009.

Defelipe, J. *et al.* (2013) 'New insights into the classification and nomenclature of cortical GABAergic interneurons', *Nature Reviews Neuroscience 2013 14:3*, 14(3), pp. 202–216. doi: 10.1038/nrn3444.

Denninger, J. K., Smith, B. M. and Kirby, E. D. (2018) 'Novel object recognition and object location behavioral testing in mice on a budget', *Journal of Visualized Experiments*, 2018(141), p. 58593. doi: 10.3791/58593.

Ding, S.-L. *et al.* (2020) 'Distinct Transcriptomic Cell Types and Neural Circuits of the Subiculum and Prosubiculum along the Dorsal-Ventral Axis', *Cell Reports*, 31(7), p. 107648. doi: 10.1016/j.celrep.2020.107648.

Dong, H.-W. *et al.* (2009) 'Genomic-anatomic evidence for distinct functional domains in hippocampal field CA1', *Proceedings of the National Academy of Sciences of the United States of America*, 106(28), pp. 11794–11799. doi: 10.1073/pnas.0812608106.

Drevets, W. C. *et al.* (1997) 'Subgenual prefrontal cortex abnormalities in mood disorders', *Nature*, 386(6627), pp. 824–827. doi: 10.1038/386824a0.

Estanislau, C. (2013) 'Cues to the usefulness of grooming behavior in the evaluation of anxiety in the elevated plus-maze.', *Psychology & Neuroscience*, 5(1), p. 105. doi: 10.3922/J.PSNS.2012.1.14.

Fanselow, M. S. and Dong, H.-W. (2010) 'Are the Dorsal and Ventral Hippocampus Functionally Distinct Structures?', *Neuron*, 65(1), pp. 7–19. doi: 10.1016/ j.neuron.2009.11.031.

Fenno, L. E. *et al.* (2014) 'INTRSECT: single-component targeting of cells using multiple-feature Boolean logic', *Nature methods*, 11(7), p. 763. doi: 10.1038/ NMETH.2996.

Ferreira-Fernandes, E. *et al.* (2019) 'A Gradient of Hippocampal Inputs to the Medial Mesocortex', *Cell Reports*, 29(10), pp. 3266-3279.e3. doi: 10.1016/ j.celrep.2019.11.011.

Fisher, D. W. *et al.* (2018) 'HCN channels in the hippocampus regulate active coping behavior', *Journal of neurochemistry*, 146(6), p. 753. doi: 10.1111/ JNC.14539.

Floriou-Servou, A. *et al.* (2018) 'Distinct Proteomic, Transcriptomic, and Epigenetic Stress Responses in Dorsal and Ventral Hippocampus', *Biological*

Psychiatry, 84(7), pp. 531–541. doi: 10.1016/j.biopsych.2018.02.003.

Fox, M. A. *et al.* (2010) 'The serotonin 5-HT2A receptor agonist TCB-2: A behavioral and neurophysiological analysis', *Psychopharmacology*, 212(1), pp. 13–23. doi: 10.1007/S00213-009-1694-1/FIGURES/6.

Fuentealba, P. *et al.* (2008) 'Ivy Cells: A Population of Nitric-Oxide-Producing, Slow -Spiking GABAergic Neurons and Their Involvement in Hippocampal Network Activity', *Neuron*, 57(6), pp. 917–929. doi: 10.1016/J.NEURON.2008.01.034/ ATTACHMENT/D2695D19-870F-4DD8-96BE-88368E94B54C/MMC1.PDF.

Fuzik, J. *et al.* (2015) 'Integration of electrophysiological recordings with single-cell RNA-seq data identifies neuronal subtypes', *Nature Biotechnology 2015 34:2*, 34(2), pp. 175–183. doi: 10.1038/nbt.3443.

Gandal, M. J. *et al.* (2018) 'Transcriptome-wide isoform-level dysregulation in ASD, schizophrenia, and bipolar disorder', *Science*, 362(6420). doi: 10.1126/ SCIENCE.AAT8127/SUPPL_FILE/AAT8127_TABLE_S9.XLSX.

George, E. D. *et al.* (2010) 'Maternal separation with early weaning: A novel mouse model of early life neglect', *BMC Neuroscience*, 11(1), p. 123. doi: 10.1186/1471-2202-11-123.

Gerfen, C. R., Paletzki, R. and Heintz, N. (2013) 'GENSAT BAC Cre-recombinase driver lines to study the functional organization of cerebral cortical and basal ganglia circuits', *Neuron*, 80(6), pp. 1368–1383. doi: 10.1016/ J.NEURON.2013.10.016.

Di Giovanni, G. *et al.* (2020) 'Serotonergic control of excitability: from neuron to networks', *Handbook of Behavioral Neuroscience*, 31, pp. 197–215. doi: 10.1016/B978-0-444-64125-0.00010-4.

Goodwill, H. L. *et al.* (2018) 'Early Life Stress Drives Sex-Selective Impairment in Reversal Learning by Affecting Parvalbumin Interneurons in Orbitofrontal Cortex of Mice', *Cell Reports*, 25(9), pp. 2299-2307.e4. doi: 10.1016/ J.CELREP.2018.11.010/ATTACHMENT/E119A22E-DA57-457F-9468-B3E8727B612D/MMC1.PDF.

Gorman-Sandler, E. and Hollis, F. (2022) 'The forced swim test: Giving up on behavioral despair (Commentary on Molendijk & de Kloet, 2021)', *European Journal of Neuroscience*, 55(9–10), pp. 2832–2835. doi: 10.1111/EJN.15270.

Gould, N. F. *et al.* (2007) 'Performance on a virtual reality spatial memory navigation task in depressed patients', *American Journal of Psychiatry*, 164 (3), pp. 516–519. doi: 10.1176/ajp.2007.164.3.516.

Guilloux, J. P. *et al.* (2011) 'Integrated behavioral z-scoring increases the sensitivity and reliability of behavioral phenotyping in mice: Relevance to emotionality and sex', *Journal of Neuroscience Methods*, 197(1), pp. 21–31. doi: 10.1016/J.JNEUMETH.2011.01.019.

Gurok, U. *et al.* (2004) 'Gene Expression Changes in the Course of Neural Progenitor Cell Differentiation', *The Journal of Neuroscience*, 24(26), p. 5982. doi: 10.1523/JNEUROSCI.0809-04.2004.

Hamani, C., Diwan, M., Macedo, C. E., *et al.* (2010) 'Antidepressant-Like Effects of Medial Prefrontal Cortex Deep Brain Stimulation in Rats', *Biological Psychiatry*, 67(2), pp. 117–124. doi: 10.1016/J.BIOPSYCH.2009.08.025.

Hamani, C., Diwan, M., Isabella, S., *et al.* (2010) 'Effects of different stimulation parameters on the antidepressant-like response of medial prefrontal cortex deep brain stimulation in rats', *Journal of Psychiatric Research*, 44(11), pp. 683–687. doi: 10.1016/J.JPSYCHIRES.2009.12.010.

Hao, Y. *et al.* (2019) 'Selecting an appropriate animal model of depression', *International Journal of Molecular Sciences*. MDPI AG. doi: 10.3390/ ijms20194827.

Hao, Z. Y. *et al.* (2020) 'Abnormal resting-state functional connectivity of hippocampal subfields in patients with major depressive disorder', *BMC Psychiatry*, 20(1), p. 71. doi: 10.1186/s12888-020-02490-7.

Harris, J. A. *et al.* (2014) 'Anatomical characterization of Cre driver mice for neural circuit mapping and manipulation', *Frontiers in Neural Circuits*, 8(JULY), p. 76. doi: 10.3389/FNCIR.2014.00076/ABSTRACT.

Harris, K. D. and Shepherd, G. M. G. (2015) 'The neocortical circuit: themes and variations', *Nature Neuroscience 2015 18:2*, 18(2), pp. 170–181. doi: 10.1038/nn.3917.

He, M. *et al.* (2016) 'Strategies and Tools for Combinatorial Targeting of GABAergic Neurons in Mouse Cerebral Cortex', *Neuron*, 91(6), pp. 1228–1243. doi: 10.1016/j.neuron.2016.08.021.

Heilbronner, S. R. and Hayden, B. Y. (2016) 'Dorsal Anterior Cingulate Cortex: A Bottom-Up View', *Annual Review of Neuroscience*, 39(1), pp. 149–170. doi: 10.1146/annurev-neuro-070815-013952.

Henningsen, K. *et al.* (2009) 'Cognitive deficits in the rat chronic mild stress model for depression: Relation to anhedonic-like responses', *Behavioural Brain Research*, 198(1), pp. 136–141. doi: 10.1016/j.bbr.2008.10.039.

Herman, J. P. and Mueller, N. K. (2006) 'Role of the ventral subiculum in stress integration', *Behavioural Brain Research*. Elsevier, pp. 215–224. doi: 10.1016/j.bbr.2006.05.035.

Hestrin, S. and Armstrong, W. E. (1996) 'Morphology and Physiology of Cortical Neurons in Layer I', *The Journal of Neuroscience*, 16(17), pp. 5290–5300. doi: 10.1523/JNEUROSCI.16-17-05290.1996.

Ho, T. C. *et al.* (2022) 'Subcortical shape alterations in major depressive disorder: Findings from the ENIGMA major depressive disorder working group', *Human Brain Mapping*, 43(1), pp. 341–351. doi: 10.1002/hbm.24988.

Hooks, B. M. *et al.* (2015) 'Dual-Channel Circuit Mapping Reveals Sensorimotor Convergence in the Primary Motor Cortex', *Journal of Neuroscience*, 35(10), pp. 4418–4426. doi: 10.1523/JNEUROSCI.3741-14.2015.

Hooks, B. M. (2018) 'Dual-Channel Photostimulation for Independent Excitation of Two Populations', *Current Protocols in Neuroscience*, 85(1), p. e52. doi: 10.1002/cpns.52.

Hoover, W. B. and Vertes, R. P. (2007) 'Anatomical analysis of afferent projections to the medial prefrontal cortex in the rat', *Brain Structure and Function*, 212 (2), pp. 149–179. doi: 10.1007/s00429-007-0150-4.

Hu, C. *et al.* (2017) 'Re-evaluation of the interrelationships among the behavioral tests in rats exposed to chronic unpredictable mild stress', *PLoS ONE*, 12(9). doi: 10.1371/journal.pone.0185129.

Hu, H., Gan, J. and Jonas, P. (2014) 'Fast-spiking, parvalbumin+ GABAergic interneurons: From cellular design to microcircuit function', *Science*, 345 (6196). doi: 10.1126/SCIENCE.1255263.

Huang, Z. J. (2014) 'Toward a genetic dissection of cortical circuits in the mouse', *Neuron*. NIH Public Access, pp. 1284–1302. doi: 10.1016/

j.neuron.2014.08.041.

Huang, Z. J. and Paul, A. (2019) 'The diversity of GABAergic neurons and neural communication elements', *Nature Reviews Neuroscience 2019 20:9*, 20(9), pp. 563–572. doi: 10.1038/s41583-019-0195-4.

Hyman, J. M., Holroyd, C. B. and Seamans, J. K. (2017) 'A Novel Neural Prediction Error Found in Anterior Cingulate Cortex Ensembles', *Neuron*, 95(2), pp. 447 -456.e3. doi: 10.1016/J.NEURON.2017.06.021.

Iñiguez, S. D. *et al.* (2014) 'Social defeat stress induces a depression-like phenotype in adolescent male c57BL/6 mice', *Stress*, 17(3), pp. 247–255. doi: 10.3109/10253890.2014.910650.

Ishihara, Y. and Fukuda, T. (2016) 'Immunohistochemical investigation of the internal structure of the mouse subiculum', *Neuroscience*, 337, pp. 242–266. doi: 10.1016/j.neuroscience.2016.09.027.

Jay, T. M. and Witter, M. P. (1991) 'Distribution of hippocampal CA1 and subicular efferents in the prefrontal cortex of the rat studied by means of anterograde transport of Phaseolus vulgaris-leucoagglutinin', *Journal of Comparative Neurology*, 313(4), pp. 574–586. doi: 10.1002/cne.903130404.

Jeffery, K. J. *et al.* (2019) 'Space and Memory (Far) Beyond the Hippocampus: Many Subcortical Structures Also Support Cognitive Mapping and Mnemonic Processing'. doi: 10.3389/fncir.2019.00052.

Kanari, L. *et al.* (2019) 'Objective Morphological Classification of Neocortical Pyramidal Cells', *Cerebral Cortex*, 29(4), pp. 1719–1735. doi: 10.1093/ cercor/bhy339.

Kantrowitz, J. T. (2020) 'Targeting Serotonin 5-HT2A Receptors to Better Treat Schizophrenia: Rationale and Current Approaches', *CNS Drugs*. Adis. doi: 10.1007/s40263-020-00752-2.

Karege, F. *et al.* (2002) 'Decreased serum brain-derived neurotrophic factor levels in major depressed patients', *Psychiatry Research*, 109(2), pp. 143–148. doi: 10.1016/S0165-1781(02)00005-7.

Karege, F. *et al.* (2005) 'Neurotrophin levels in postmortem brains of suicide victims and the effects of antemortem diagnosis and psychotropic drugs', *Molecular Brain Research*, 136(1–2), pp. 29–37. doi: 10.1016/

J.MOLBRAINRES.2004.12.020.

Kawaguchi, Y. (1995) 'Physiological subgroups of nonpyramidal cells with specific morphological characteristics in layer II/III of rat frontal cortex', *Journal of Neuroscience*, 15(4), pp. 2638–2655. doi: 10.1523/jneurosci.15-04-02638.1995.

Kempermann, G. and Kronenberg, G. (2003) 'Depressed new Neurons?—Adult hippocampal neurogenesis and a cellular plasticity hypothesis of major depression', *Biological Psychiatry*, 54(5), pp. 499–503. doi: 10.1016/S0006-3223(03)00319-6.

Kessaris, N. *et al.* (2014) 'Genetic programs controlling cortical interneuron fate', *Current Opinion in Neurobiology*, 26, pp. 79–87. doi: 10.1016/J.CONB.2013.12.012.

Killcross, S. and Coutureau, E. (2003) 'Coordination of Actions and Habits in the Medial Prefrontal Cortex of Rats', *Cerebral Cortex*, 13(4), pp. 400–408. doi: 10.1093/cercor/13.4.400.

Kim, C. S., Brager, D. H. and Johnston, D. (2018) 'Perisomatic changes in h-channels regulate depressive behaviors following chronic unpredictable stress', *Molecular Psychiatry*, 23(4), pp. 892–903. doi: 10.1038/mp.2017.28.

Kim, C. S. and Johnston, D. (2018) 'A Possible Link Between HCN Channels and Depression', *Chronic Stress*. SAGE Publications, p. 247054701878778. doi: 10.1177/2470547018787781.

Kim, E. J. *et al.* (2020) 'Extraction of Distinct Neuronal Cell Types from within a Genetically Continuous Population', *Neuron*, 107(2), pp. 274-282.e6. doi: 10.1016/j.neuron.2020.04.018.

Kim, Y. and Spruston, N. (2012) 'Target-specific output patterns are predicted by the distribution of regular-spiking and bursting pyramidal neurons in the subiculum', *Hippocampus*, 22(4), pp. 693–706. doi: 10.1002/hipo.20931.

Kinnavane, L. *et al.* (2018) 'Collateral Projections Innervate the Mammillary Bodies and Retrosplenial Cortex: A New Category of Hippocampal Cells', *eNeuro*, 5 (1). doi: 10.1523/ENEURO.0383-17.2018.

Kinnavane, L., Albasser, M. M. and Aggleton, J. P. (2015) 'Advances in the behavioural testing and network imaging of rodent recognition memory',

Behavioural Brain Research, 285, pp. 67–78. doi: 10.1016/j.bbr.2014.07.049.

Kitanishi, T., Umaba, R. and Mizuseki, K. (2021) 'Robust information routing by dorsal subiculum neurons', *Science Advances*, 7(11). doi: 10.1126/sciadv.abf1913.

Kjelstrup, K. G. *et al.* (2002) 'Reduced fear expression after lesions of the ventral hippocampus', *Proceedings of the National Academy of Sciences of the United States of America*, 99(16), pp. 10825–10830. doi: 10.1073/pnas.152112399.

Klapoetke, N. C. *et al.* (2014) 'Independent Optical Excitation of Distinct Neural Populations', *Nature methods*, 11(3), p. 338. doi: 10.1038/NMETH.2836.

Klein, J. *et al.* (2010) 'Lesion of the medial prefrontal cortex and the subthalamic nucleus selectively affect depression-like behavior in rats', *Behavioural Brain Research*, 213(1), pp. 73–81. doi: 10.1016/j.bbr.2010.04.036.

Knable, M. B. *et al.* (2004) 'Molecular abnormalities of the hippocampus in severe psychiatric illness: postmortem findings from the Stanley Neuropathology Consortium', *Molecular Psychiatry 2004 9:6*, 9(6), pp. 609–620. doi: 10.1038/sj.mp.4001471.

Knierim, J. J., Neunuebel, J. P. and Deshmukh, S. S. (2014) 'Functional correlates of the lateral and medial entorhinal cortex: Objects, path integration and local - Global reference frames', *Philosophical Transactions of the Royal Society B: Biological Sciences*. doi: 10.1098/rstb.2013.0369.

Knox, D. *et al.* (2021) 'Maternal Separation Induces Sex-Specific Differences in Sensitivity to Traumatic Stress', *Frontiers in Behavioral Neuroscience*, 15, p. 312. doi: 10.3389/FNBEH.2021.766505/BIBTEX.

Krishnan, V. and Nestler, E. J. (2011) 'Animal models of depression: Molecular perspectives', *Current Topics in Behavioral Neurosciences*, 7(1), pp. 121–147. doi: 10.1007/7854_2010_108.

Ku, S. P. *et al.* (2017) 'Regional specific evidence for memory-load dependent activity in the dorsal subiculum and the lateral entorhinal cortex', *Frontiers in Systems Neuroscience*, 11, p. 51. doi: 10.3389/fnsys.2017.00051.

de Landeta, A. B. *et al.* (2020) 'Anterior retrosplenial cortex is required for long-term object recognition memory', *Scientific Reports*, 10(1), pp. 1–13. doi:

10.1038/s41598-020-60937-z.

Lee, S. *et al.* (2010) 'The Largest Group of Superficial Neocortical GABAergic Interneurons Expresses Ionotropic Serotonin Receptors', *Journal of Neuroscience*, 30(50), pp. 16796–16808. doi: 10.1523/JNEUROSCI.1869-10.2010.

Leger, M. *et al.* (2013) 'Object recognition test in mice', *Nature Protocols*, 8(12), pp. 2531–2537. doi: 10.1038/nprot.2013.155.

Lehtinen, K., Nokia, M. S. and Takala, H. (2022) 'Red Light Optogenetics in Neuroscience', *Frontiers in Cellular Neuroscience*, 15, p. 532. doi: 10.3389/FNCEL.2021.778900/BIBTEX.

Lein, E. S. *et al.* (2007) 'Genome-wide atlas of gene expression in the adult mouse brain', *Nature*, 445(7124), pp. 168–176. doi: 10.1038/nature05453.

Lein, E. S., Borm, L. E. and Linnarsson, S. (2017) 'The promise of spatial transcriptomics for neuroscience in the era of molecular cell typing', *Science*, 358(6359), pp. 64–69. doi: 10.1126/SCIENCE.AAN6827.

Lever, C. *et al.* (2009) 'Boundary vector cells in the subiculum of the hippocampal formation', *Journal of Neuroscience*, 29(31), pp. 9771–9777. doi: 10.1523/JNEUROSCI.1319-09.2009.

Levone, B. R., Cryan, J. F. and O'Leary, O. F. (2021) 'Specific sub-regions of the longitudinal axis of the hippocampus mediate behavioural responses to chronic psychosocial stress', *Neuropharmacology*, 201, p. 108843. doi: 10.1016/j.neuropharm.2021.108843.

Li, Y. *et al.* (2017) 'Detection of volume alterations in hippocampal subfields of rats under chronic unpredictable mild stress using 7T MRI: A follow-up study', *Journal of Magnetic Resonance Imaging*, 46(5), pp. 1456–1463. doi: 10.1002/jmri.25667.

Lim, L. *et al.* (2018) 'Development and Functional Diversification of Cortical Interneurons', *Neuron*, pp. 294–313. doi: 10.1016/j.neuron.2018.10.009.

Liu, B. *et al.* (2017) 'From Serotonin to Neuroplasticity: Evolvement of Theories for Major Depressive Disorder', *Frontiers in Cellular Neuroscience*, 11, p. 305. doi: 10.3389/fncel.2017.00305.

Liu, X. and Carter, A. G. (2018) 'Ventral Hippocampal Inputs Preferentially Drive

Corticocortical Neurons in the Infralimbic Prefrontal Cortex', *The Journal of Neuroscience*, 38(33), pp. 7351–7363. doi: 10.1523/JNEUROSCI.0378-18.2018.

López-Giménez, J. F. and González-Maeso, J. (2017) 'Hallucinogens and Serotonin 5-HT2A Receptor-Mediated Signaling Pathways', in *Current Topics in Behavioral Neurosciences*. Springer Verlag, pp. 45–73. doi: 10.1007/7854_2017_478.

Luo, Y. *et al.* (2014) 'Dynamic study of the hippocampal volume by structural MRI in a rat model of depression', *Neurological Sciences*, 35(11), pp. 1777–1783. doi: 10.1007/s10072-014-1837-y.

Macdougall, M. J. and Howland, J. G. (2013) 'Acute stress and hippocampal output: Exploring dorsal CA1 and subicular synaptic plasticity simultaneously in anesthetized rats', *Physiological Reports*, 1(2). doi: 10.1002/phy2.35.

Madisen, L. *et al.* (2010) 'A robust and high-throughput Cre reporting and characterization system for the whole mouse brain', *Nature neuroscience*, 13 (1), p. 133. doi: 10.1038/NN.2467.

Maeng, S. *et al.* (2008) 'Cellular Mechanisms Underlying the Antidepressant Effects of Ketamine: Role of α-Amino-3-Hydroxy-5-Methylisoxazole-4-Propionic Acid Receptors', *Biological Psychiatry*, 63(4), pp. 349–352. doi: 10.1016/J.BIOPSYCH.2007.05.028.

Maramis, M. M., Mahajudin, M. S. and Khotib, J. (2020) 'Impaired Cognitive Flexibility and Working Memory Precedes Depression: A Rat Model to Study Depression', *Neuropsychobiology*, pp. 1–9. doi: 10.1159/000508682.

Mason, A. and Larkman, A. (1990) 'Correlations Between Morphology and Electrophysiology of Pyramidal Neurons in Slices of Rat Visual Cortex. II. Electrophysiology', *The Journal of Neuroscience*, 70(5), pp. 1415–1428.

Mathis, A. *et al.* (2018) 'DeepLabCut: markerless pose estimation of user-defined body parts with deep learning', *Nature Neuroscience 2018 21:9*, 21(9), pp. 1281–1289. doi: 10.1038/s41593-018-0209-y.

Matho, K. *et al.* (2021) 'Genetic dissection of the glutamatergic neuron system in cerebral cortex', *Nature*, 598(7879), pp. 182–187. doi: 10.1038/s41586-021-03955-9.

Matsumoto, N., Kitanishi, T. and Mizuseki, K. (2018) 'The subiculum: Unique hippocampal hub and more', *Neuroscience Research*, 143, pp. 1–12. doi: 10.1016/j.neures.2018.08.002.

Matsushita, N. *et al.* (2022) 'Highly Selective Transgene Expression Through Double-Floxed Inverted Orientation System by Using a Unilateral Spacer Sequence', *SSRN Electronic Journal*. doi: 10.2139/ssrn.4083378.

Matthews, K. and Robbins, T. W. (2003) 'Early experience as a determinant of adult behavioural responses to reward: the effects of repeated maternal separation in the rat', *Neuroscience & Biobehavioral Reviews*, 27(1–2), pp. 45–55. doi: 10.1016/S0149-7634(03)00008-3.

McLean, T. H. *et al.* (2006) '1-Aminomethylbenzocycloalkanes: Conformationally restricted hallucinogenic phenethylamine analogues as functionally selective 5-HT2A receptor agonists', *Journal of Medicinal Chemistry*, 49(19), pp. 5794 –5803. doi: 10.1021/JM060656O.

Mihaljević, B. *et al.* (2019) 'Classification of GABAergic interneurons by leading neuroscientists', *Scientific Data*, 6(1), pp. 1–6. doi: 10.1038/s41597-019-0246 -8.

Moreira, P. S. *et al.* (2016) 'Impact of chronic stress protocols in learning and memory in rodents: Systematic review and meta-analysis', *PLoS ONE*, 11(9). doi: 10.1371/journal.pone.0163245.

Moser, M. B. *et al.* (1995) 'Spatial learning with a minislab in the dorsal hippocampus', *Proceedings of the National Academy of Sciences of the United States of America*, 92(21), pp. 9697–9701. doi: 10.1073/ pnas.92.21.9697.

Naber, P. A. and Witter, M. P. (1998) 'Subicular efferents are organized mostly as parallel projections: A double-labeling, retrograde-tracing study in the rat', *The Journal of Comparative Neurology*, 393(3), pp. 284–297. doi: 10.1002/ (SICI)1096-9861(19980413)393:3<284::AID-CNE2>3.0.CO;2-Y.

Nagel, G. *et al.* (2005) 'Channelrhodopsins: directly light-gated cation channels', *Biochemical Society transactions*, 33(Pt 4), pp. 863–866. doi: 10.1042/ BST0330863.

Nakamura, H., Katayama, Y. and Kawakami, Y. (2010) 'Hippocampal CA1/ subiculum-prefrontal cortical pathways induce plastic changes of nociceptive

responses in cingulate and prelimbic areas', *BMC Neuroscience*, 11(1), p. 100. doi: 10.1186/1471-2202-11-100.

Namura, S. *et al.* (1994) 'Topographical organization of subicular neurons projecting to subcortical regions', *Brain Research Bulletin*, 35(3), pp. 221–231. doi: 10.1016/0361-9230(94)90126-0.

Narayanan, R. T., Udvary, D. and Oberlaender, M. (2017) 'Cell Type-Specific Structural Organization of the Six Layers in Rat Barrel Cortex', *Frontiers in Neuroanatomy*, 11, p. 91. doi: 10.3389/fnana.2017.00091.

Newton, D. F. *et al.* (2022) 'Chronic Stress Induces Coordinated Cortical Microcircuit Cell–Type Transcriptomic Changes Consistent With Altered Information Processing', *Biological Psychiatry*, 91(9), pp. 798–809. doi: 10.1016/J.BIOPSYCH.2021.10.015.

O'Mara, S. M. *et al.* (2009) 'Roles for the subiculum in spatial information processing, memory, motivation and the temporal control of behaviour', *Progress in Neuro-Psychopharmacology and Biological Psychiatry*, 33(5), pp. 782–790. doi: 10.1016/j.pnpbp.2009.03.040.

Olave, F. A. *et al.* (2022) 'Chronic restraint stress produces sex-specific behavioral and molecular outcomes in the dorsal and ventral rat hippocampus', *Neurobiology of Stress*, 17, p. 100440. doi: 10.1016/J.YNSTR.2022.100440.

Opalka, A. N. and Wang, D. V (2020) 'Hippocampal efferents to retrosplenial cortex and lateral septum are required for memory acquisition', *Learning & Memory*, 27(8), pp. 310–318. doi: 10.1101/lm.051797.120.

Overstreet-Wadiche, L. and McBain, C. J. (2015) 'Neurogliaform cells in cortical circuits', *Nature Reviews Neuroscience*. Nature Publishing Group, pp. 458–468. doi: 10.1038/nrn3969.

Page, C. E. *et al.* (2019) 'Prefrontal parvalbumin cells are sensitive to stress and mediate anxiety-related behaviors in female mice', *Scientific Reports*, 9(1), pp. 1–9. doi: 10.1038/s41598-019-56424-9.

Papp, M., Willner, P. and Muscat, R. (1991) 'An animal model of anhedonia: attenuation of sucrose consumption and place preference conditioning by chronic unpredictable mild stress', *Psychopharmacology*, 104(2), pp. 255–259. doi: 10.1007/BF02244188.

Paul, A. *et al.* (2017) 'Transcriptional Architecture of Synaptic Communication Delineates GABAergic Neuron Identity', *Cell*, 171(3), pp. 522-539.e20. doi: 10.1016/J.CELL.2017.08.032/ATTACHMENT/375ACDF0-B7C8-4698-911C-DAF0E15AC885/MMC8.PDF.

Peng, H. *et al.* (2021) 'Morphological diversity of single neurons in molecularly defined cell types', *Nature*, 598(7879), pp. 174–181. doi: 10.1038/s41586-021-03941-1.

Perlman, G., Tanti, A. and Mechawar, N. (2021) 'Parvalbumin interneuron alterations in stress-related mood disorders: A systematic review', *Neurobiology of Stress*, 15, p. 100380. doi: 10.1016/J.YNSTR.2021.100380.

Petreanu, L. *et al.* (2007) 'Channelrhodopsin-2–assisted circuit mapping of long-range callosal projections', *Nature Neuroscience*, 10(5), pp. 663–668. doi: 10.1038/nn1891.

Pizzagalli, D. A. and Roberts, A. C. (2022) 'Prefrontal cortex and depression', *Neuropsychopharmacology*, 47(1), pp. 225–246. doi: 10.1038/s41386-021-01101-7.

Planchez, B., Surget, A. and Belzung, C. (2019) 'Animal models of major depression: drawbacks and challenges', *Journal of Neural Transmission*. Springer-Verlag Wien, pp. 1383–1408. doi: 10.1007/s00702-019-02084-y.

Posener, J. A. *et al.* (2003) 'High-Dimensional Mapping of the Hippocampus in Depression', *American Journal of Psychiatry*, 160(1), pp. 83–89. doi: 10.1176/appi.ajp.160.1.83.

Pothuizen, H. H. J. *et al.* (2004) 'Dissociation of function between the dorsal and the ventral hippocampus in spatial learning abilities of the rat: A within-subject, within-task comparison of reference and working spatial memory', *European Journal of Neuroscience*, 19(3), pp. 705–712. doi: 10.1111/j.0953-816X.2004.03170.x.

Qin, X. *et al.* (2019) 'Moderate maternal separation mitigates the altered synaptic transmission and neuronal activation in amygdala by chronic stress in adult mice', *Molecular Brain*, 12(1), pp. 1–12. doi: 10.1186/S13041-019-0534-4/FIGURES/6.

Rajkowska, G. *et al.* (2006) 'GABAergic Neurons Immunoreactive for Calcium Binding Proteins are Reduced in the Prefrontal Cortex in Major Depression',

Neuropsychopharmacology, 32(2), pp. 471–482. doi: 10.1038/sj.npp.1301234.

Ramón y Cajal, S. (1899) *Textura del sistema nervioso del hombre y de los vertebrados*. Imprenta y Librería de Nicolás Moya.

Ravnkilde, B. *et al.* (2002) 'Cognitive deficits in major depression', *Scandinavian Journal of Psychology*, 43(3), pp. 239–251. doi: 10.1111/1467-9450.00292.

Reincke, S. A. J. and Hanganu-Opatz, I. L. (2017) 'Early-life stress impairs recognition memory and perturbs the functional maturation of prefrontal-hippocampal-perirhinal networks', *Scientific Reports*, 7(1), pp. 1–16. doi: 10.1038/srep42042.

Richardson, R. *et al.* (2021) 'Does maternal separation accelerate maturation of perineuronal nets and parvalbumin-containing inhibitory interneurons in male and female rats?', *Developmental cognitive neuroscience*, 47. doi: 10.1016/J.DCN.2020.100905.

Rocha, M. *et al.* (2021) 'Deficits in hippocampal-dependent memory across different rodent models of early life stress: systematic review and meta-analysis', *Translational Psychiatry*, 11(1). doi: 10.1038/s41398-021-01352-4.

Rock, P. L. *et al.* (2014) 'Cognitive impairment in depression: A systematic review and meta-analysis', *Psychological Medicine*. Cambridge University Press, pp. 2029–2040. doi: 10.1017/S0033291713002535.

Rojas-Carvajal, M. and Brenes, J. C. (2020) 'Acute stress differentially affects grooming subtypes and ultrasonic vocalisations in the open-field and home-cage test in rats', *Behavioural Processes*, 176, p. 104140. doi: 10.1016/J.BEPROC.2020.104140.

Romeo, R. D. *et al.* (2003) 'Anxiety and fear behaviors in adult male and female C57BL/6 mice are modulated by maternal separation', *Hormones and Behavior*, 43(5), pp. 561–567. doi: 10.1016/S0018-506X(03)00063-1.

Rotherme, M. *et al.* (2013) 'Transgene expression in target-defined neuron populations mediated by retrograde infection with adeno-associated viral vectors', *The Journal of neuroscience : the official journal of the Society for Neuroscience*, 33(38), pp. 15195–15206. doi: 10.1523/JNEUROSCI.1618-13.2013.

Roy, D. S. *et al.* (2017) 'Distinct Neural Circuits for the Formation and Retrieval of Episodic Memories', *Cell*, 170(5), pp. 1000-1012.e19. doi: 10.1016/j.cell.2017.07.013.

Rudy, B. *et al.* (2011) 'Three groups of interneurons account for nearly 100% of neocortical GABAergic neurons', *Developmental Neurobiology*, 71(1), pp. 45–61. doi: 10.1002/DNEU.20853.

Ruhé, H G *et al.* (2021) 'Molecular Imaging of Depressive Disorders', *PET and SPECT in Psychiatry*, pp. 85–207. doi: 10.1007/978-3-030-57231-0_4.

Salminen, L. E. *et al.* (2019) 'Hippocampal subfield volumes are uniquely affected in PTSD and depression: International analysis of 31 cohorts from the PGC-ENIGMA PTSD Working Group', *bioRxiv*. doi: 10.1101/739094.

Sánchez-Bellot, C. *et al.* (2022) 'Two opposing hippocampus to prefrontal cortex pathways for the control of approach and avoidance behaviour', *Nature Communications 2022 13:1*, 13(1), pp. 1–17. doi: 10.1038/s41467-022-27977-7.

Savitz, J., Lucki, I. and Drevets, W. C. (2009) '5-HT1A Receptor Function in Major Depressive Disorder', *Progress in neurobiology*, 88(1), p. 17. doi: 10.1016/J.PNEUROBIO.2009.01.009.

Scheggi, S., De Montis, M. G. and Gambarana, C. (2018) 'Making sense of rodent models of anhedonia', *International Journal of Neuropsychopharmacology*, 21(11), pp. 1049–1065. doi: 10.1093/ijnp/pyy083.

Schmaal, L. *et al.* (2020) 'ENIGMA MDD: seven years of global neuroimaging studies of major depression through worldwide data sharing', *Translational Psychiatry*, 10(1), pp. 1–19. doi: 10.1038/s41398-020-0842-6.

Schuman, B. *et al.* (2019) 'Four Unique Interneuron Populations Reside in Neocortical Layer 1.', *The Journal of neuroscience : the official journal of the Society for Neuroscience*, 39(1), pp. 125–139. doi: 10.1523/JNEUROSCI.1613-18.2018.

Serafini, G. (2012) 'Neuroplasticity and major depression, the role of modern antidepressant drugs', *World Journal of Psychiatry*, 2(3), p. 49. doi: 10.5498/wjp.v2.i3.49.

Shalev, U. and Kafkafi, N. (2002) 'Repeated maternal separation does not alter

sucrose-reinforced and open-field behaviors', *Pharmacology Biochemistry and Behavior*, 73(1), pp. 115–122. doi: 10.1016/S0091-3057(02)00756-6.

Sharp, P. E. (1997) 'Subicular cells generate similar spatial firing patterns in two geometrically and visually distinctive environments: Comparison with hippocampal place cells', *Behavioural Brain Research*, 85(1), pp. 71–92. doi: 10.1016/S0166-4328(96)00165-9.

Shepard, R. and Coutellier, L. (2018) 'Changes in the Prefrontal Glutamatergic and Parvalbumin Systems of Mice Exposed to Unpredictable Chronic Stress', *Molecular Neurobiology*, 55(3), pp. 2591–2602. doi: 10.1007/S12035-017-0528-0/FIGURES/5.

Sibille, E. *et al.* (2011) 'GABA-related transcripts in the dorsolateral prefrontal cortex in mood disorders', *The international journal of neuropsychopharmacology*, 14(6), pp. 721–734. doi: 10.1017/S1461145710001616.

Simonnet, J. and Brecht, M. (2019) 'Burst firing and spatial coding in subicular principal cells', *Journal of Neuroscience*, 39(19), pp. 3651–3662. doi: 10.1523/JNEUROSCI.1656-18.2019.

Slattery, D. A., Neumann, I. D. and Cryan, J. F. (2011) 'Transient inactivation of the infralimbic cortex induces antidepressant-like effects in the rat', *Journal of Psychopharmacology*, 25(10), pp. 1295–1303. doi: 10.1177/0269881110368873.

Sorensen, S. A. *et al.* (2015) 'Correlated Gene Expression and Target Specificity Demonstrate Excitatory Projection Neuron Diversity', *Cerebral Cortex*, 25(2), pp. 433–449. doi: 10.1093/cercor/bht243.

Spellman, T. and Liston, C. (2020) 'Toward circuit mechanisms of pathophysiology in depression', *American Journal of Psychiatry*, 177(5), pp. 381–390. doi: 10.1176/appi.ajp.2020.20030280.

Staff, N. P. *et al.* (2000) 'Resting and active properties of pyramidal neurons in subiculum and CA1 of rat hippocampus', *Journal of Neurophysiology*, 84(5), pp. 2398–2408. Available at: https://journals.physiology.org/doi/abs/10.1152/jn.2000.84.5.2398 (Accessed: 27 September 2020).

Stedenfeld, K. A. *et al.* (2011) 'Novelty-seeking behavior predicts vulnerability in a rodent model of depression', *Physiology & Behavior*, 103(2), pp. 210–216.

doi: 10.1016/J.PHYSBEH.2011.02.001.

Strange, B. A. *et al.* (2014) 'Functional organization of the hippocampal longitudinal axis', *Nature Reviews Neuroscience*. Nature Publishing Group, pp. 655–669. doi: 10.1038/nrn3785.

Stuart, S. A., Hinchcliffe, J. K. and Robinson, E. S. J. (2019) 'Evidence that neuropsychological deficits following early life adversity may underlie vulnerability to depression', *Neuropsychopharmacology 2019 44:9*, 44(9), pp. 1623–1630. doi: 10.1038/s41386-019-0388-6.

Sun, Y. *et al.* (2019) 'CA1-Projecting Subiculum Neurons Facilitate Object-Place Learning', *Nature neuroscience*, 22(11), p. 1857. doi: 10.1038/S41593-019-0496-Y.

Svenningsen, K. *et al.* (2016) 'MicroRNA profiling in the medial and lateral habenula of rats exposed to the learned helplessness paradigm: Candidate biomarkers for susceptibility and resilience to inescapable shock', *PLoS ONE*, 11(8). doi: 10.1371/journal.pone.0160318.

Tamás, G. *et al.* (2003) 'Identified sources and targets of slow inhibition in the neocortex', *Science*, 299(5614), pp. 1902–1905. doi: 10.1126/science.1082053.

Tan, S. *et al.* (2017) 'Maternal separation does not produce a significant behavioral change in mice', *Experimental Neurobiology*, 26(6), pp. 390–398. doi: 10.5607/en.2017.26.6.390.

Taniguchi, H. *et al.* (2011) 'A Resource of Cre Driver Lines for Genetic Targeting of GABAergic Neurons in Cerebral Cortex', *Neuron*, 71(6), pp. 995–1013. doi: 10.1016/J.NEURON.2011.07.026/ATTACHMENT/9DAB21D6-26D0-4299-ABDF-9A2A3F66CA3A/MMC5.AVI.

Tanti, A. and Belzung, C. (2013) 'Neurogenesis along the septo-temporal axis of the hippocampus: Are depression and the action of antidepressants region-specific?', *Neuroscience*, 252, pp. 234–252. doi: 10.1016/j.neuroscience.2013.08.017.

Tasic, B. *et al.* (2016) 'Adult mouse cortical cell taxonomy revealed by single cell transcriptomics', *Nature Neuroscience 2016 19:2*, 19(2), pp. 335–346. doi: 10.1038/nn.4216.

Tasic, B. *et al.* (2018) 'Shared and distinct transcriptomic cell types across neocortical areas', *Nature*, 563(7729), pp. 72–78. doi: 10.1038/s41586-018-0654-5.

Tchenio, A. *et al.* (2017) 'Limiting habenular hyperactivity ameliorates maternal separation-driven depressive-like symptoms', *Nature Communications*, 8(1), pp. 1–8. doi: 10.1038/s41467-017-01192-1.

Thaweethee-Sukjai, B. *et al.* (2019) 'Parvalbumin Promoter Methylation Altered in Major Depressive Disorder', *International journal of medical sciences*, 16(9), pp. 1207–1214. doi: 10.7150/IJMS.36131.

Thompson, S. M. *et al.* (2015) 'An excitatory synapse hypothesis of depression', *Trends in Neurosciences*, 38(5), pp. 279–294. doi: 10.1016/J.TINS.2015.03.003.

Thomson (2010) 'Neocortical layer 6, a review', *Frontiers in Neuroanatomy*, 4, p. 13. doi: 10.3389/fnana.2010.00013.

Tian, M. K., Schmidt, E. F. and Lambe, E. K. (2016) 'Serotonergic Suppression of Mouse Prefrontal Circuits Implicated in Task Attention', *eNeuro*, 3(5). doi: 10.1523/ENEURO.0269-16.2016.

Torromino, G. *et al.* (2019) 'Offline ventral subiculum-ventral striatum serial communication is required for spatial memory consolidation', *Nature Communications*, 10(1), pp. 1–9. doi: 10.1038/s41467-019-13703-3.

Tractenberg, S. G. *et al.* (2016) 'An overview of maternal separation effects on behavioural outcomes in mice: Evidence from a four-stage methodological systematic review', *Neuroscience and Biobehavioral Reviews*. Elsevier Ltd, pp. 489–503. doi: 10.1016/j.neubiorev.2016.06.021.

Treadway, M. T. *et al.* (2015) 'Illness Progression, Recent Stress, and Morphometry of Hippocampal Subfields and Medial Prefrontal Cortex in Major Depression', *Biological Psychiatry*, 77(3), pp. 285–294. doi: 10.1016/J.BIOPSYCH.2014.06.018.

Tricoire, L. *et al.* (2010) 'Common Origins of Hippocampal Ivy and Nitric Oxide Synthase Expressing Neurogliaform Cells', *Journal of Neuroscience*, 30(6), pp. 2165–2176. doi: 10.1523/JNEUROSCI.5123-09.2010.

Tripp, A. *et al.* (2012) 'Brain-Derived Neurotrophic Factor Signaling and Subgenual

Anterior Cingulate Cortex Dysfunction in Major Depressive Disorder', *The American journal of psychiatry*, 169(11), p. 1194. doi: 10.1176/APPI.AJP.2012.12020248.

Vidal-Gonzalez, I. *et al.* (2006) 'Microstimulation reveals opposing influences of prelimbic and infralimbic cortex on the expression of conditioned fear.', *Learning & memory (Cold Spring Harbor, N.Y.)*, 13(6), pp. 728–33. doi: 10.1101/lm.306106.

Wang, M. *et al.* (2014) 'Synaptic modifications in the medial prefrontal cortex in susceptibility and resilience to stress', *Journal of Neuroscience*, 34(22), pp. 7485–7492. doi: 10.1523/JNEUROSCI.5294-13.2014.

Webster, J. F. *et al.* (2021) 'NDNF is selectively expressed by neocortical, but not habenular neurogliaform cells', *European Journal of Neuroscience*, 53(11), pp. 3561–3575. doi: 10.1111/ejn.15237.

Willner, P. (2017) 'Reliability of the chronic mild stress model of depression: A user survey', *Neurobiology of Stress*, 6, pp. 68–77. doi: 10.1016/j.ynstr.2016.08.001.

Witter, M. P. (2006) 'Connections of the subiculum of the rat: Topography in relation to columnar and laminar organization', *Behavioural Brain Research*, 174(2), pp. 251–264. doi: 10.1016/j.bbr.2006.06.022.

Witter, M. P., Ostendorf, R. H. and Groenewegen, H. J. (1990) 'Heterogeneity in the Dorsal Subiculum of the Rat. Distinct Neuronal Zones Project to Different Cortical and Subcortical Targets', *European Journal of Neuroscience*, 2(8), pp. 718–725. doi: 10.1111/j.1460-9568.1990.tb00462.x.

Woodruff, A. *et al.* (2009) 'Depolarizing effect of neocortical chandelier neurons', *Frontiers in Neural Circuits*, 3(OCT), p. 15. doi: 10.3389/neuro.04.015.2009.

Wozny, C. *et al.* (2018) 'VGLUT2 functions as a differential marker for hippocampal output neurons', *Frontiers in Cellular Neuroscience*, 12. doi: 10.3389/fncel.2018.00337.

Wozny, C. and Williams, S. R. (2011) 'Specificity of Synaptic Connectivity between Layer 1 Inhibitory Interneurons and Layer 2/3 Pyramidal Neurons in the Rat Neocortex', *Cerebral Cortex*, 21(8), pp. 1818–1826. doi: 10.1093/cercor/bhq257.

Yamawaki, N. *et al.* (2019) 'Differential Contributions of Glutamatergic Hippocampal→Retrosplenial Cortical Projections to the Formation and Persistence of Context Memories', *Cerebral Cortex*, 29(6), pp. 2728–2736. doi: 10.1093/cercor/bhy142.

Yang, Y. *et al.* (2018) 'Ketamine blocks bursting in the lateral habenula to rapidly relieve depression', *Nature*, 554(7692), pp. 317–322. doi: 10.1038/nature25509.

Yankelevitch-Yahav, R. *et al.* (2015) 'The forced swim test as a model of depressive-like behavior', *Journal of Visualized Experiments*, 2015(97). doi: 10.3791/52587.

Yao, Z. *et al.* (2021) 'A taxonomy of transcriptomic cell types across the isocortex and hippocampal formation', *Cell*, 184(12), pp. 3222-3241.e26. doi: 10.1016/j.cell.2021.04.021.

Yu, J. Y. *et al.* (2018) 'Dorsal CA1 interneurons contribute to acute stress-induced spatial memory deficits', *Neuropharmacology*, 135, pp. 474–486. doi: 10.1016/J.NEUROPHARM.2018.04.002.

Yu, T. *et al.* (2011) 'Cognitive and neural correlates of depression-like behaviour in socially defeated mice: An animal model of depression with cognitive dysfunction', *International Journal of Neuropsychopharmacology*, 14(3), pp. 303–317. doi: 10.1017/S1461145710000945.

Yuen, E. Y. and Yan, Z. (2007) 'Serotonergic regulation of NMDA receptor trafficking and function in prefrontal cortex', *Monoaminergic Modulation of Cortical Excitability*, pp. 91–101. doi: 10.1007/978-0-387-72256-6_5/COVER.

Yuste, R. *et al.* (2020) 'A community-based transcriptomics classification and nomenclature of neocortical cell types', *Nature Neuroscience*. Nature Publishing Group, pp. 1456–1468. doi: 10.1038/s41593-020-0685-8.

Zacharko, R. M. and Anisman, H. (1991) 'Stressor-induced anhedonia in the mesocorticolimbic system', *Neuroscience and biobehavioral reviews*, 15(3), pp. 391–405. doi: 10.1016/S0149-7634(05)80032-6.

Zhang, X. *et al.* (2020) 'Effects of BDNF Signaling on Anxiety-Related Behavior and Spatial Memory of Adolescent Rats in Different Length of Maternal Separation', *Frontiers in Psychiatry*, 11. doi: 10.3389/fpsyt.2020.00709.

Zhang, Y. P. and Oertner, T. G. (2007) ‘Optical induction of synaptic plasticity using a light-sensitive channel’, *Nature Methods*, 4(2), pp. 139–141. doi: 10.1038/NMETH988.

Zhang, Z. W. and Deschênes, M. (1997) ‘Intracortical Axonal Projections of Lamina VI Cells of the Primary Somatosensory Cortex in the Rat: A Single-Cell Labeling Study’, *The Journal of Neuroscience*, 17(16), p. 6365. doi: 10.1523/JNEUROSCI.17-16-06365.1997.

Zingg, B. *et al.* (2019) ‘Anterograde Trans-Synaptic AAV Strategies for Probing Neural Circuitry’, *The Journal of Neuroscience*, p. 2019.12.24.888172. doi: 10.1101/2019.12.24.888172.

Zufferey, R. *et al.* (1999) ‘Woodchuck hepatitis virus posttranscriptional regulatory element enhances expression of transgenes delivered by retroviral vectors’, *Journal of virology*, 73(4), pp. 2886–2892. doi: 10.1128/JVI.73.4.2886-2892.1999.